A FINITE ELEMENT MODELING STUDY ON THE SEISMIC RESPONSE OF CANTILEVER RETAINING WALLS

A THESIS SUBMITTED TO
THE GRADUATE SCHOOL OF NATURAL AND APPLIED SCIENCES
OF
MIDDLE EAST TECHNICAL UNIVERSITY

BY

ÖZGÜR LÜTFİ ERTUĞRUL

IN PARTIAL FULFILLMENT OF THE REQUIREMENTS
FOR
THE DEGREE OF MASTER OF SCIENCE
IN
CIVIL ENGINEERING

SEPTEMBER 2006

Approval of the Graduate School of Natural And Applied Sciences

Prof.Dr. Canan ÖZGEN
Director

I certify that this thesis satisfies all the requirements as a thesis for the degree of Master of Science.

Prof.Dr. Erdal ÇOKÇA
Head of Department

This is to certify that we have read this thesis and that in our opinion it is fully adequate, in scope and quality, as a thesis for the degree of Master of Science.

Prof.Dr.M. Ufuk ERGUN
Co-Supervisor

Prof.Dr. M. Yener ÖZKAN
Supervisor

Examining Committee Members

Prof. Dr. Erdal ÇOKÇA (METU-CE) _____

Prof. Dr. M. Yener ÖZKAN (METU-CE) _____

Prof. Dr. M. Ufuk ERGUN (METU-CE) _____

Dr. Oğuz ÇALIŞAN (ÇALIŞAN PROJE) _____

Dr. Mehmet ÖZYAZICIOĞLU (METU-CE) _____

I hereby declare that all information in this document has been obtained and presented in accordance with academic rules and ethical conduct. I also declare that, as required by these rules and conduct, I have fully cited and referenced all material and results that are not original to this work.

Name, Last name : Özgür L. ERTUĞRUL

Signature:

ABSTRACT

A FINITE ELEMENT MODELING STUDY ON THE SEISMIC RESPONSE OF CANTILEVER RETAINING WALLS

ERTUĞRUL, Özgür L.
MSc., Department of Civil Engineering
Supervisor: Prof. Dr. M. Yener ÖZKAN
Co-Supervisor: Prof. Dr. M. Ufuk ERGUN

September 2006, 107 Pages

A numerical study was performed in order to investigate the effects of base excitation characteristics (peak acceleration amplitude and frequency of the excitation), soil strength and wall flexibility on the dynamic response of cantilever earth-retaining walls. In this study, Plaxis v8.2 dynamic finite element code was used. Previous 1-g shake table tests performed by Çalışan (1999) and Yunatçı (2003) were used to compare the experimental results with those obtained by finite element analysis. Comparison of experimental and numerical results indicated that the code was capable of predicting the dynamic lateral thrust values and bending moment profiles on the wall stems. In the light of these validation studies, a parametric study was carried on for a configuration that consists of an 8 meters high retaining wall supporting the same height of dry cohesionless backfill. Total and incremental dynamic thrust values, points of application and dimensionless bending moment values were presented together with the results obtained from commonly used pseudo static Mononobe-Okabe method and Steedman-Zeng approaches. According to the finite element analyses results, total dynamic active thrust act at approximately 0.30H above wall base. Base motion frequency becomes an important factor on magnitudes of dynamic active thrust when it approaches to the natural frequency of the system. Significantly high overturning moments were predicted at wall base in this case. It was observed that increasing wall rigidity increases forces acting on the wall stem during dynamic motion.

Keywords: Cantilever Earth-retaining Walls, Soil Strength, Wall Flexibility, Base Excitation Characteristics, Dynamic Lateral Thrust

ÖZ

ANKASTRE İSTİNAT DUVARLARININ SİSMİK DAVRANIŞININ SONLU ELEMANLAR METODU KULLANILARAK MODELLENMESİ

ERTUĞRUL, Özgür L.
Yüksek Lisans , İnşaat Mühendisliği Bölümü
Tez Yöneticisi: Prof. Dr. M. Yener ÖZKAN
Yardımcı Yönetici: Prof. Dr. M. Ufuk ERGUN

Eylül 2006, 107 sayfa

Yer ivmesi özellikleri (en büyük ivme , frekans) , zemin mukavemeti ve duvar rijitliğinin , ankastre istinat duvarlarının dinamik davranışları üzerindeki etkilerinin incelenmesi amacıyla modelleme çalışmaları gerçekleştirilmiştir. Sayısal analizlerde Plaxis sürüm 8.2 programı kullanılmıştır. Çalışan (1999) ve Yunatçı (2003) tarafından gerçekleştirilen 1-g sarsma tablası testlerinin sonuçlarından, deneysel sonuçların sonlu eleman analiz sonuçlarıyla karşılaştırılması hususunda faydalanılmıştır. Sayısal ve deneysel modellemelerin sonuçları karşılaştırıldığında, programın , model duvar gövdesinde oluşan dinamik yanal zemin itkileri ve bu kuvvetlerden kaynaklanan momentleri tahmin edebildiği gözlenmiştir. Bu doğrulama çalışmaları ışığında , sekiz metre derinliğinde kuru kum dolguyu destekleyen aynı yükseklikte bir ankastre duvar modellenerek bir parametrik çalışma yapılmıştır. Toplam ve ilave dinamik zemin itki değerleri ve uygulama noktaları ile duvar üzerinde oluşması tahmin edilen eğilme momenti değerleri, sıkça kullanılan yarı-statik Mononobe-Okabe ve Steedman-Zeng metotlarıyla elde edilen sonuçlarla karşılaştırılmıştır.Sonlu elemanlar metodu ile yapılan analiz sonuçlarına göre, maksimum toplam aktif itki, duvar tabanından yaklaşık olarak 0.30H yüksekliğinde etki etmektedir. Dinamik yer hareketinin frekansı, dolgu-duvar sisteminin doğal frekanslarına yaklaştığında etkili bir faktör olmakta ve duvar tabanında yüksek devrilme momentlerin oluşmasına sebep olmaktadır. Artan duvar rijitliğinin , dinamik hareket esnasında duvar üzerine etkiyen kuvvetlerin artmasına sebep olduğu gözlenmiştir

Anahtar kelimeler: Ankastre İstinat Duvarı, Zemin Mukavemeti, Duvar Esnekliği , Yer İvmesi Özellikleri , Dinamik Yanal İtki

TO MY FAMILY

ACKNOWLEDGMENTS

The author wishes to express his deepest gratitude to his supervisors Prof. Dr. M. Yener ÖZKAN and Prof. Dr. M. Ufuk ERGUN for their guidance, advice, criticism, encouragements and positive attitude throughout the whole phases of this research. Without their valuable support, the completion of this study would be nearly impossible.

The author would also like to thank Dr. Oğuz Çalışan, Mr. Anıl Yunatçı and Mr. Ersan Yıldız for their valuable suggestions and comments.

TABLE OF CONTENTS

LIST OF FIGURES

LIST OF TABLES

CHAPTER 1

INTRODUCTION

1.1 General

Failure of retaining walls in seismic events is a frequently observed problem. Retaining wall damages recorded in large earthquakes are in the form of translational displacements, rotations of the foundation, structural failure due to bending and large settlement of the backfills which effect the stability of the engineered structures located on the backfills. For a long time, the seismic performance of these structures is not considered in the designs because of incomplete understanding of the problem. Because the interactions occurring during and after a seismic excitation are complicated as compared to the static responses.

Existing seismic design methodologies are extensions of the static methods and far from accounting for the different parameters affecting the nature of the dynamic response. Since 1930's, the seismic analysis of retaining walls has been based on a simple extension of Coulomb's limit equilibrium analysis, which has become widely known as the Mononobe–Okabe method (1924). The method, modified and simplified by Seed and Whitman (1970), has been preferred mainly due to its simplicity and the familiarity of engineers with the Coulomb method.

Experimental studies in the 1970s using small-scale shaking table tests proved that in many cases the Mononobe–Okabe method was quite good in predicting dynamic thrusts, at least if the outward displacement of the wall (either due to translation, or rotation, or bending deformation) was large enough to cause the formation of a Coulomb-type sliding surface in the retained soil. A significant further development on the Mononobe–Okabe method is introduced by Richards and Elms (1979) who proposed to determine the permanent (inelastic) outward displacements using the sliding block concept proposed by Newmark (1965). Veletsos and Younan (1997) proposed elastic solutions for simple retaining wall systems which considers soil as a visco-elastic medium but this method gets complicated in modeling soil-structure interaction phenomena. The verification of these theories and methods using full-scale structures or scaled models is difficulty and has practical limitations.

The concept of building and instrumenting a full-scale structure and waiting for an earthquake to occur is impractical.

Since soil is a stress dependent material, the use of 1-g models allows only a limited insight into the actual prototype behavior. The most realistic modeling of this type of interaction problem can be performed by using centrifuge facilities.

1.2 Aim of the Study

Dynamic response of retaining wall systems were modeled via finite element method approach. The objective of the this study is to improve our understanding about the effects of

i. dynamic base excitation in terms of altered wave amplitude and frequency
ii. physical properties of the backfill and foundation material
iii. flexibility of the cantilever retaining wall

on the maximum dynamic thrust acting on the walls, the point of application of the resultant and bending moment profiles occurring on the walls.

In this thesis, the dynamic behavior of concrete cantilever walls retaining dry sand backfill is studied by Plaxis 8.2 finite element code with dynamic module which is an implicit non-linear solver. Newmark time-integration procedure is utilized in the dynamic module of the program for dynamic steps. The results of the dynamic finite element analyses can serve as a good source of high quality information for use in the assessment, verification, and development of numerical predictive methods. Considering this, results obtained from finite element analyses were compared with the results of experiments which were previously conducted at METU. Following this, a parametric study was carried on to investigate the effects of the base excitation characteristics (peak acceleration and frequency), flexibility of the considered cantilever retaining wall and the strength of the backfill. Also results of this study are compared with solutions of commonly used Mononobe-Okabe and Steedman-Zeng methods.

CHAPTER 2

LITERATURE REVIEW ON SEISMIC RESPONSE OF RETAINING WALLS

2.1 General

This literature review gives a brief summary of the studies performed up to now to model the dynamic response of cantilever retaining wall-soil systems. For this purpose, analytical solutions, numerical and experimental modeling studies will be considered.

Seismic behavior of retaining walls has been a field of interest to civil engineers since the beginning of 1900's.Since that time, different researchers compiled damage data for the retaining walls in previous strong earthquakes. But, it must be known that there exist only a few well documented case histories. The damage changes according to the type of the retaining wall, and the magnitude of the earthquake. Besides these, different conditions exist in each case such as orientation of the wall with respect to wave propagation direction, backfill and underlying soil characteristics, wall stiffness, ground water level etc. Primarily permanent deformations and/or rotations occur in retaining walls after a strong shaking episode. In some cases, only small deformation occurs, in others collapse occurs with large physical and economical consequences. It is very difficult to classify all the damage and reasons. But a brief summary on recorded damage data for a group of strong earthquakes is shown in Table 2-1.

A considerable effort has been devoted to study this concept. Many different types of retaining walls exist (i.e. gravity, cantilever, counter fort etc) and researchers developed various analytical and numerical models to predict the dynamic behavior of these structures. Besides these studies, lots of experimental study are performed to observe the mechanisms of soil-structure interaction and to verify the analytical and numerical modeling studies. Experimental studies were conducted on 1-g and centrifuge environments. An extensive 1-g modeling study on dynamic behavior of gravity retaining walls was conducted by Çalışan (1999). Nowadays, use of centrifuge techniques are considered to be more reliable because they are one step better to represent the stress dependency of soils on experiments carried on. In these tests, stress field is artificially changed to simulate prototype stress conditions.

Table 2-1 Retaining Wall Damage Due to Past Strong Earthquakes
(after Stadler 1997)

Earthquake	Date	Magn.	Damage
Kitaizu, Japan	1930	7,1	Failure of gravity walls (approx. 26 ft of mvt)
Tonankai, Japan	1944	8,2	Sliding of retaining wall. Outward movement of bulkhead with relieving platform (10-13 ft. of mvt.).
Tokachioi, Japan	1952	7,8	Outward movement of gravity wall (approx. 18 ft. of mvt)
Chile	1960	8,5	Complete overturning of gravity walls (>15 ft of mvt.) Outward movement of anchored bulkheads
Alaska, USA	1964	8,4	Lateral displacement of bridge abutments. Spreading and settlement of abutment fills.
Niigata, Japan	1964	7,5	Complete failure of 4.4 miles of earth retaining waterfront structures (sheetpile and gravity walls)
San Fernando, USA	1971	6,2	Severely damaged flood control channels (L-type reinforced concrete sections),
Friuli, Italy	1976	6,5	Complete collapse of retaining wall due to liquefied backfill.
Tangshan, China	1976	7,8	Lateral movement of bridge abutments. Buckling of superstructures.

Table 2.1 (continued) Retaining Wall Damage Due to Past Strong Earthquakes (after Stadler 1997)

Loma Prieta, USA	1989	7,1	Vertical cracking of reinforced concrete walls. Formation of gaps between top of walls and backfill soil.
Northridge, USA	1994	6,7	Continuous cracking and differential settlement of concrete crib walls.
Hyogoken-Nanbu, Japan	1995	7,2	Overturning and outward tilting with subsequent backfill settlement of gravity walls. Complete failure of stem of reinforced concrete cantilever retaining walls.

Numerous analytical solutions to the problem of dynamic lateral earth pressure on retaining walls have been proposed up to now. As suggested by Nazarian and Hadjian (1979), the proposed analytical solutions can be divided into four broad categories based on the methodologies of the investigators. The categories include rigid plastic, elastic, elasto-plastic and nonlinear methods. Typically, the magnitude of the anticipated retaining wall deflection determines which analysis method should be used. The rigid plastic and elastic methods represent the two extremes of displacement. A fundamental assumption of the rigid plastic methods is relatively large displacement. Very small displacements are assumed in the elastic methods. For displacements between these two extremes, elasto-plastic and nonlinear methods are appropriate. Numerical methods, most commonly using finite element analysis methods, are typically used when the intermediate displacement conditions are expected. Relevant work in each of the methodologies is presented in the following sections.

2.2 Analytical Methods for Calculating Seismic Pressures on Retaining Walls

According to Kramer (1996) one common approach for designing retaining walls for the seismic loads involves estimating the loads imposed on the wall during earthquake excitation and then ensuring that the wall can resist these loads. The actual loading phenomena on the retaining wall is actually a very complicated soil structure interaction problem and depends on the modes of wall movement. Therefore, simplified methodologies were developed.

2.2.1 Rigid Plastic Methods

2.2.1.1 Mononobe-Okabe Method

It is an approximate method which was developed in Japan in the 1920's by Okabe (1924) and Mononobe and Matsuo (1929) for determining the resultant of dynamic lateral earth pressures due to earthquake motions. Still widely used, this approach is called the Mononobe-Okabe (M-O) method. It is based on Coulomb's classical earth pressure theory for dry sand backfill. Coulomb's theory was modified by treating the inertial forces due to horizontal and vertical backfill accelerations as additional static forces. The model used for the M-0 method of analysis is shown in Figure 2.1. In this analysis, pseudo static accelerations are applied to a Coulomb active or passive wedge. The pseudo static soil thrust is then obtained from force equilibrium of the wedge.

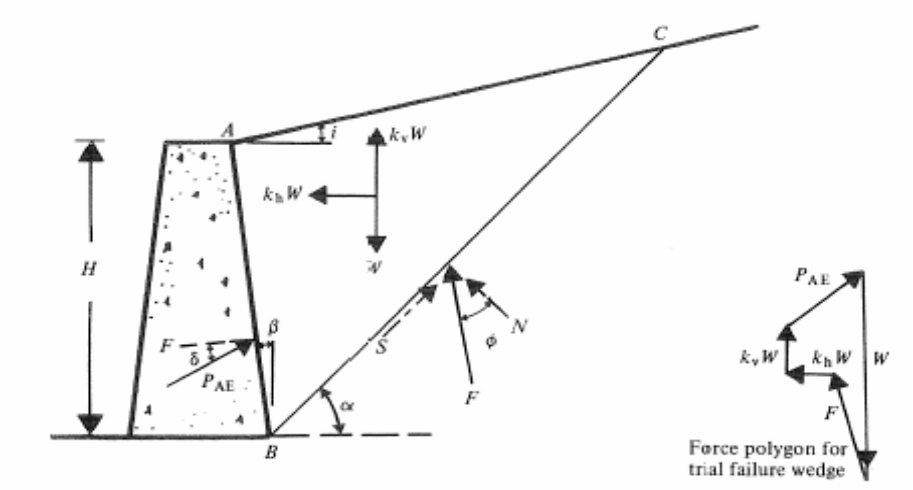

Figure 2.1 Forces for M-O method in active case (after Das,1983)

Seed and Whitman (1970) summarized the fundamental assumptions of Mononobe-Okabe method:

(a) The driving soil wedge and the retaining structure act as rigid bodies and therefore experience uniform accelerations throughout the respective bodies.

(b) Wall movement is sufficient to ensure either active or passive conditions, as the case may be.

(c) The driving soil wedge inducing the lateral earth pressures is formed by a planar failure surface starting at the heel of the wall and extending to the free surface of the backfill. Along this failure plane the maximum shear strength of the backfill is mobilized.

(d) When the minimum soil pressures are developed, the soil wedge behind the wall is at the point of failure and the maximum shear strength developed along the failure surface.

(e) The point of application of the seismic lateral thrust is at H/3 above the base of the wall where H is the wall height.

As demonstrated by Seed and Whitman (1970), the dynamic earth pressures may be determined from analogous static conditions. Accordingly, the Mononobe-Okabe expressions for dynamic earth pressures can be derived from the Coulomb's expressions for static earth pressures. The analogous static conditions are achieved by rotating the wall-backfill system by an angle ψ, such that the vector sum of the horizontal and vertical inertial coefficients (k_h and k_v, respectively) is oriented vertically, where:

$$\tan(\psi) = \frac{k_h}{1 - k_v} \qquad (2.1)$$

This procedure is illustrated in Figure 2.2 and Figure 2.3 for active and passive stress conditions, respectively. In regards to the mathematical expressions, the Mononobe-Okabe expressions can be derived from the Coulomb's expressions by replacing the static values for the total unit weight of the soil (γ_t), height of the wall (H), inclination of the backfill (β), and inclination of the wall face from the vertical (θ), with the corresponding dynamic values (i.e., $\gamma_{td}, H_d, \beta_d$ and θ_d).

This substitution is demonstrated in the following set of equations.

For the static conditions in active case:

$$P_a = \frac{1}{2}\gamma_t H^2 K_a \tag{2.2}$$

$$K_a = \frac{\cos^2(\phi-\theta)}{\cos^2(\theta).\cos(\theta+\delta).\left[1+\sqrt{\frac{\sin(\phi+\delta).\sin(\phi-\beta)}{\cos(\delta+\theta).\cos(\beta-\theta)}}\right]^2} \tag{2.3}$$

For the dynamic conditions, these expressions are modified as:

$$P_{AE} = \frac{1}{2}\gamma_{td} H_d^2 K_a(\beta_d,\theta_d) = \frac{1}{2}\gamma_t H^2.(1-k_v).K_{AE} \tag{2.4}$$

$$K_{AE} = \frac{\cos^2(\phi-\theta-\psi)}{\cos(\psi).\cos^2(\theta).\cos(\delta+\theta+\psi).\left[1+\sqrt{\frac{\sin(\phi+\delta).\sin(\phi-\beta-\psi)}{\cos(\delta+\theta+\psi).\cos(\beta-\theta)}}\right]^2} \tag{2.5}$$

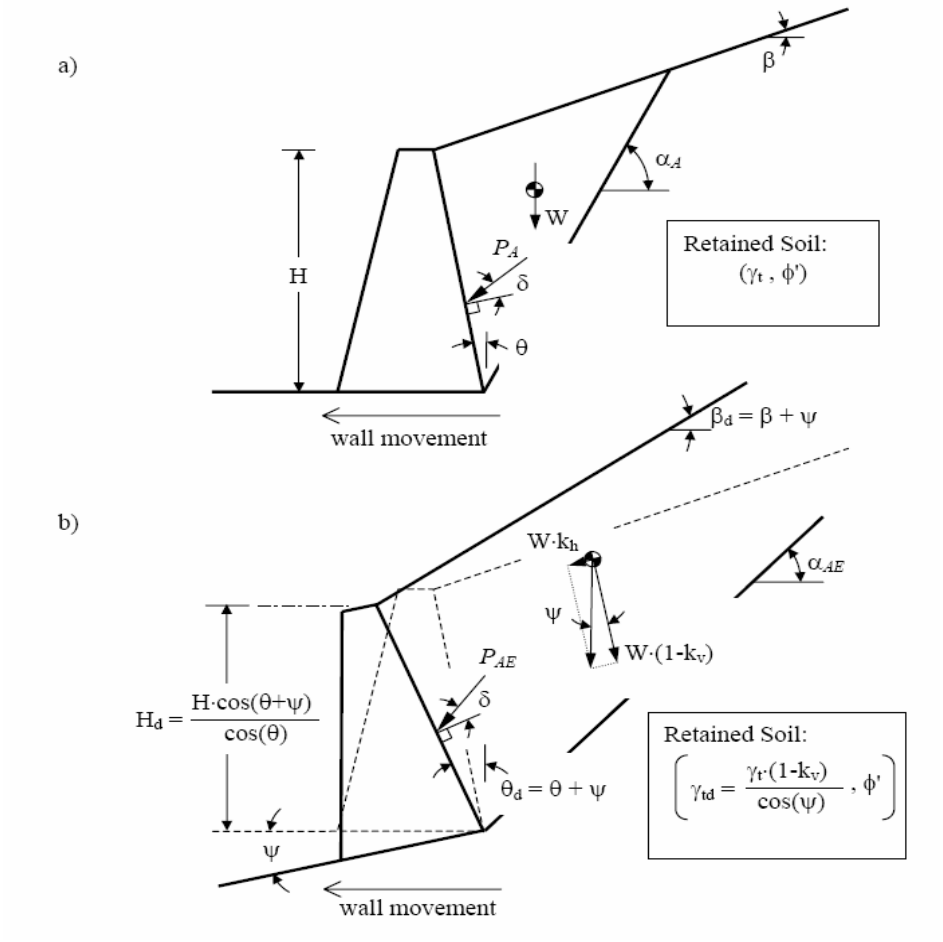

Figure 2.2 Active earth pressures for a)static conditions b) for dynamic conditions (after Green et al. ,2003)

For the static conditions in passive case:

$$P_p = \frac{1}{2}\gamma_t H^2 K_p \tag{2.6}$$

$$K_p = \frac{\cos^2(\phi+\theta)}{\cos^2(\theta).\cos(\delta-\theta).\left[1-\sqrt{\frac{\sin(\phi+\delta).\sin(\phi+\beta)}{\cos(\delta-\theta).\cos(\beta-\theta)}}\right]^2} \tag{2.7}$$

For the dynamic conditions, these expressions are modified as:

$$P_{PE} = \frac{1}{2}\gamma_{td} H_d^2 K_p(\beta_d, \theta_d) = \frac{1}{2}\gamma_t H^2.(1-k_v)K_{PE} \qquad (2.8)$$

$$K_{PE} = \frac{\cos^2(\phi+\theta-\psi)}{\cos(\psi).\cos^2(\theta).\cos(\delta-\theta+\psi).\left[1-\sqrt{\frac{\sin(\phi+\delta).\sin(\phi+\beta-\psi)}{\cos(\delta-\theta+\psi).\cos(\beta-\theta)}}\right]^2} \qquad (2.9)$$

Although M-O method implies that the total active thrust should act at a point H/3 above the base of the wall height, H , experimental results suggest that it actually acts at a higher point under dynamic loading conditions. The total active thrust calculated in (2.4) can be divided into a static component, P_a [from (2.2)]and a dynamic component ΔP_{AE} as shown in Eq.(2.10).

$$P_{AE} = P_A + \Delta P_{AE} \qquad (2.10)$$

The static component is known to act at H/3 above the base of the wall. Seed and Whitman(1970) suggested that the dynamic component be taken to act at approximately 0.6H. On this basis, the total active thrust will act at a height:

$$h = \frac{P_A H/3 + \Delta P_{AE}.(0.6H)}{P_{AE}} \qquad (2.11)$$

above the base of the wall. The value of h depends on the relative magnitudes of P_A and P_{AE}. Generally it occurs near the midheight of the wall.

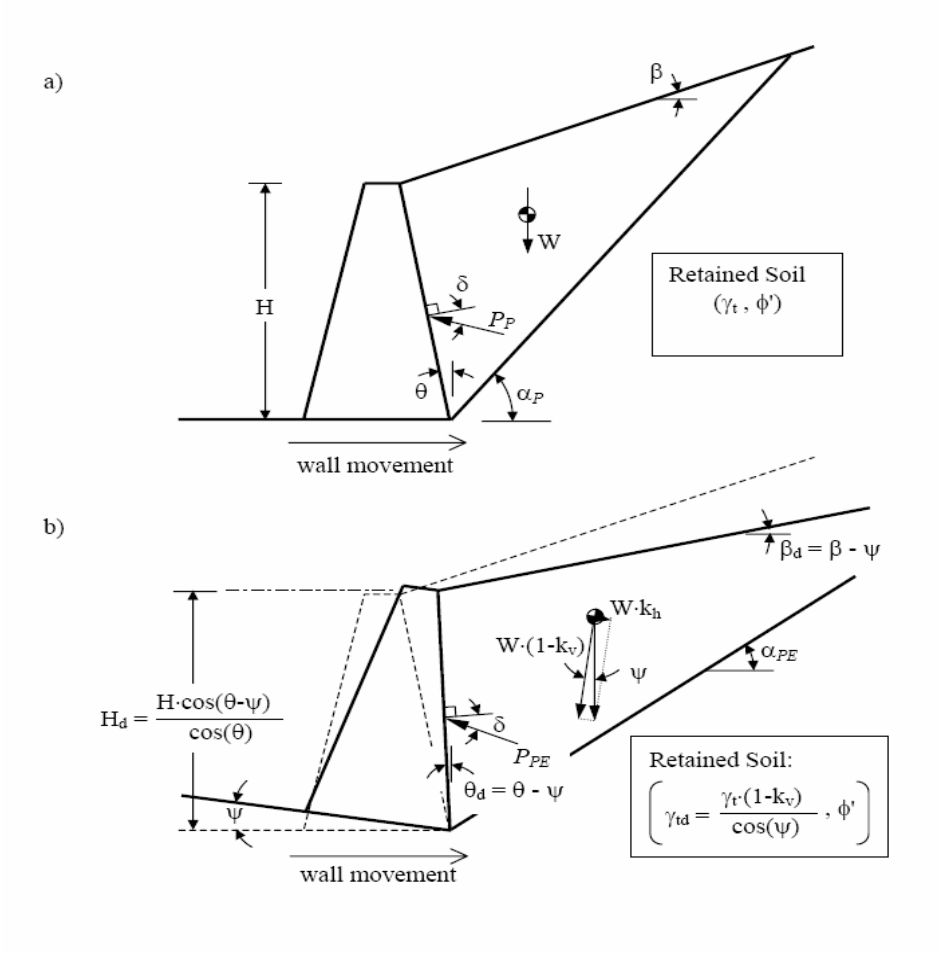

Figure 2.3 Passive earth pressures for a)static conditions b) for dynamic conditions (after Green et al. ,2003)

Although quite simple, the M-O method gives a useful means of estimating earthquake induced loads on retaining walls. A positive horizontal acceleration causes the total active thrust to exceed the static active thrust and the total passive thrust to be less than the static passive thrust.

But, as a pseudo static extension of the Coulombs analyses, The M-O analysis is subject to all the limitations of the pseudo static analyses as well as the limitations of the Coulomb's theory and must be carefully examined.

2.2.1.2 Steedman-Zeng Method

Mononobe-Okabe method mentioned previously accounts the dynamic nature of earthquake loading in a very approximate way. A finer approximation of these phenomena was suggested by Steedman and Zeng (1991).

Steedman – Zeng method is a pseudo dynamic analysis which accounts for phase differences and amplification effects developing during an earthquake (Kramer,1996). If the active wedge shown in Figure 2.4 is considered, acceleration at a depth z can be expressed as follows:

$$a(z,t) = a_h \sin\left[\omega\left(t - \frac{H - z}{v_s}\right)\right] \qquad (2.12)$$

where

a_h= amplitude of harmonic horizontal input acceleration

ω = cyclic frequency of harmonic input motion

t = time

v_s = velocity of vertically propagating harmonic shear wave

H = height of the wall

Z = depth

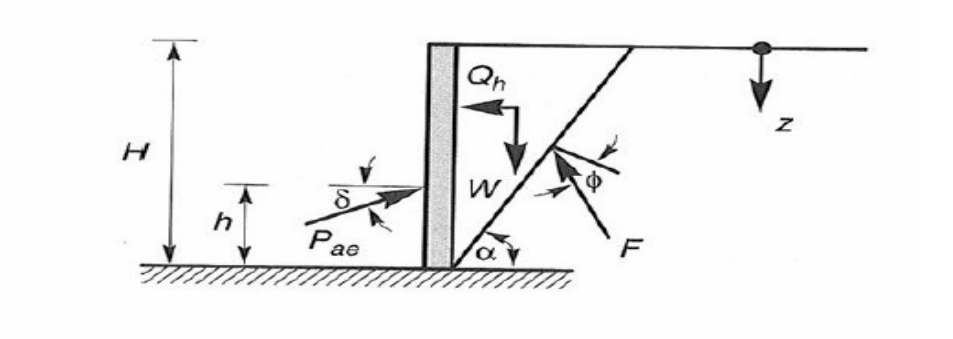

Figure 2.4 A Steedman-Zeng Wedge and the forces acting on it. (After Kramer,1996)

The mass of a thin element in the active wedge is:

$$m(z) = \frac{\gamma}{g}.\frac{H-z}{\tan\alpha}dz \qquad (2.13)$$

where

γ = unit weight of the backfill material

g= gravitational acceleration

The total inertial force acting on the wall can therefore be given as:

$$Q_h(t) = \int_0^H m(z).a(z,t).dz = \frac{\lambda\gamma a_h}{4\pi^2 g\tan(\alpha)}\left[2\pi H\cos\omega\zeta + \lambda\left(\sin\omega\zeta - \sin\omega t\right)\right] \qquad (2.14)$$

where

$$\lambda = \frac{2\pi v_s}{\omega} \qquad (2.15)$$

and

$$\zeta = t - \frac{H}{v_s} \qquad (2.16)$$

By resolving the forces on the wedge we can obtain the total soil thrust as follows:

$$P_{AE}(t) = \frac{Q_h(t)\cos(\alpha-\phi) + W\sin(\alpha-\phi)}{\cos(\delta+\phi-\alpha)} \qquad (2.17)$$

If we differentiate the total soil thrust we can obtain the total earth pressure distribution as follows:

$$P_{AE}(t) = \frac{\gamma z}{\tan\alpha}\frac{\sin(\alpha-\phi)}{\cos(\delta+\phi-\alpha)} + \frac{k_h\gamma z}{\tan\alpha}\frac{\cos(\alpha-\phi)}{\cos(\delta+\phi-\alpha)}\sin\left(\omega\left(t-\frac{z}{V_s}\right)\right) \qquad (2.18)$$

The height of application of total thrust varies with time according to the following formula:

$$h_d = H - \frac{2\pi^2 H^2 \cos\omega\zeta + 2\pi\lambda H \sin\omega\zeta - \lambda^2\left(\cos\omega\zeta - \cos\omega t\right)}{2\pi H \cos\omega\zeta + \pi\lambda\left(\sin\omega\zeta - \sin\omega t\right)} \qquad (2.19)$$

Steedman and Zeng (1991) observed that the soil thrusts for backfills of different stiffnesses were close to those obtained when shear wave velocities of the backfill were used in the pseudo-dynamic analyses. Backfill amplification effects can also be reflected in the equations by expressing a_h as a function of depth rather than using a constant acceleration value thought the height of the backfill. The results of Steedman-Zeng shows good agreement with the centrifuge results but this method can not have the ability to represent the effects of flexibility of the wall.

2.2.2 Displacement Based Methods

Performance based design can be considered in retaining wall applications, because in many of the cases, post-earthquake serviceability of these structures are more important and closely related to the permanent deformations that occur after a strong shaking episode. Large permanent displacements may be acceptable in some walls, but some of them are sensitive to large displacements. By considering these, some methodologies were developed by researchers. In the following paragraph, these methods will be summarized.

Richards and Elms (1977) modified the Mononobe-Okabe theory to include the inertial forces due to the retaining wall. Another group of rigid plastic analysis techniques may be termed as the displacement-based methods. Newmark (1965) presented results of standardized maximum displacements of earth embankments under earthquake loadings on the basis of a sliding block model and four earthquake records. Franklin and Chang (1977) extended Newmark's data base by similarly analyzing more than 100 published earthquake records. Richards and Elms (1979) proposed that gravity retaining walls be designed to permit a small amount of displacement in a large earthquake.

According to their method, using the simplified M-O formulation, a yielding wall may be designed using either a limit-equilibrium force approach (conventional retaining wall design) or an approach that permits movement of the wall up to tolerable amounts.

Using Franklin and Chang's data, they presented a function that predicts the maximum displacement for a maximum earthquake velocity.

Based on a certain amount of permissible displacement, the designer can calculate an acceleration coefficient value somewhat less than the maximum. This reduced acceleration coefficient is used in the M-0 method to determine the lateral force. Wall inertia must also be considered. To account for uncertainties, they recommended a safety factor of 1.5 be applied to the weight of the wall.

Others, including Zarrabi (1979) and Jacobson (1980), have extended the sliding block model to account for such things as the relative accelerations of the soil wedge and the retaining wall.

2.2.3 Elastic Methods Based on Wave Theory

Elastic solutions are applicable to non- yielding walls where displacements do not cause plastic displacements in the soil body.

Matsuo and Ohara (1960) determined an approximate elastic solution for the dynamic soil pressure on a rigid wall using a two-dimensional analytical model. In this methodology bending of the wall was not considered and no vertical displacement of the soil mass was allowed. Assuming the wall was stationary, lateral soil stresses were derived using classical wave theory.

Tajimi (1973) derived the pressures induced by a harmonically forced rigid-wall in translation and base rotation by employing a quarter infinite field and two-dimensional elastic wave theory. The formulation of this problem is illustrated in Figure 2.5. The results are given in the form of equations and charts. The solutions may be used to calculate the approximate impedance functions for embedded structures. However, the boundary conditions used by Tajimi are such that his solutions are not directly relevant to the problem of base shaking of a wall-soil system of finite size (Steedman, 1984).

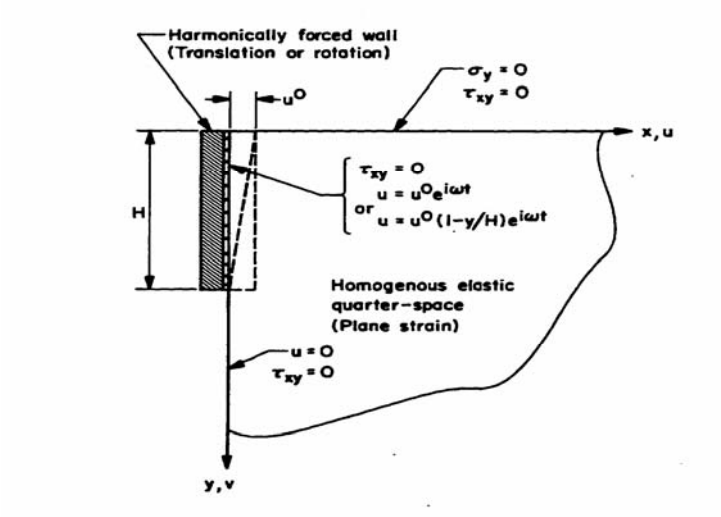

Figure 2.5 Tajimi's Problem (after Wood,1973)

Scott (1973) studied the dynamic behavior of a rigid retaining wall by modeling the soil backfill as a one-dimensional, elastic, shear beam attached to the wall by Winkler springs. This model is shown in Figure 2.6. He solved this problem for two soil conditions: constant soil properties with depth and shear modulus increasing parabolically with depth. His results show that the first mode is primarily responsible for the pressures on the wall. According to his solution, the first-mode dynamic pressure increment distribution is a cosine function which decreases with depth from a maximum at the surface to zero at the base. The resultant acts at approximately 2H/3.

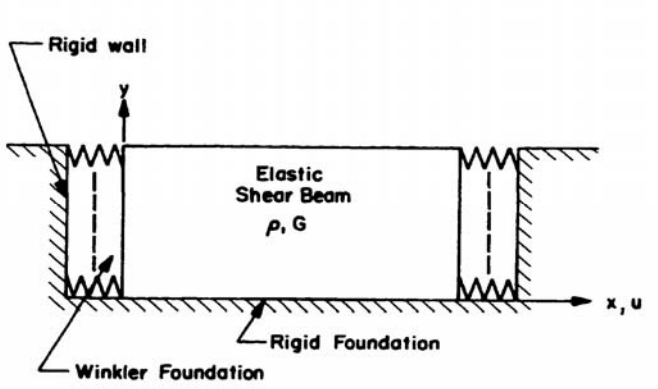

Figure 2.6 Scott's Model (after Wood,1973)

Wood (1973) has presented an extensive study of the behavior of rigid soil retaining structures subjected to earthquake motions. The study is based on linear elastic theory and idealized representations of wall-soil systems. He derived the normal mode solution for the free vibration of the elastic solid and presented solutions for the cases of arbitrary horizontal forcing of the rigid boundaries and a uniform horizontal body force. The formulation for the case of a uniform horizontal body force is illustrated in Figure 2.7.Results from this case were presented as normalized pressure profiles and are shown in Figure 2.8. Analytical solutions were augmented by finite element solutions for those cases where analytical results would be difficult to obtain. Similar results were presented for the case of rotational forcing of the wall about its base.

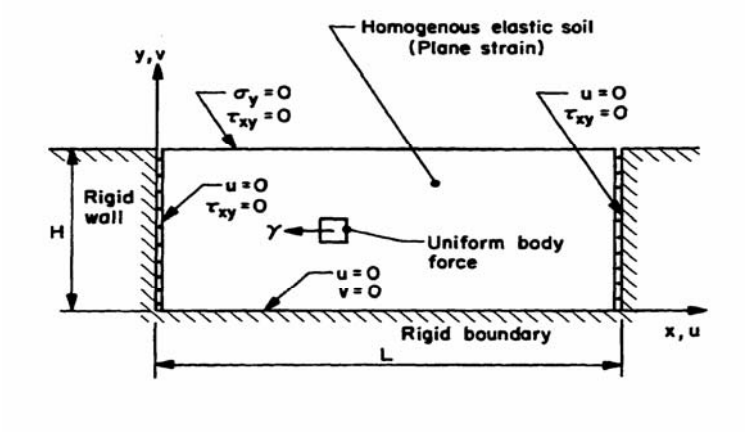

Figure 2.7 Wood's Model (after Nazarian and Hadjian,1979)

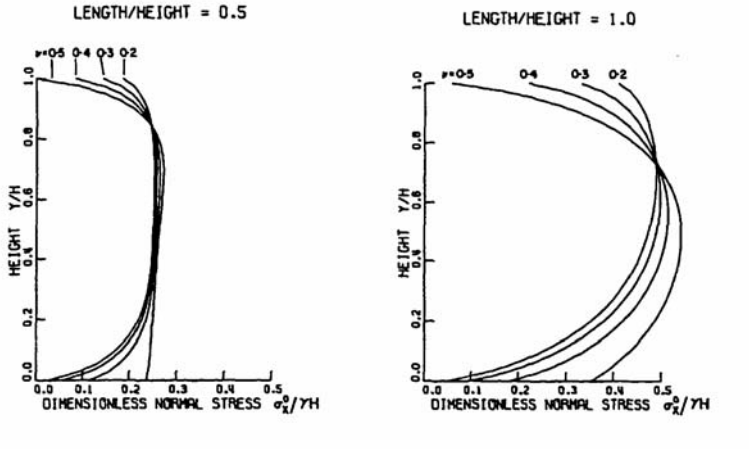

Figure 2.8 Pressure Distributions for 1-g Static Horizontal Body Force
(after Wood,1973)

2.3 Numerical Methods

The development of the computational capabilities are giving researchers to model soil with much more advanced models and carry non-linear analyses. Nowadays, finite element computer codes are frequently used in modeling and analyzing complex soil-structure interaction problems.

The actual behavior of the retaining walls depend on the interaction of the structure with the backfill and underlain soil layers, therefore it is logical to use stress-deformation techniques such as finite element methods. Clough and Duncan(1971) stated that finite-element analyses are very useful for estimating the retaining wall pressures and movements and in addition to this, they can help to explain unexpected field measurements of actual wall behavior.

The accuracy of these stress-deformation techniques depends on how well the actual field conditions are represented. According to Kramer (1996), a useful method for this purpose is to model to behavior of soil with nonlinear constitutive models, the wall elements with linear model, to consider the stress-displacement of the soil-wall interface, and the sequence of wall construction and backfill placement.

For dynamic finite element analysis, the variations of acceleration in the soil is of great importance because these variations lead to equivalent thrusts through application of Newton's laws. Therefore, methodologies are developed to implement the effect of inertia into finite element modeling. The details of dynamic finite element modeling will be discussed in chapter four.

2.3.1 A Brief Summary of the Development of Finite Element Procedures for Modeling the Dynamic Response of the Retaining Walls

One of the first investigators applying finite element method to retaining wall problem were Clough and Duncan (1971), They performed finite element modeling techniques to inspect the behavior of the soil-wall interface .

Wood (1973) modeled selected retaining wall-backfill soil systems with linear, plane-strain finite elements. He compared the numerical results with analytical calculations and found generally good agreement.

Aggour and Brown (1973) studied the effects of wall flexibility, soil moduli, backfill length and backfill shape on the dynamic earth pressure distribution. Two-dimensional, plane strain analyses were performed on a 6 m. wall with backfill extending to 60 meters Wall thicknesses of 0.4, 0.6 and 1.2 meters were studied. 0.1g amplitude sinusoidal excitation with varying frequencies was used as the input acceleration.

Byrne and Salgado (1981) derived a simple elasto-plastic model. Soil spring stiffnesses, with limiting forces based on the active and passive values, are calculated based on the recommendations of Terzaghi (1934). Elastic vibrations are superimposed on plastic slippage and observed. Byrne and Salgado conclude that the initial static stress condition has only a small effect on the maximum force on the wall.

Nadim and Whitman (1982) considered some of the limitations of the sliding block model using a finite element formulation. They recommended that the limiting displacement method be used for design with modifications to the design acceleration.

Steedman (1984) developed a quasi-static, elasto-plastic interaction model. He concludes that stress state and stress path are important parameters.

Siddharthan and Maragakis (1987) studied the dynamic behavior of flexible walls supporting dry sand backfill. Soil response under dynamic loading was modeled as nonlinear and hysteretic. Their model also accounts for the increase in lateral stresses and settlement related to grain slip caused by cyclic loads, the soil was represented by plane-strain, isoparametric elements and the wall was represented by beam elements. Sinusoidal base excitation was used. A centrifuge test of an aluminum wall retaining dry sand (Steedman, 1983) was modeled numerically. Experimental wall is shown in Figure 2.9. Computed and measured dynamic bending moments showed good agreement. Finite element model they developed was used to study the effect of different backfill densities and wall flexibilities on the wall response. They concluded that the base bending moment was smaller and the deflection was greater for the more flexible walls.

Finn et al (1989) presented a numerical method of analysis for cantilever retaining walls and compared the results with centrifuge test data. The finite element code employed a nonlinear dynamic effective stress analysis method. Deformations, bending moments, and accelerations were numerically estimated and compared with the centrifuge test results. Good agreement was found between the two.

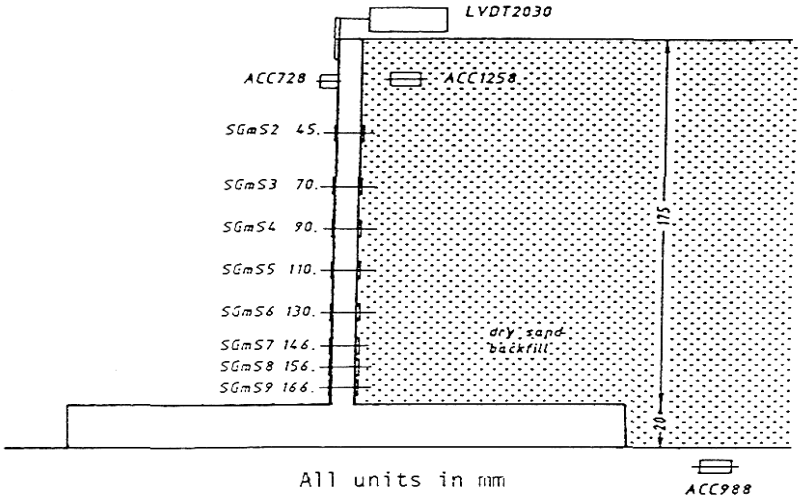

Figure 2.9 Model Retaining Wall used in Steedman's centrifuge tests (after Siddarthan and Maragakis, 1987)

Bakeer, Bhatia and Ishibashi (1990) performed finite element analysis in order to investigate the dynamic pressures and the point of application for different wall movement modes. Translation (AT), rotation about the top (ART) and rotation about the bottom (ARB) were selected failure modes. They found that dynamic lateral earth pressures are larger than predicted by Mononobe-Okabe for all wall movement modes. Distribution of pressure is not hydrostatic either. For ART and AT modes, location of the resultant thrust was higher than the one third of the wall height; whereas for the ARB mode, location was lower than M-O values for small acceleration values, exceeding at accelerations larger than 0.3g. Bakeer et al. used results of shaking table tests to verify their finite element analysis results. The comparison of their studies and experimental results are shown in Figure 2.10 to Figure 2.13 .

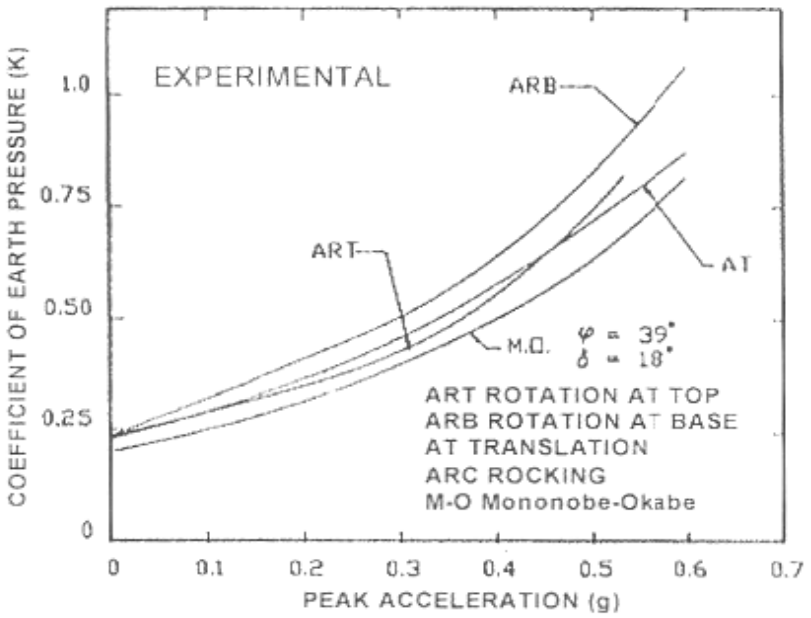

Figure 2.10 Experimental values of coefficient of earth pressure for different wall movement modes (after Bakeer,Bhatia and Ishibashi,1990)

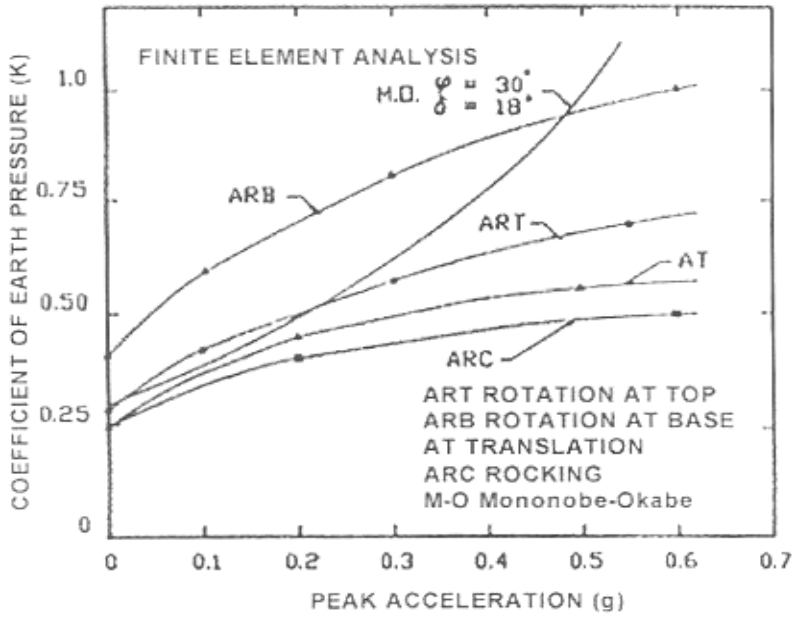

Figure 2.11 Finite Element analysis results for coefficient of earth pressure for different wall movement modes (after Bakeer, Bhatia and Ishibashi, 1990)

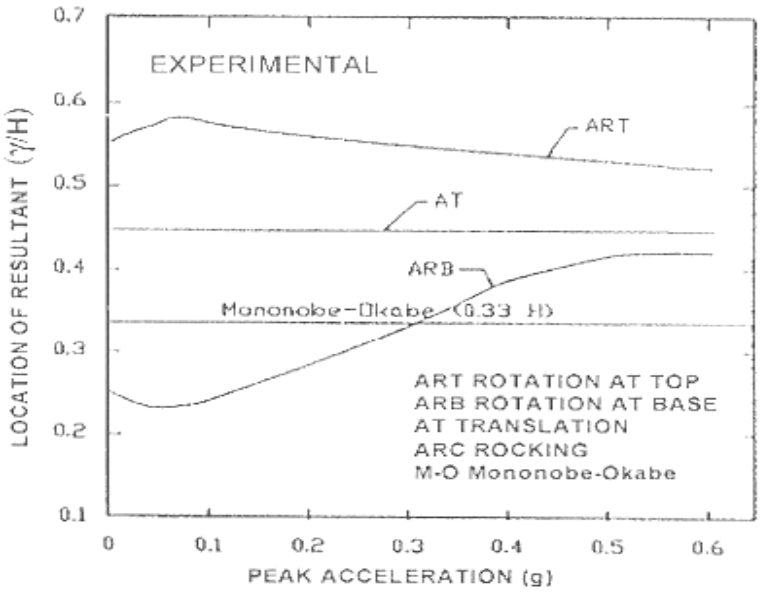

Figure 2.12 Experimental values of application point of resultant for various wall movement modes(after Bakeer,Bhatia and Ishibashi,1990)

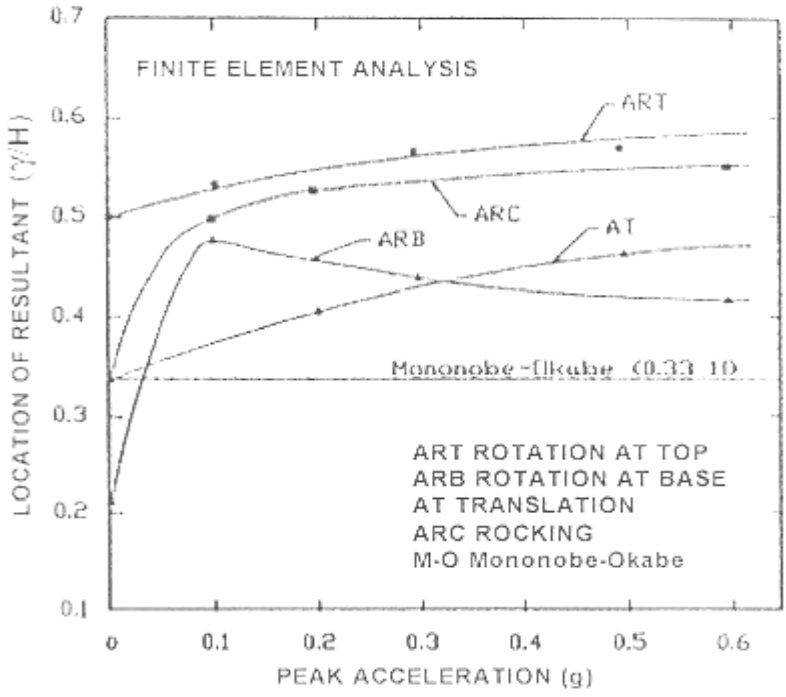

Figure 2.13 Finite element results of the application point of the resultant for different wall modes (after Bakeer,Bhatia and Ishibashi,1990)

Bangash (1991) performed finite element modeling studies of tied-back retaining walls to identify the variables that most affect the seismic behavior of these walls. His parametric study shows that simulated wall generally moves together with its backfill. The parameters he studied involves the depth of bedrock, input frequency, input acceleration, soil strength, backfill slope, anchor inclination and actual earthquake record. At the beginning of his finite element studies, a one dimensional wave propagation analysis is performed to validate the finite element code. Same results are obtained with finite element analysis results. The discretised model he used in his studies is shown in Figure 2.14.

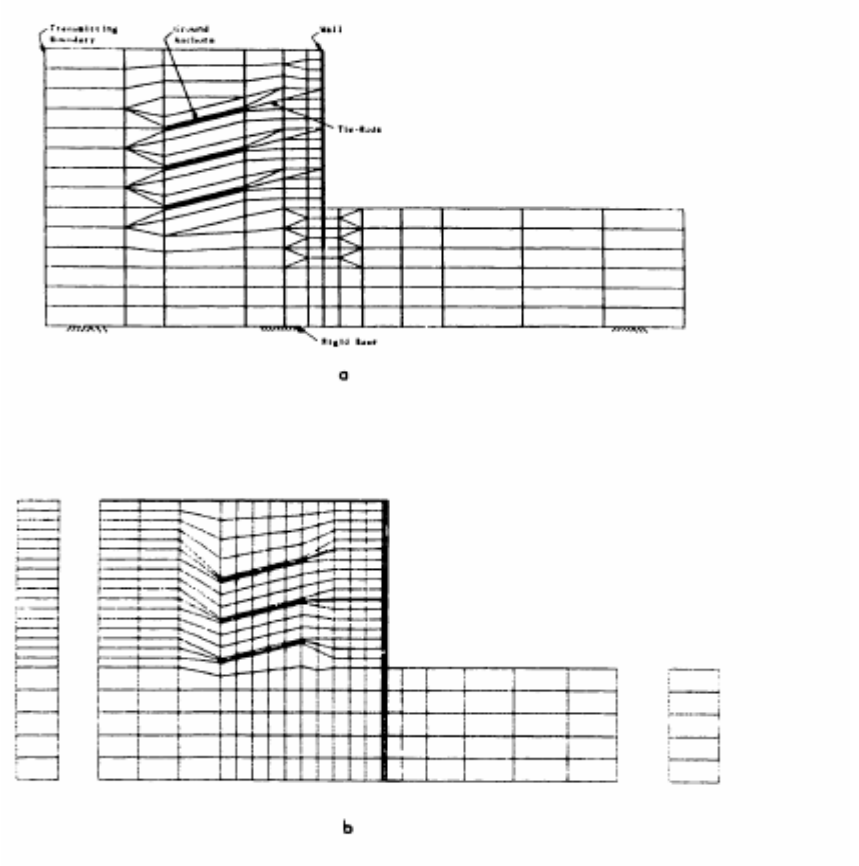

Figure 2.14 Discretised finite element model of the anchored bulkhead (after Bangasah,1991)

In his study, very large bending moments observed due to the displacements toward the excavation versus those toward the retained soil side. As the wall moves towards the excavation, passive resistance limits the movement of the embedded portion, producing large bending moments. His quantitative results may serve as a basis for preliminary design guidelines.

Veletsos and Younan (1994) studied the dynamic behavior of rigid vertical walls. Their study examines the semi-infinite, uniform, visco-elastic stratum of soil having constant thickness which has excited by both harmonic and transient excitations.

The studies are carried by assuming constant and frequency dependent parameters. Then they reduced the model to frequency independent parameters for obtaining more generalized characteristics. In their studies, they also aimed to assess the reliability of the Scott's model (1973). In this model; the radiational damping capacity of the medium is ignored and the wall pressures are considered to be proportional with the relative motions of the soil at the far field. But they concluded that this procedure may lead to large errors.

Veletsos and Younan (1997) carried analytical studies to examine the effect of wall and base stiffnesses on the wall pressures and distributions. The model they used are shown in Figure 2.15 . According to their studies on rigid retaining walls which are elastically constrained against rotation at their base, both the magnitudes and distributions of dynamic earth pressures are heavily dependent on the flexibility of the base constraint.

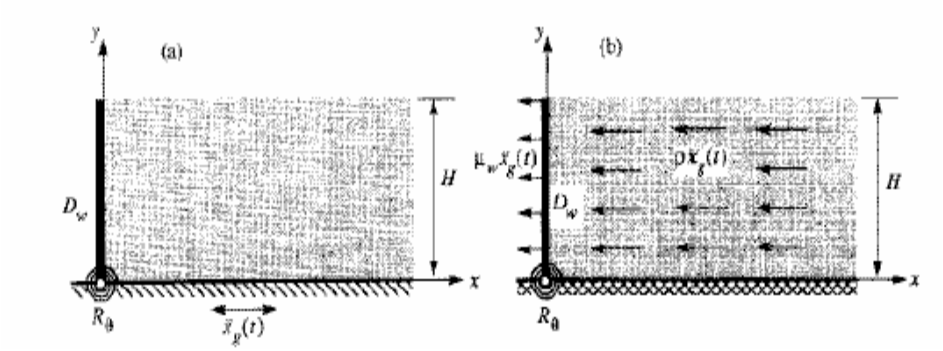

Figure 2.15 Soil wall system investigated by Velestos and Younan (1997)
(a) Base-excited system (b) Force – excited system
(after Velestos and Younan, 1997)

Increasing flexibility of the base and the wall reduces the horizontal extensional stiffness of the retained medium relative to its shearing stiffness, and this reduction decreases the proportion of the soil inertia forces that gets transferred to the wall and, hence, the forces developed in it. Wall pressures for different wall flexibilities are shown in Figure 2.16.

In this figure: η axis of the graph is the dimensionless vertical position coordinate which is equal to y/H, d_θ denotes the relative flexibility of the rotational base constrained and the retained medium, d_w ,the relative flexibility of the wall and the retained medium, ρ, mass density of the soil medium, H , height of the wall and $\ddot{X}_g$, maximum ground acceleration. They concluded in their study that the total wall force or base shear is one-half or less than the values obtained for a fixed based rigid wall and large reductions are observed for the base moments.

Gazetas (2004) investigated the dynamic earth pressures on various kinds of earth retaining structures such as L-shaped reinforced-concrete walls, piled walls with horizontal or strongly inclined anchors, and reinforced soil walls. In their analyses, base excitations of either high or moderately low dominant frequencies having a peak value of 0.4g are used. Time of excitation was short. For modeling the soil, non-linear Mohr-Coulomb model is used as well as linear model. The soil modeled was under dry conditions. For the L-shaped reinforced-concrete retaining walls they observed that the failure shapes indicated in Figure 2.17.

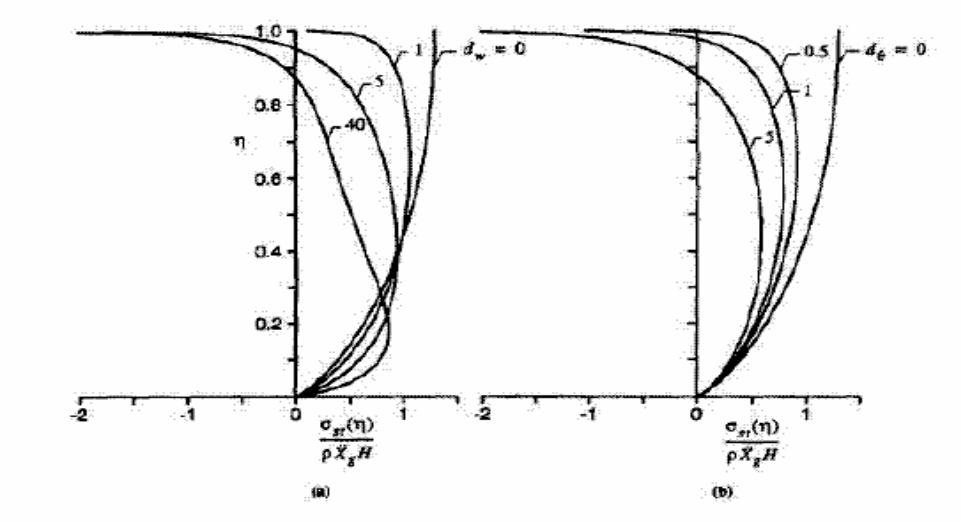

Figure 2.16 Distributions of wall pressure for excited systems with different wall and base flexibilities (a) for d_θ (b) for $d_w=0$ (after Velestos and Younan, 1997)

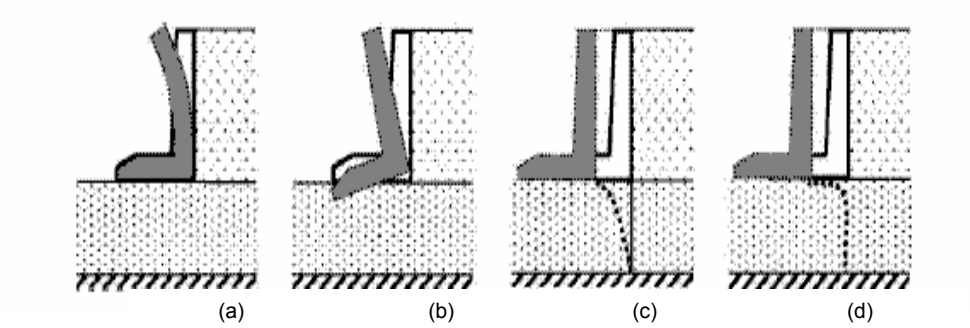

Figure 2.17 Possible modes of displacement of an L-shaped wall: (a) structural flexure, (b) base rotation, (c) elastic base translation, and (d) inelastic base translation (sliding) (after Gazetas et al,2004)

In Figure 2.18, the pressure distributions for walls of different flexibilities in Gazetas' study are plotted. There is a considerable change in pressure distributions for increasing flexibilities. As compared with Wood's solutions, smaller pressure values are obtained in these analyses.

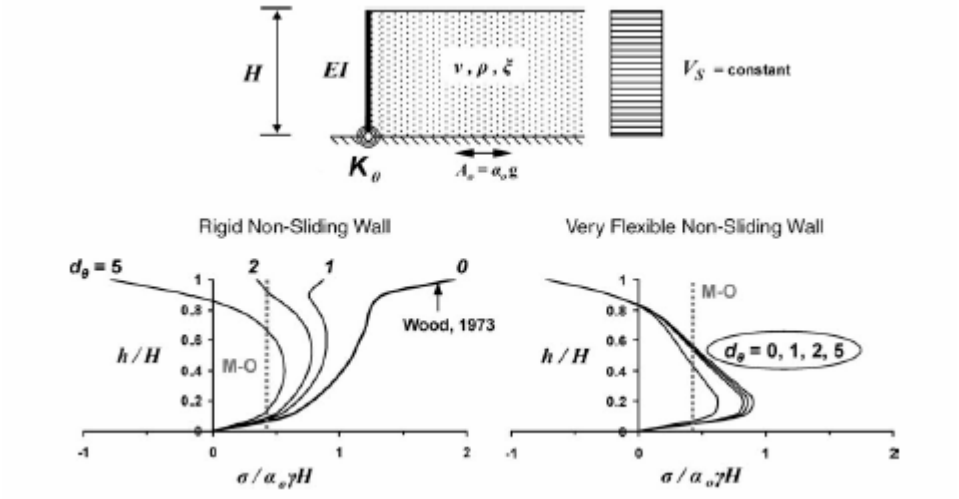

Figure 2.18 Elastic dynamic earth-pressure distribution of a pseudo-statically excited one-layer system for a non-sliding wall (after Gazetas et al., 2004)

Gazetas, compared results of a numerical analysis of a reinforced soil zone with centrifuge experiment results of Koseki (2002) in a quantitative manner. A visual

comparison of the soil wedge at failure from finite element analysis and the centrifuge experiments is shown in Figure 2.19.

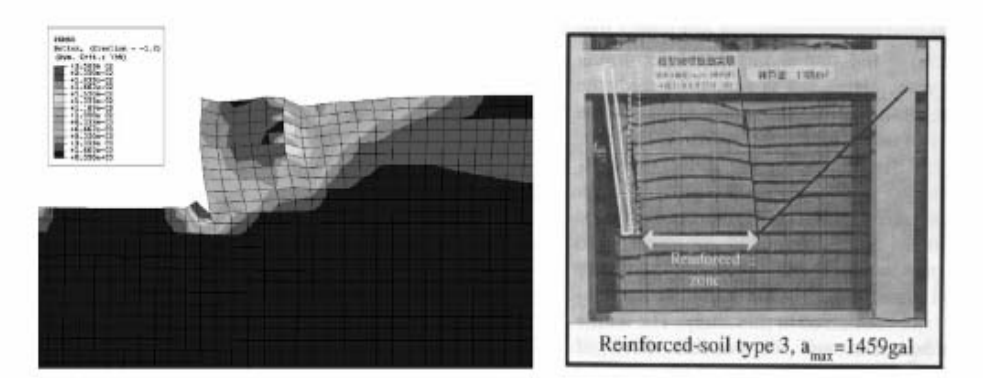

Figure 2.19 A quantitative comparison of finite element analysis Of Gazetas (2004) and centrifuge experiments for plastic deformation magnitude. (Experiment by Koseki, 2002)

As can be observed from the figure, the soil tends to move as a block and with the failure mechanism developing behind the wall. According to their numerical analysis results, the dynamic wall pressures are small as long as the soil behavior remains in the linear range, but when the soil wedge behind the wall occurs, or in other words, when failure mechanism activates, significant dynamic wall pressures occur.

In 2003, Veletsos and Younan developed their previous study on cantilever retaining walls. They performed comprehensive numerical solutions for their parametric study. Different from their previous study, they observed walls with a top support, and they also include the characteristics of the input motions in their parametric studies. The response quantities they examined include the displacements of the wall relative to its base, the dynamic wall pressures, and the total wall force, base shear and base moment.

Psarrapoulos et al. (2004) conducted finite element analyses to verify the elastic solutions of Veletsos and Younan. They developed a more general finite-element method of solution, and the results are in agreement with the available analytical results for the distribution of the dynamic earth pressures on rigid and flexible walls. They also observed parametric effects such as flexural wall rigidity and the rocking base compliance. They modeled the soil both as a homogeneous and inhomogeneous media.

In the first part of their numerical analyses, they examined single layer backfill retaining wall systems with the wall having different flexural rigidities and rotational base constraints by assuming soil as homogeneous media, therefore constant shear wave velocity is considered through the soil, and in the second part of this study inhomogeneous soil properties are used by considering a variable shear wave velocity.

In the third part of the study, two layer soil systems with a rigid gravity retaining wall are modeled. In this part, homogeneous soil properties are assumed for the both of the layers. The systems examined in this study are shown in Figure 2.20.

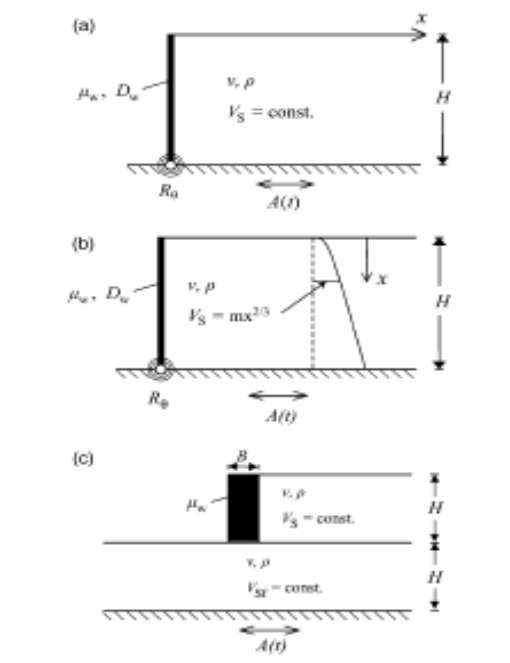

Figure 2.20 (a) flexible wall retaining a homogeneous soil layer, (b)flexible wall retaining inhomogeneous soil layer and (c) rigid gravity wall in a two-layer soil system (after Psarrapaulos,2005)

In their analyses, they used ABAQUS general finite element package by presuming plane strain conditions, In their trial analyses, they observed that wall height is an important factor in dynamic earth pressures, Taking that into account they performed analyses by considering a 8m-high wall. In discretisation of the model soil, four-noded quadrilateral plane strain elements are used. Since finite element mesh cannot be extended infinitely, they assume absorbing boundary elements at the end lines of the geometry. The base of the model remains fixed, no absorbing boundaries are used at this location.

The excitation are given as a base excitation of sinusoidal acceleration time history, it is prescribed to the nodes of the wall and soil-stratum bases. They used frequencies of maximum three times the natural frequency of the considered soil stratum.

In their analyses results, they observed that the soil pressure profiles in the dynamic case are highly dependent on the wall flexibilities and the rotational base constraints of the modeled walls. Dynamic earth pressures for different wall flexibilities are shown in Figure 2.21.

According to Psarrapoulos (2005), there are limitations in the use of elastic solutions in the literature and the analytical methods available; one main limitation is the assumption of complete bonding in the soil-wall interface. This causes unexpected behavior due to occurring tensile forces at this boundary.

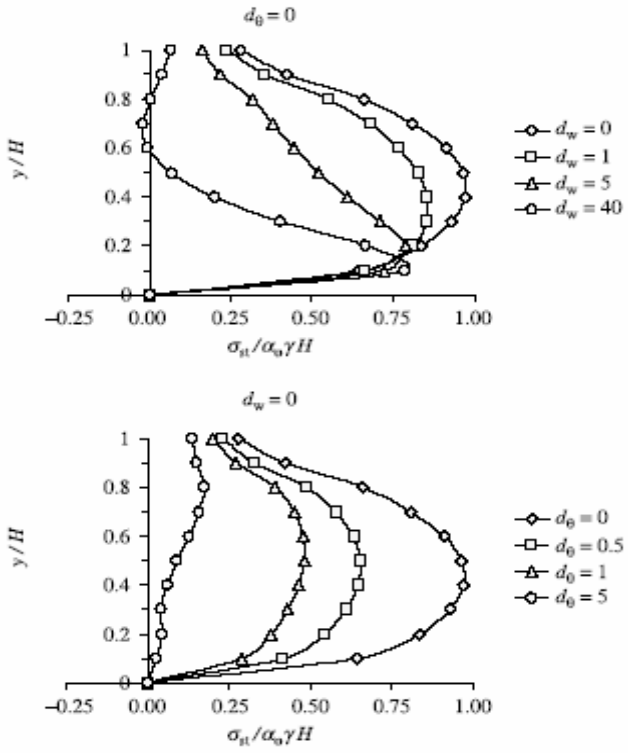

Figure 2.21 Earth pressure distributions for statically excited walls retaining soil, with different wall and base flexibilities (after Psarrapoulos, 2005)

CHAPTER 3

SOIL CONSTITUTIVE MODELING

3.1 Introduction

Typical behavior of the soils are highly non-linear in most of the progressive failure cases and use of elastic and elastic –perfectly plastic models are causing errors in these types of failure problems. For this reason, in this study nonlinear hardening soil model (Schanz et al. 1999) will be used. Details of the model are discussed in this chapter. For setting context, a review of plasticity is made beforehand.

3.2 Plasticity

Plasticity is a property of a material to undergo a non-reversible change of shape in response to an applied force. In Figure 3.1, a stress-strain curve of a metal behaving in a non-linear manner is shown. In this curve, after point A, nonlinear behavior begins and after the yielding point B, plastic deformations start to form in the material although the load is not applied. At point C, if the sample is unloaded, an elastic strain of DE is recovered but a plastic strain of OD remains in the sample.

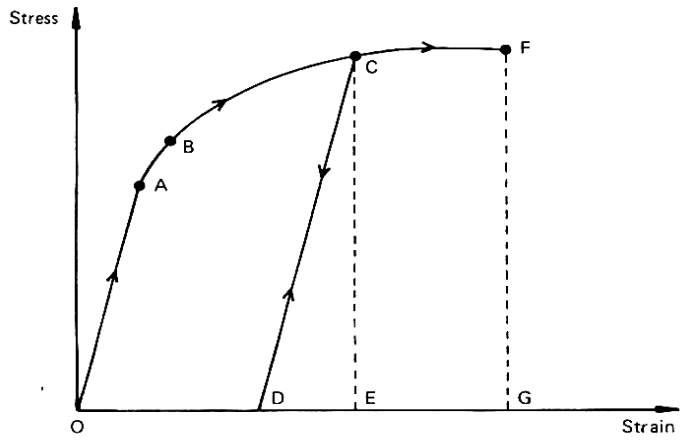

Figure 3.1 Typical non-linear stress-strain curve for metals (Britto and Gunn 1987)

To model the materials having plastic behavior, some idealizations have to be made. In such idealizations, the main features of the behavior are identified but aspects of secondary importance are ignored. The basic principle of elastoplasticity is that strains and strain rates are decomposed into an elastic part and a plastic part:

$$\underline{\varepsilon} = \underline{\varepsilon}^{e} + \underline{\varepsilon}^{p} \qquad (3.1)$$

Britto and Gunn (1987) summarized the generalized statements of the elasto-plastic model as below:

1- A yield function that generalizes the concept of yield stress for stress states.

2- A flow rule which specifies the relative magnitudes of the incremental plastic strains when the material is yielding.

3- A hardening rule which is the relationship between the amount of hardening and plastic strain when the material is yielding. Thus the hardening rule determines the changes in the yield surface.

4- A relationship between the directions of the principal plastic strain increments and the principal stresses.

3.2.1 Yield Function

For determining whether or not plasticity occurs at some stress condition, a yield function, f is introduced as a function of stress and strain. A yield function can often be presented as a surface in principal stress space. A perfectly-plastic model is a constitutive model with a fixed yield surface, i.e. a yield surface that is fully defined by model parameters and not affected by (plastic) straining. For stress states represented by points within the yield surface, the behavior is purely elastic and all strains are reversible.

All of the stress components must be considered for determining whether the material will behave elastic or plastic. But if an isotropic material is considered, then it is sufficient to consider only principal stresses (σ_a , σ_b and σ_c), and generally the yield functions are expressed in terms of them (Yıldız , 2003).

A yield function represents a surface in three-dimensional stress space. Generally yield function is written in such a way that, the negative value of the function for the current stress state indicates that the behavior is elastic (inside the yield surface). A zero value of the function indicates that yielding takes place and positive values are not allowed.

3.2.2 Hardening Rule

Changes in the size, shape and location of the yield surface during plastic loadings are determined by hardening rule. Three types of hardening rule are used to define the motion of the yield surface. These are, isotropic hardening, kinematic hardening and mixed hardening. Examples of hardening surfaces are shown in Figure 3.2. In isotropic hardening, yield surface expands uniformly. Different from this isotropic hardening, it moves as a rigid body in kinematic hardening. In mixed hardening, superposition of these two kinds of movements is available. For monotonic loadings, isotropic hardening rule is used to describe the behavior. But for cyclic and reversed type loadings, kinematic hardening is suitable (Chen and Mizuno 1990).

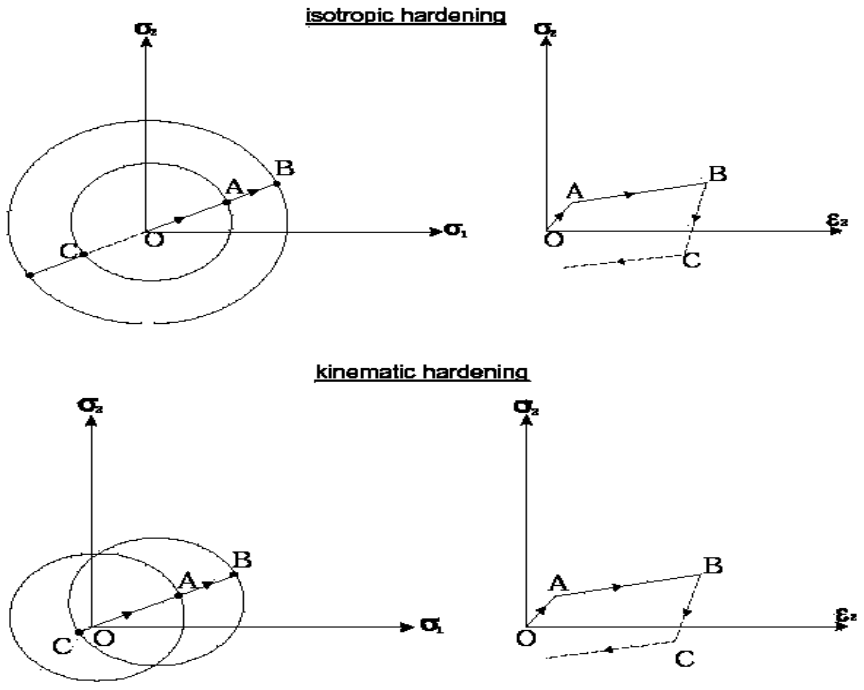

Figure 3.2 Isotropic and kinematic hardening (Britto and Gunn 1987)

3.2.3 Flow Rule

It defines the relative sizes of individual strain increments. For defining the ratios of plastic strain increments of the yielding material, flow rule is required. It can be defined as in the following expression:

$$\delta\varepsilon^{p} = \delta\lambda \frac{\partial g}{\partial \sigma} \qquad (3.2)$$

Where $\delta\varepsilon^{p}$ is the plastic strain increment, $\delta\lambda$ is the proportionality factor and g is the plastic potential function.

Similar to yield function, plastic potential function, $g(\sigma_a,\sigma_b,\sigma_c) = 0$ defines a surface in principal stress space. Individual plastic strain increment vectors are normal to this surface as can be observed in Figure 3.3.

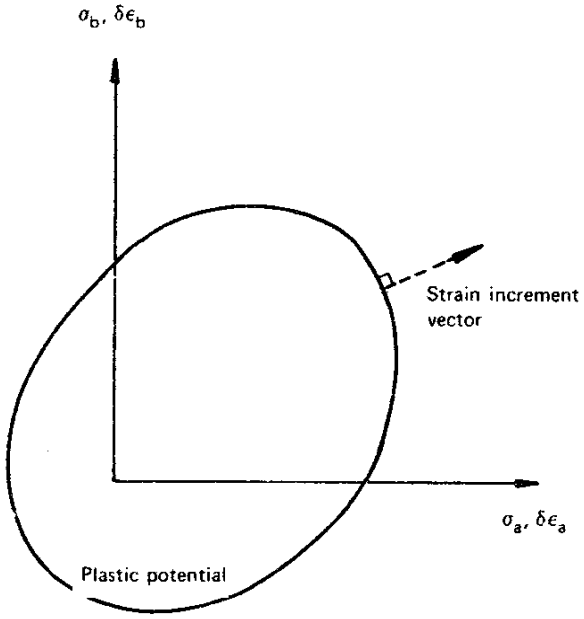

Figure 3.3 The plastic potential (Britto and Gunn 1987)

3.3 Duncan and Chang Hyperbolic Model

Stress-strain curves for both clays and sands are formulated by the following hyperbolic equation :

$$(\sigma_1 - \sigma_3) = \frac{\varepsilon}{\frac{1}{E_i} + \frac{\varepsilon}{(\sigma_1 - \sigma_3)_{ult}}} \qquad (3.3)$$

where σ_1 and σ_3 are the major and minor principal stresses respectively, ε is the major principal strain, E_i is the initial tangent modulus and $(\sigma_1-\sigma_3)_{ult}$ is the asymptotic value at infinite strain. In Figure 3.4 , this hyperbolic relation is shown .

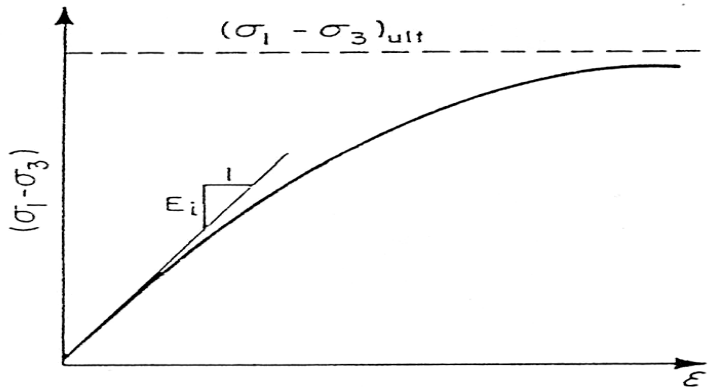

Figure 3.4 Hyperbolic representation of a stress-strain curve (Duncan et al. 1980)

According to Duncan and Chang (1970) , E_i should be dependent on the confining pressure, σ_3 , and vary according to the following relation:

$$E_i = K(\frac{\sigma_3}{P_a})^n P_a \qquad (3.4)$$

Where K represents the modulus number and n, the modulus exponent. P_a is the atmospheric pressure. They further suggested that:

$$(\sigma_1 - \sigma_3)_f = R_f(\sigma_1 - \sigma_3)_{ult} \qquad (3.5)$$

where $(\sigma_1-\sigma_3)_f$ is the principal stress difference at failure and R_f is the failure ratio. R_f changes from 0.5 to 0.9 for most soils.

The compressive strength can be calculated by Mohr-Coulomb criterion as:

$$(\sigma_1-\sigma_3)_f=\frac{2(c\cos\phi+\sigma_3\sin\phi)}{1-\sin\phi} \qquad (3.6)$$

where c is the cohesion intercept and ϕ is the internal angle of friction for the soil. The tangent modulus, E_t is calculated by differentiating Equation (3.3) with respect to ε and substituting Equations.(3.4), (3.5) and (3.6). The resulting expression is :

$$E_t=\left[1-\frac{R_f(1-\sin\phi)(\sigma_1-\sigma_3)}{2(c\cos(\phi)+\sigma_3\sin(\phi))}\right]^2 KP_a\left(\frac{\sigma_3}{P_a}\right) \qquad (3.7)$$

In the case of unloading and reloading, Duncan and Chang (1970) proposed the use of the unloading-reloading modulus, E_{ur} , for both cases. E_{ur} is expressed similarly to E_i as :

$$E_{ur}=K_{ur}P_a\left(\frac{\sigma_3}{P_a}\right)^n \qquad (3.8)$$

Where K_{ur} is the unloading-reloading modulus number. The modulus exponent, n, is assumed to be the same for both unloading-reloading and primary loading. Duncan and Chang (1970) assumed the second elastic constant, Poisson's ratio, to be constant. This assumption is modified by Duncan et al. (1980) by introducing a bulk modulus (B) for the soil. The bulk modulus is assumed to vary with the confining pressure. The variation of B with σ_3 is approximated similarly to variation of E_i with σ_3 as:

$$B=K_bP_a\left(\frac{\sigma_3}{P_a}\right)^m \qquad (3.9)$$

where K_b is the bulk modulus number and m is the bulk modulus exponent both of which are dimensionless.

Non-linear and stress dependent stress-strain characteristics of soils are defined by tangent values of Young's modulus (E_t) which vary with confining pressure and the percentage of the strength mobilized and values of bulk modulus (B) which vary with confining pressure and are independent of the percentage of the strength mobilized (Duncan et al. 1980).

3.4 Hardening Soil Model

The hardening soil model by Schanz et al. (1999) is an advanced model for simulating the stress-strain behavior of different types of soil by using theory of plasticity. This model is used to represent the stress-strain characteristics of the soil in the finite element analyses using PLAXIS version 8.2 in this study.

In this model, yield surface is not fixed in principal stress space but it can expand due to plastic hardening and distinction is made between two types of hardening: Shear hardening is used to model irreversible strains due to primary deviatoric loading. Compression hardening is used to model irreversible strains due to primary compression in oedometer loading and isotropic loading. Soil dilatancy and a yield cap are considered in the model.

3.4.1 Equations of the Model

Equations are formed by considering a hyperbolic relationship between the axial strain and the deviatoric stress. In the special case of a drained triaxial test, the relationship between the axial strain and the deviatoric stress can be approximated by a hyperbola that can be described by :

$$-\varepsilon_1 = \frac{q_a}{2E_{50}} \frac{(\sigma_1 - \sigma_3)}{q_a - (\sigma_1 - \sigma_3)} \qquad \text{For } q_a \le q_f \qquad (3.10)$$

The ultimate deviatoric stress, q_f, is obtained from the Mohr-Coulomb failure criterion as follows:

$$q_f = (c.\cot(\phi) - \sigma_3') \frac{2\sin(\phi)}{1-\sin(\phi)} \qquad (3.11)$$

where c and φ are the strength parameters of the soil. σ'_3 is assumed to be negative for compression. The asymptotic value, q_a , is defined as :

$$q_a = q_f / R_f \qquad (3.12)$$

where R_f is the failure ratio, which is always smaller than 1. R_f = 0.9 is often a suitable value to use for most soils. This hyperbolic relationship is shown in Figure 3.5.

The parameter E_{50} is the confining stress dependent stiffness modulus for primary loading. It is expressed as:

$$E_{50} = E_{50}^{ref} \left(\frac{c.\cot(\phi) - \sigma_3'}{c.\cot(\phi) + p^{ref}} \right)^m \qquad (3.13)$$

E_{50}^{ref} is the reference stiffness modulus corresponding to the reference stress (effective confining pressure) p^{ref}. It is determined from a triaxial stress-strain curve for the mobilization of 50 % of the maximum shear strength q_f as can be observed in Figure 3.5. The amount of stress dependency is given by the power m.

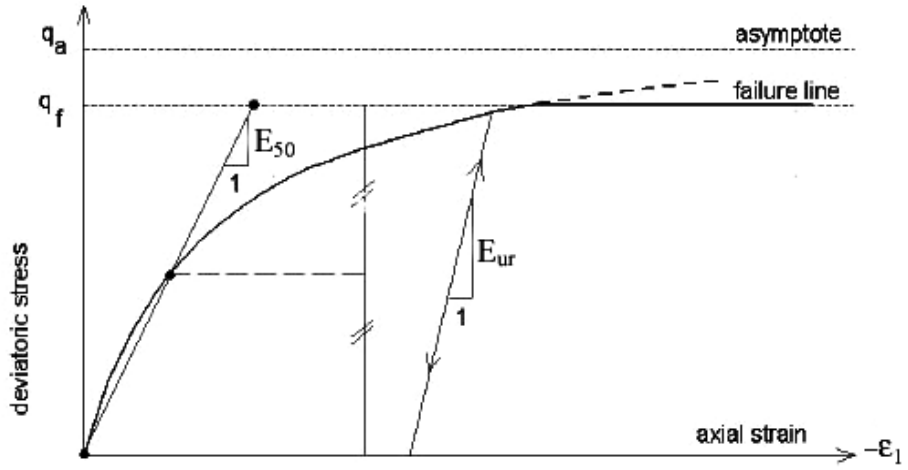

Figure 3.5 Hyperbolic stress strain relationship in primary loading for a standard drained triaxial test (Schanz et al. 1999)

For unloading and reloading, another stress-dependent stiffness modulus, E_{ur} is used and expressed as:

$$E_{ur} = E_{ur}^{ref} \left(\frac{c.\cot(\phi) - \sigma_3'}{c.\cot(\phi) + p^{ref}} \right)^m \qquad (3.14)$$

where E_{ur}^{ref} is the reference modulus for unloading and reloading corresponding to the reference pressure p^{ref}.

To simulate the oedometer loading or isotropic loading, the tangent stiffness modulus for oedometer loading, E_{oed} is used as:

$$E_{oed} = E_{oed}^{ref} \left(\frac{c.\cot(\phi) - \sigma_1'}{c.\cot(\phi) + p^{ref}} \right)^m \qquad (3.15)$$

where E_{oed}^{ref} is the tangent stiffness at a vertical stress of p^{ref} shown in Figure 3.6.

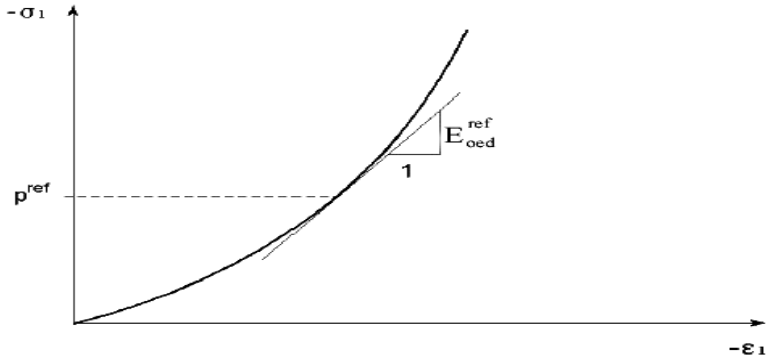

Figure 3.6 Definition of E_{oed}^{ref} in oedometer test results (Schanz et al. 1999)

3.4.2 Yield Surface, Failure Criterion and Hardening Rule

Considering the triaxial case, two yield functions f_{12} and f_{13} are defined as:

$$f_{12} = \frac{q_a}{E_{50}} \frac{(\sigma_1 - \sigma_2)}{q_a - (\sigma_1 - \sigma_2)} \frac{2(\sigma_1 - \sigma_2)}{E_{ur}} - \gamma^p$$
$$f_{13} = \frac{q_a}{E_{50}} \frac{(\sigma_1 - \sigma_3)}{q_a - (\sigma_1 - \sigma_3)} \frac{2(\sigma_1 - \sigma_3)}{E_{ur}} - \gamma^p \qquad (3.16)$$

with the definition of γ^p as :

$$\gamma^p = -(\varepsilon_1^p - \varepsilon_2^p - \varepsilon_3^p) = -(2\varepsilon_1^p - \varepsilon_v^p) \approx -2\varepsilon_1^p \qquad (3.17)$$

Here, the measure of plastic strain, γ^p, is used as the relevant parameter for frictional hardening. In reality, plastic volumetric strain ε_v^p will never be zero, but it is small compared to axial strain for hard soils, so it is neglected in the determination of γ^p.

3.4.3 Flow Rule, Plastic Potential Functions

We require some way of describing the mechanism of plastic deformation. This can conveniently be achieved just in the same way as for the perfectly plastic model using a plastic potential to indicate the ratio of the several strain components and to show that the plastic strains are controlled by the current stresses at yield.

3.4.4 Cap Yield Surface

A cap type of yield surface is required to formulate a model with independent inputs of E_{50} and E_{oed}. The triaxial modulus, E_{50} , largely controls the shear yield surface; and the oedometer modulus, E_{oed} , controls the cap yield surface. In fact, E_{50}^{ref} largely controls the magnitude of the plastic strains associated with the shear yield surface. Similarly, E_{oed}^{ref} controls the magnitude of plastic strains that originate from the yield cap.

The cap yield surface is considered as:

$$f^c = \frac{\tilde{q}^2}{\alpha^2} + p^2 - p_p{}^2 \qquad (3.18)$$

where α is an auxiliary model parameter related to K_o^{nc} as will be discussed later. It must be also reminded that $p = -(\sigma_1 + \sigma_2 + \sigma_3)/3$ and $\tilde{q} = \sigma_1 + (\delta - 1)\sigma_2 - \delta\sigma_3$ with $\delta = (3 + \sin(\phi))/(3 - \sin(\phi))$. $\tilde{q}$ is a special stress measure for deviatoric stresses. The magnitude of the yield cap is determined by the isotropic pre-consolidation stress p_p. We have a hardening law relating p_p to volumetric cap strain ε_v^{pc} as:

$$\varepsilon_v^{pc} = \frac{\beta}{m+1}\left(\frac{p_p}{p^{ref}}\right)^{m+1} \qquad (3.19)$$

The volumetric cap strain is the plastic volumetric strain in isotropic compression. α and β are cap parameters which are related to K_o^{nc} and E_{oed}^{ref} .

Yield surface is shown in Figure 3.7. Both the shear locus and the yield cap have the hexagonal shape of the classical Mohr-Coulomb failure criterion. In fact, the shear yield locus can expand up to the ultimate Mohr-Coulomb failure surface; the yield surface expands as a function of the pre-consolidation stress p_p. (Schanz et al. 1999)

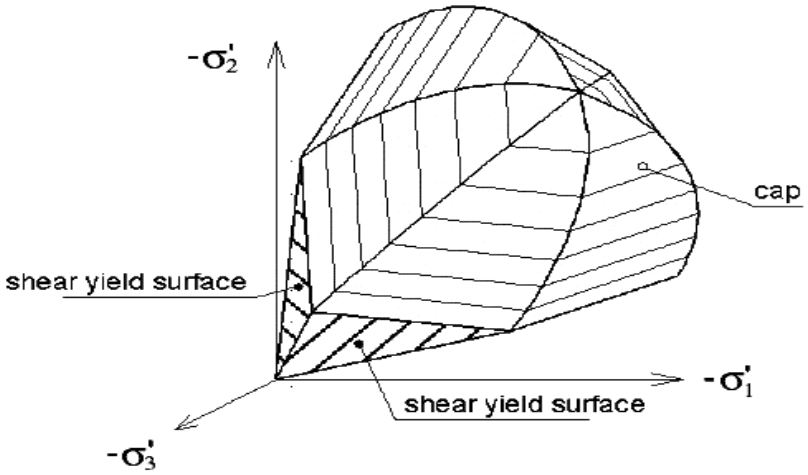

Figure 3.7 Representation of total yield contour in principal stress space for cohesionless soil (Schanz et al. 1999)

CHAPTER 4

DYNAMIC FINITE ELEMENT MODELING OF GEOTECHNICAL PROBLEMS

4.1 General

In this chapter, fundamental theory of dynamic finite element modeling and element types used to model the geotechnical system are briefly discussed.

4.2 Geotechnical Considerations

There are some features particular to geotechnical engineering that must be added to the general finite element theory before any real problems can be analyzed. The most significant difference between soil and other engineering materials is that it is composed of two separate phases, the soil skeleton and the fluid which fills the pores between the individual soil particles. This difference requires the finite element program to include the presence of the pore fluid in the equilibrium. However, in this study, it is assumed that all the geometry of the problem is above the water table which means no coupled conditions occur.

4.2.1 Element Types Required to Model Geotechnical Problems

For modeling the soil continuum, different kinds of element types can be utilized. In this study, 15-node triangular elements which are available as a default setting of Plaxis software are used for the plane strain conditions .

Structural components can also be modeled with different element types. Two different kinds of element types are frequently used to model the structural components in geotechnical problems. In this study structural components are modeled by a simplified two dimensional beam element that is conveniently formulated in terms of axial, bending and shear strains. Finite element formulation of a Mindlin beam which is used in Plaxis for modeling the structural elements will be explained in detail in the following parts.

Another type of special element used in geotechnical problems is a zero thickness interface element which allows the relative movement of two adjoining elements. One of the fundamental requirements of finite element analysis is that continuity is maintained between connected nodes. However, in practice discontinuities may develop within the ground. Examples of this are a tension crack forming behind a retaining wall, at the top of a slope or behind a pile subjected to lateral loading. To overcome this problem without invalidating the continuity requirement, zero thickness elements have been developed that can open up when their tensile strength is exceeded (Plaxis 8.2 User's Manual ,2002). User predicts where a discontinuity may occur and place interface elements at that location. The material properties assigned to these interface elements also cause complications. Due to the nature of their formulation, the material properties have different units to the surrounding solid elements. This causes difficulties because the interface elements are trying to replicate the deformational behavior of the surrounding soil and therefore some investigation is required before choosing the shear stiffness and normal stiffness of the interface elements. A detailed information on the formulation for interface elements and their implementation and performance can be found in Day (1990) and Potts and Zdravković (1999), (2001).

4.3 Brief summary of element types used in Plaxis

Two kind of triangular elements are present in PLAXIS for the plane strain conditions which are 6-node and 15-node elements. 15-node triangular elements are used in this study for a more accurate calculation of the stresses. The 15-node triangular element consists of 15 nodes as shown in Figure 4.1. The displacements are calculated at these nodes. In contrast to displacements, stresses are calculated at individual stress points rather than at the nodes. The 15-node element has 12 stress points as shown in Figure 4.1. In Plaxis, 15 node element which is shown in Figure 4.1, provides a fourth order interpolation for displacements and the numerical integration involves twelve Gauss points(stress points). A 15-node element can be considered as a combination of four 6-node elements, since the total number of the nodes and stress points are equal. But these elements are more powerful than 6-node elements of Plaxis The 15-node element is a very accurate element that has produced high quality stress results for difficult problems. But usage of these elements utilizes large amounts of memory and processing time.

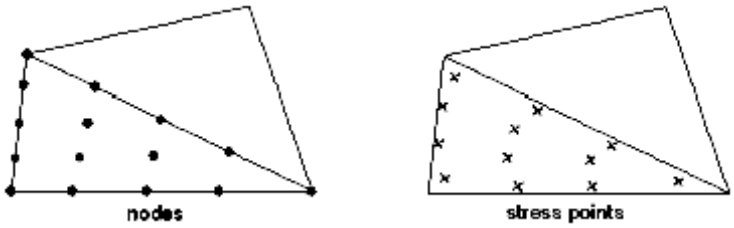

Figure 4.1 Nodes and stress points for 15-node triangular elements (Plaxis 8 Scientific Manual, 2002)

For triangular elements there are two local coordinate systems (i.e. ξ and η). An auxiliary coordinate system, ζ=1-ξ-η can also be used. For 15 node triangular elements, the shape functions can be written in the following form:

$$
\begin{aligned}
N_1 &= \zeta\,(4\zeta\text{-}1)\,(4\zeta\text{-}2)\,(4\zeta\text{-}3)\,/6 \\
N_2 &= \xi\,(4\xi\text{-}1)\,(4\xi\text{-}2)\,(4\xi\text{-}3)\,/6 \\
N_3 &= \eta\,(4\eta\text{-}1)\,(4\eta\text{-}2)\,(4\eta\text{-}3)\,/6 \\
N_4 &= 4\,\zeta\,\xi\,(4\zeta\text{-}1)\,(4\xi\text{-}1) \\
N_5 &= 4\,\xi\,\eta\,(4\xi\text{-}1)\,(4\eta\text{-}1) \\
N_6 &= 4\,\eta\,\zeta\,(4\eta\text{-}1)\,(4\zeta\text{-}1) \\
N_7 &= \xi\,\zeta\,(4\zeta\text{-}1)\,(4\zeta\text{-}2)\,*8/3 \\
N_8 &= \zeta\,\xi\,(4\xi\text{-}1)\,(4\xi\text{-}2)\,*8/3 \\
N_9 &= \eta\,\xi\,(4\xi\text{-}1)\,(4\xi\text{-}2)\,*8/3 \\
N_{10} &= \xi\,\eta\,(4\eta\text{-}1)\,(4\eta\text{-}2)\,*8/3 \\
N_{11} &= \zeta\,\eta\,(4\eta\text{-}1)\,(4\eta\text{-}2)\,*8/3 \\
N_{12} &= \eta\,\zeta\,(4\zeta\text{-}1)\,(4\zeta\text{-}2)\,*8/3 \\
N_{13} &= 32\,\eta\,\xi\,\zeta\,(4\zeta\text{-}1) \\
N_{14} &= 32\,\eta\,\xi\,\zeta\,(4\xi\text{-}1) \\
N_{15} &= 32\,\eta\,\xi\,\zeta\,(4\eta\text{-}1)
\end{aligned}
\qquad (4.1)
$$

Local numbering for these shape functions are shown in Figure 4.2.

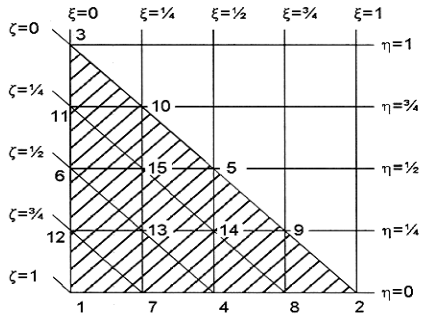

Figure 4.2 Local numbering and positioning of the nodes for 15-node triangular element (Plaxis 8 Scientific Manual,2002)

One can formulate the numerical integration over triangular elements as:

$$\int\int F(\xi,\eta)d\xi d\eta = \sum_{i=1}^{K} F(\xi_i,\eta_i)w_i \qquad (4.2)$$

In Plaxis, Gaussian integration within the triangular elements is used. For 6-node elements the integration is based on 3 sample points, whereas for 15-node elements 12 sample points are used. In the following tables, integration points and their weights are given for 6-node and 15-node elements .

Table 4-1 3-point integration for 6-node elements

Point	ξ_i	η_i	ζ_i	w_i
1,2 & 3	1/6	1/6	2/3	1/3

Table 4-2 12-point integration for 15-node elements

Point	ξ_i	η_i	ζ_i	w_i
1,2 & 3	0.063089...	0.063089...	0.873821...	0.050845...
4.. 6	0.249286...	0.249286...	0.501426...	0.116786...
7..12	0.310352...	0.053145...	0.636502...	0.082851...

In order to calculate Cartesian strain components from displacements, derivatives need to be taken with respect to the global system of axes *(x,y,z)*.

$$\underline{\varepsilon} = \underline{\underline{B_i}}\,\underline{v_i} \tag{4.3}$$

where

$$\underline{\underline{B_i}} = \begin{pmatrix} \frac{\partial N_i}{\partial x} & 0 & 0 \\ 0 & \frac{\partial N_i}{\partial y} & 0 \\ 0 & 0 & \frac{\partial N_i}{\partial z} \\ \frac{\partial N_i}{\partial y} & \frac{\partial N_i}{\partial x} & 0 \\ 0 & \frac{\partial N_i}{\partial z} & \frac{\partial N_i}{\partial y} \\ \frac{\partial N_i}{\partial z} & 0 & \frac{\partial N_i}{\partial x} \end{pmatrix} \tag{4.4}$$

$$\left\{ \frac{\partial N_i}{\partial S} \frac{\partial N_i}{\partial T} \right\}^T = [J] \left\{ \frac{\partial N_i}{\partial x} \frac{\partial N_i}{\partial y} \right\}^T \tag{4.5}$$

Within the elements , derivatives are calculated with respect to the local coordinated system (ξ ,η ,ζ). By using the relationship given in Eq.(4.5) , a relationship is obtained between the global and local derivatives in the form of:

$$\begin{pmatrix} \frac{\partial N_i}{\partial x} \\ \frac{\partial N_i}{\partial y} \\ \frac{\partial N_i}{\partial z} \end{pmatrix} = J^{-1} \begin{pmatrix} \frac{\partial N_i}{\partial \xi} \\ \frac{\partial N_i}{\partial \eta} \\ \frac{\partial N_i}{\partial \zeta} \end{pmatrix} \tag{4.6}$$

The Cartesian strain components can now be calculated by summation of all the nodal contributions as shown in the following equation:

$$\begin{pmatrix} \varepsilon_{xx} \\ \varepsilon_{yy} \\ \varepsilon_{zz} \\ \gamma_{xy} \\ \gamma_{yz} \\ \gamma_{zx} \end{pmatrix} = \sum_i \underline{\underline{B_i}} \begin{bmatrix} v_{x,i} \\ v_{y,i} \\ v_{z,i} \end{bmatrix} \qquad (4.7)$$

For plane strain analyses, strain components in z-direction are zero by definition i.e. $\varepsilon_{zz} = \gamma_{yz} = \gamma_{zx} = 0$

In addition to plane strain soil elements, compatible plate elements are used to simulate the behavior of walls, plates and shells. Plates in the 2-D finite element model are composed of beam elements (line elements) with three degrees of freedom per node: Two translational degrees of freedom *(u_x,* u_v) and one rotational degrees of freedom (rotation in the x-y plane: *φ_z)*. When 6-node soil elements are employed then each beam element is defined by three nodes whereas 5-node beam elements are used together with the 15-node soil elements . These element types are shown in Figure 4.3. The beam elements are based on Mindlin's beam theory. This theory allows for beam deflections due to shearing as well as bending. In addition, the element can change length when an axial force is applied. Beam elements can become plastic if a prescribed maximum bending moment or maximum axial force is reached.

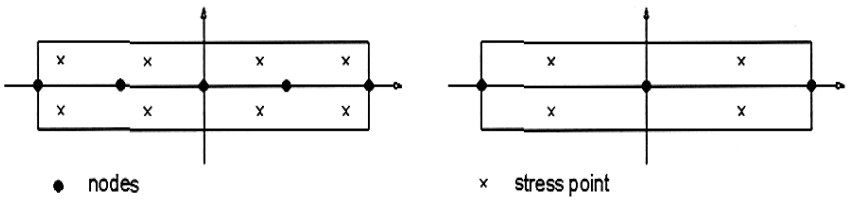

Figure 4.3 Nodes and stress points in 3-node and 5-node beam elements (Plaxis 8 Scientific Manual,2002)

For 3-node beam elements each node has three degrees of freedom, two displacements and one rotation, the overall deformational behavior of the element is assumed to be given by a product of a shape function and the values of the degrees of freedom at the nodes. In Figure 4.4 Shape functions for 3-node element which is compatible with 6 node triangle element are shown.

For 3 node elements where the nodes 1,2 and 3 are located at ξ=-1,0,1 respectively, the shape functions are given by:

$$
\begin{aligned}
N_1 &= -\frac{1}{2}(1-\xi)\xi \\
N_2 &= (1+\xi)(1-\xi) \\
N_3 &= \frac{1}{2}(1+\xi)\xi
\end{aligned}
\qquad (4.8)
$$

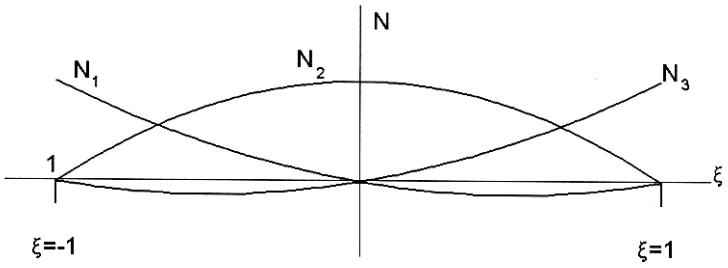

Figure 4.4 Shape functions for 3-node element (Plaxis 8 Scientific Manual,2002)

When using 15-noded triangles, there are 5 nodes at a side. For 5-node line-elements, where nodes 1 to 5 are at ξ=-1,-1/2,0,1/2,1 respectively, we have

$$
\begin{aligned}
N_1 &= -(1-\xi)(1-2\xi)\xi(-1-2\xi)/6 \\
N_2 &= 4(1-\xi)(1-2\xi)\xi(-1-2\xi)/3 \\
N_3 &= (1-\xi)(1-2\xi)(-1-2\xi)(-1-\xi) \\
N_4 &= 4(1-\xi)(-1-2\xi)(-1-\xi)/3 \\
N_5 &= (1-2\xi)(-1-2\xi)(-1-\xi)/6
\end{aligned}
\qquad (4.9)
$$

The graphical representation of the shape functions is shown in Figure 4.5. Element stiffness matrix is:

$$
[K_E] = \int_{-1}^{1} t[B]^T [D][B]|J|\,ds \qquad (4.10)
$$

where t is the element thickness and J is the determinant of the Jacobian matrix where

$$|J| = \left[\left(\frac{dx}{d\xi} \right)^2 + \left(\frac{dy}{d\xi} \right)^2 \right]^{1/2} \qquad (4.11)$$

And [B] is the matrix containing the derivatives of the shape functions.

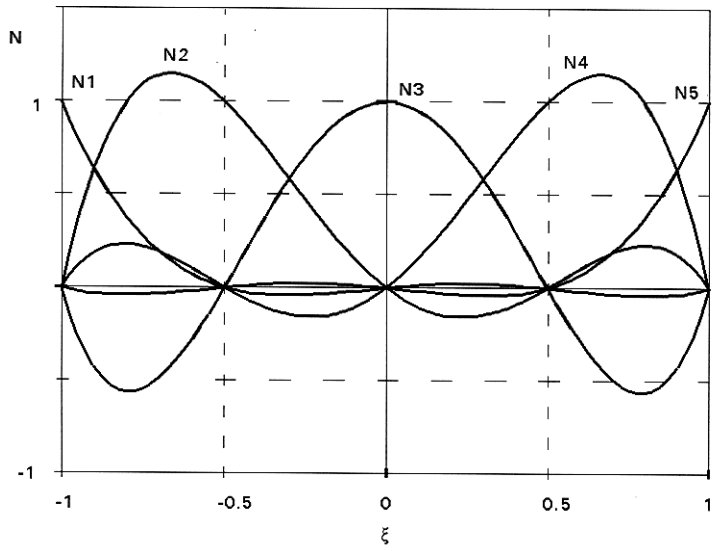

Figure 4.5 Shape functions for 5-node element (Plaxis 8 Scientific Manual,2002)

4.4 Interface Elements

In Plaxis each interface has a virtual thickness which is an imaginary dimension used to define the material properties of the interface. The higher the virtual thickness is, the more elastic deformations are generated. In general, interface elements are supposed to generate very little elastic deformations and therefore the virtual thickness should be small. On the other hand, if the virtual thickness is too small, numerical ill-conditioning may occur. The virtual thickness is calculated by multiplying virtual thickness factor by the average element size. The average element size is determined by the global coarseness setting for the mesh generation of Plaxis Input module. If interface elements are subjected to very large normal stresses, it may be required to reduce the virtual thickness factor.

A typical application of interfaces is to model the interaction between a sheet pile wall and the soil, which is intermediate between smooth and fully rough. The roughness of the interaction is modeled by choosing a suitable value for the strength reduction factor *(R_{inter})* which relates the interface strength (wall friction and adhesion) to the soil strength (friction angle and cohesion).

Interfaces are composed of interface elements. Figure 4.6 shows how interface elements are connected to soil elements. When using 15-node soil elements, the corresponding interface elements are defined by five pairs of nodes, whereas for 6-node soil elements the corresponding interface elements are defined by three pairs of nodes.

In the figure, the interface elements are shown to have a finite thickness, but in the finite element formulation the coordinates of each node pair are identical, which means that the element has a zero thickness.

The stiffness matrix for interface elements is obtained by means of Newton Cotes integration. The position of the Newton Cotes stress points coincides with the node pairs. Hence, five stress points are used for a 10-node interface element whereas three stress points are used for a 6-node interface element.

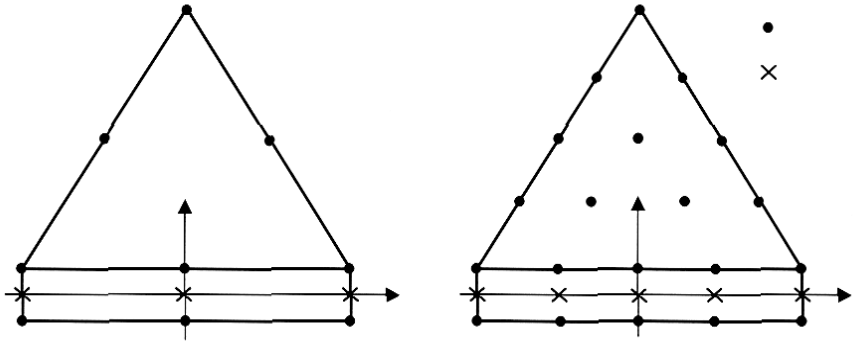

Figure 4.6 Distributions of nodes in interface elements and their connections with triangular elements (Plaxis 8 Scientific Manual, 2002)

In Plaxis software, an elastic-plastic model is used to describe the behavior of interfaces for the modeling of soil-structure interaction. The Coulomb criterion is used to distinguish between elastic behavior, where small displacements can occur within the interface, and plastic interface behavior when permanent slip may occur.

For the interface to remain elastic the shear stress τ is given by:

$$|\tau| \prec \sigma_n \tan\psi_i + c_i \qquad (4.12)$$

and for plastic behavior it is given by:

$$|\tau| = \sigma_n \tan\psi_i + c_i \qquad (4.13)$$

where ψ_i and c_i are the friction angle and cohesion (adhesion) of the interface.

The strength properties of interfaces are linked to the strength properties of a soil layer. Each data set has an associated strength reduction factor for interfaces *(R_{inter})*. The interface properties are calculated from the soil properties in the associated data set and the strength reduction factor by applying the following rules:

$$\begin{aligned} c_i &= R_{inter} c_{soil} \\ \tan\psi_i &= R_{inter} \tan\psi_{soil} \le \tan\psi_{soil} \end{aligned} \qquad (4.14)$$

When the interface is elastic then both slipping (relative movement parallel to the interface) and gapping or overlapping (i.e. relative displacements perpendicular to the interface) could be expected to occur.

The magnitudes of these displacements are:

$$\begin{aligned} \text{Elastic gap displacement} &= \frac{\sigma t_i}{E_{oed,i}} \\ \text{Elastic slip displacement} &= \frac{\tau t_i}{G_i} \end{aligned} \qquad (4.15)$$

where G, is the shear modulus of the interface, $E_{oed,i}$ is the one-dimensional compression modulus of the interface and t_i is the virtual thickness of the interface, generated during the creation of interfaces in the geometry model. The shear and compression moduli are related by the expressions:

$$\begin{aligned} E_{oed,i} &= 2G_i \frac{1-\upsilon_i}{1-2\upsilon_i} \\ G_i &= R_{inter}{}^2 G_{soil} \le G_{soil} \\ \upsilon_i &= 0.45 \end{aligned} \qquad (4.16)$$

4.5 Dynamic Finite Element Formulation

4.5.1 Fundamentals of Dynamic Equilibrium

In dynamic analyses we are concerned with variations of acceleration within the soil which leads to equivalent forces through the application of Newton's laws. For this purpose we must have the ability to write equations of motion in terms of time derivatives of nodal displacements. The mass of the total system must also be assigned to individual nodal degrees of freedoms to carry on the analyses.

The equation for the time-dependent movement of a volume under the influence of a (dynamic) load is:

$$M\ddot{u} + C\dot{u} + Ku = F \qquad (4.17)$$

Here, M is the mass matrix, u is the displacement vector, C is the damping matrix, K is the stiffness matrix and F is the load vector. The displacement, *u,* the velocity, $\acute{u}$, and the acceleration, ü, can vary with time. The last two terms in the equation *(K u = F)* correspond to the static deformation.

All models of static Plaxis can also be used in dynamic analyses. The soil behavior can be drained or undrained. Plaxis takes into account of mass of any material (soil, water or any kind of structure) as a lumped mass in matrix M.All the theory developed in the static finite element method remains unchanged except the addition of the inertial forces. According to Hardy (2003) ,the process begins with dividing the solution domain into finite element meshes. During this procedure, it must be given importance to select an element size which is small enough to solve the dynamic equilibrium equations before the vibration wave travels the whole element length during the selected time step. More detail in this limitation will be given in proceeding parts.

Following the process of dividing the solution domain into a finite element mesh, the dynamic formulation must begin by redefining the incremental potential energy of a single element. Using D'Alemberts principle, an incremental energy equation is obtained as:

Incremental potential energy (ΔE) = Incr. strain energy (ΔW)
+Incr. inertial energy (ΔI)
– Incr. work done by
applied loads (ΔL) (4.18)

According to Newton's second law, the force applied to a body is equal to the rate of change of momentum. This reduces to inertial force equals mass times acceleration if the bodies mass does not change. Therefore, using the principle of virtual work the incremental inertial energy is given by :

$$\Delta I = \int \{\Delta u\, \rho \{\Delta \ddot{u}\}\, dVol \qquad (4.19)$$

where ρ is the material density and $\{\Delta u\}$ and $\{\Delta \ddot{u}\}$ are the incremental displacements and accelerations respectively. In addition to this inertial force, it is also known that, when subjected to dynamic excitations, objects tend to dissipate energy. This is usually taken into account by introducing a damping force (ΔD) into the equilibrium equation as can be observed in Eq.(4.20).

Incremental potential energy (ΔE) =Incr. strain energy (ΔW)
+Incr. inertial energy (ΔI)
+Incr. damping energy (ΔD)
– Incr. work done by
applied loads (ΔL) (4.20)

If the damping force is assumed to be velocity dependent, and again using the principle of virtual work, the incremental damping energy is given by Eq.(4.21).

$$\Delta D = \int \{\Delta u\} \kappa \{\Delta \dot{u}\}\, dVol \qquad (4.21)$$

where $\{\Delta \dot{u}\}$ is the incremental velocity and κ is a constant representing the damping characteristics of the material. Representing a material's damping characteristics with a single parameter is a large oversimplification (Hardy,2003). The options developed to overcome this problem will be discussed in following sections. To formulate the finite element equations the displacements, velocities and accelerations must be approximated in terms of their nodal values. This is achieved according to Eq. (4.22) using the same shape functions which is also used in static analyses.

$$\begin{aligned} \{u\} &= [N]\{d\} \\ \{\dot{u}\} &= [N]\{\dot{d}\} \\ \{\ddot{u}\} &= [N]\{\ddot{d}\} \end{aligned} \qquad (4.22)$$

Where $d, \dot{d}$ and $\ddot{d}$ are nodal displacements, velocities and accelerations respectively. By using above equations, dynamic equation can be written as :

$$\sum_{i=1}^{N}[M_e]_i\left(\{\Delta\ddot{u}\}_n\right)_i+\sum_{i=1}^{N}[C_e]_i\left(\{\Delta\dot{u}\}_n\right)_i+\sum_{i=1}^{N}[K_e]_i\left(\{\Delta u\}_n\right)_i=\sum_{i=1}^{N}[\Delta R_e] \tag{4.23}$$

where

$$[M_e]=\int_{vol}[N]^T\rho[N]dvol$$

$$[C_e]=\int_{vol}[N]^T\kappa[N]dvol$$

$$[K_e]=\int_{vol}[B]^T[D][B]dvol$$

$$\{\Delta R_e\}=\int_{vol}[N]^T\{\Delta F\}dVol+\int_{surf}[N]^T\{\Delta T\}dSurf$$

The general formulation is applicable to any element with a matrix of shape functions [*N*]. Special care has to be taken when formulating the equilibrium equations for the elements specially derived to allow the analysis of geotechnical problems.

4.5.2 Formulation of element mass and damping matrices

In addition to the stiffness matrix [*K*], the mass matrix [*M*] and the damping matrix [*C*] must now be evaluated for each element. First consider the evaluation of the mass matrix using Eq. (4.24).

$$[M_e]=\int_{vol}[N]^T\rho[N]dvol \tag{4.24}$$

The matrix of shape functions [*N*] is given in terms of the natural coordinate system (*S* and *T*) and therefore to evaluate the mass matrix, the integral variables must be transformed from the global system (in terms of *x* and *y*) to the natural coordinate system. This is achieved by using the determinant of the Jacobian matrix, as shown in Eq. (4.25).

$$[M_e]=\int_{-1}^{+1}\int_{-1}^{+1}t[N]^T\rho[N]|J|dSdT \tag{4.25}$$

where t is the thickness of the element. The given integral can be evaluated by Newton-Cotes or Gauss integration technique.

As mentioned previously, experimental results led to the observation that energy is lost from a body as it vibrates. This so called damping originates from three different mechanisms (Ghanooni, 1994):

i. Hysteretic damping: This type of damping is independent of the frequency of vibration and is caused by frictional loss and the non-linearity of the stress strain relationship of the material.

ii. Radiation damping: For problems in the ground, energy is lost as the waves and hence the energy propagate into the surrounding soil.

iii. Viscous damping: Caused by the viscosity of the fluid flow within the pores of the soil matrix. The energy loss is proportional to the velocity and is also dependent on the frequency of the vibration.

Including all these features in a finite element analysis is extremely difficult. The problem of radiation damping cannot easily be dealt with. A non-linear elasto-plastic soil model should be sufficient to reproduce the energy loss due to hysteresis, whilst including the presence of the pore fluid in the equilibrium equations should model the energy loss due to viscous damping. If however, an elastic soil model is to be used to simplify the analysis and the presence of the pore fluid is not to be included, it may be necessary to add a damping matrix to approximate the energy loss from these two sources. A mentioned previously, modeling viscous and hysteretic damping with a single constant κ as indicated by Eq.(4.21) is a simplification of what is a complex phenomenon and in this way cannot model the frequency dependent nature of the energy loss. The most popular assumption made to improve the performance of the damping matrix is to use Rayleigh damping. This method assumes that the damping matrix [*C*] is made of a linear combination of the mass matrix [*M*] and the stiffness matrix [*K*], i.e.

$$[C] = \alpha_R [M] + \beta_R [K] \qquad (4.26)$$

During a non-linear analysis the stiffness matrix is constantly changing and therefore to overcome the problem, Rayleigh damping is not allowed to be prescribed for elements which have a non-linear constitutive model.

This assumption is considered to be more consistent as Rayleigh damping is generally introduced to model the energy loss through hysteretic damping which should be recreated by a non-linear soil model. Generally the performance of damping matrices is not adequate as they fail to capture the true frequency and amplitude dependent nature of energy loss that has been observed in practice.

To demonstrate the variation of the material damping ratio with frequency observed when Rayleigh damping is introduced into an analysis, the example given by Bathe (1996) will be repeated here. The level of damping ξ, for any frequency ω, is given by Eq.(4.27) in terms of the Rayleigh parameters α_R *and* β_R .

$$\xi_i = \frac{\alpha_R + \beta_i \omega_i}{2\omega_i} \qquad (4.27)$$

This relationship is illustrated in Figure 4.7 for the parameters *A*=0.01498 and *B*=0.01405.

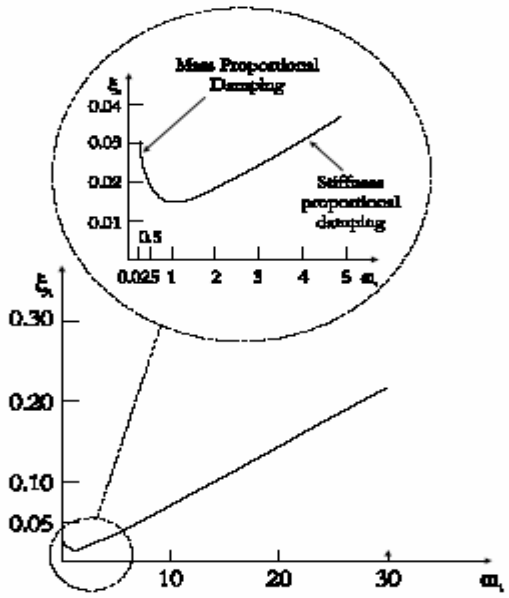

Figure 4.7 Damping as a function of frequency (after Bathe, 1996)

When using Rayleigh damping the level of damping cannot be related to strain level and is heavily dependant on the frequency of vibration. These two features illustrate the unsuitability of Rayleigh damping when trying to model the response of soils to dynamic loading. The ultimate goal is to model hysteric damping by using an appropriate cyclic soil model and to model the presence of the pore fluid to include the effects of viscous damping.

Selection of Rayleigh damping parameters requires an understanding of the effect of mass , stiffness and frequency of the input motion on them.
Generally when the contribution of matrix *M* is dominant (for example. α_R = 0.01 and β_R =0.001) more of the low frequency vibrations are damped. If the contribution of *K* is dominant (for example, α_R = 0.001 and β_R = 0.01) more of the high-frequency vibrations are assumed to be damped.

4.5.3 Time Integration Scheme

In the numerical implementation of dynamics, the formulation of the time integration constitutes an important factor for the stability and accuracy of the calculation process. Explicit and implicit integration are the two commonly used time integration schemes. The advantage of explicit integration is that it is relatively simple to formulate.However, the disadvantage is that the calculation process is not as robust and it imposes serious limitations on the time step. The implicit method is more complicated, but it produces a more reliable (more stable) calculation process and usually a more accurate solution according to Sluys (1992).

The implicit time integration scheme of Newmark is a frequently used method. With this method, the displacement and the velocity at the point in time $t+\Delta t$ are expressed respectively as:

$$\begin{aligned} u^{t+\Delta t} &= u^t + \dot{u}^t \Delta t + ((\frac{1}{2} - \alpha)\ddot{u}^t + \alpha \ddot{u}^{t+\Delta t})\Delta t^2 \\ \dot{u}^{t+\Delta t} &= \dot{u}^t + ((1-\beta)\ddot{u}^t + \beta \ddot{u}^{t+\Delta t})\Delta t \end{aligned} \qquad (4.28)$$

In the above equations, Δt is the time step. The coefficients α and β determine the accuracy of the numerical time integration. They are not equal to the α and β for the Rayleigh damping. In order to obtain a stable solution, the following condition must apply:

$$\beta \geq 0.5, \alpha \geq \frac{1}{4}\left(\frac{1}{2} + \beta\right) \qquad (4.29)$$

Equation set (4.28) can also be expressed as in following form:

$$\begin{aligned} \ddot{u}^{t+\Delta t} &= c_o \Delta u - c_2 \dot{u}^t - c_3 \ddot{u}^t \\ \dot{u}^{t+\Delta t} &= c_1 \Delta u - c_4 \dot{u}^t - c_5 \ddot{u}^t \\ u^{t+\Delta t} &= u^t + \Delta u \end{aligned} \qquad (4.30)$$

where the coefficients c_o .. c_7 can be expressed in the time step and in the integration parameters α and *β*. In this way, the displacement, the velocity and the acceleration at the end of the time step are expressed by those at the start of the time step and the displacement increment. With implicit time integration, Eq.(4.17) must be obtained at the end of a time step (t+Δt):

$$\underline{\underline{M}}\ddot{u}^{t+\Delta t} + \underline{\underline{C}}\dot{u}^{t+\Delta t} + \underline{\underline{K}}u^{t+\Delta t} = \underline{F}^{t+\Delta t} \qquad (4.31)$$

This equation, combined with the Eq.(4.30) for the displacements, velocities and accelerations at the end of the time step, produce:

$$(c_o\underline{\underline{M}} + c_1\underline{\underline{C}} + \underline{\underline{K}})\Delta u = \underline{F}_{ext}^{\ t+\Delta t} + \underline{\underline{M}}(c_2\dot{u}^t + c_3\ddot{u}^t) + \underline{\underline{C}}(c_4\dot{u}^t + c_5\ddot{u}^t) - \underline{F}_{\text{int}}^t \qquad (4.32)$$

In this form, the system of equations for a dynamic analysis reasonably matches that of a static analysis. The difference is that the stiffness matrix contains extra terms for mass and damping and that the right-hand term contains extra terms specifying the velocity and acceleration at the start of the time step (*Δt)*.

4.5.4 Critical Time Step

Despite the advantages of the implicit integration, the time step used in the calculation is subject to some limitations. If the time step is too large, the solution will display substantial deviations and the calculated response will be unreliable. For this reason, a time step criterion is defined in Plaxis. This critical time step depends on the maximum frequency and the coarseness of the finite element mesh. In general, the following expression can be used for a single element.

$$\Delta t_{critical} = \frac{B}{\alpha\sqrt{\frac{E(1-\nu)}{\rho(1+\upsilon)(1-2\nu)}}\sqrt{1+\frac{B^4}{4S^2}-\frac{B^2}{2S}\left[1+\frac{1-2\nu}{4}\frac{2S}{B^2}\right]}} \qquad (4.33)$$

The first root term represents the velocity of a (compression) wave. The factor α depends on the element type. For a 6-node element $\alpha = 1/(6\sqrt{c_6})$, with c_6= 5.1282, and for a 15-node element $\alpha = l/(19\sqrt{c_{l5}})$, with c_{15} = 4.9479. The other determining factors are the Poisson's ratio, v , the average length of an element B and the surface of the element *S.*

In a finite element model, the critical time step is equal to the minimum value of Δt according to Eq.(4.33) over all elements. This time step is chosen to ensure that a wave during a single step does not move a distance larger than the minimum dimension of an element.

4.6 Boundary Conditions

For most of the static geotechnical problems occurring in the earth there is no obvious location of where to place the outer boundaries of the finite element mesh. The choice of their location is often based on experience.

Due to the necessity of modeling the soil medium with finite number of elements, use of zero displacement boundaries are inevitable. But these kind of boundaries do not let waves to propagate, scattering waves reflect at these boundaries. In principle of dynamic analyses boundaries must be infinitely far away to prevent the reflection of waves propagating. However, locating the boundaries far away requires many extra elements and therefore a lot of extra memory and calculating time.

To counteract reflections, special measures are needed at the boundaries. In Plaxis, absorbent boundaries are used for this purpose. Various methods are used to create these boundaries, which include:

- Use of half -infinite elements (boundary elements).

- Adaptation of the material properties of elements at the boundary (low stiffness, high viscosity).
- Use of viscous boundaries (dampers).

In Plaxis for absorbent boundaries, a damper is used instead of applying fixities in a certain direction. The damper ensures that an increase in stress on the boundary is absorbed without rebounding. The boundary then starts to move for simulating free field motion . The use of absorbent boundaries in Plaxis is based on the method described by Lysmer and Kuhlmeyer , The normal and shear stress components absorbed by a damper in x-direction are:

$$\sigma_n = -c_1 \rho V_p \dot{u}_x \qquad (4.34)$$

$$\tau = -c_2 \rho V_s \dot{u}_y \qquad (4.35)$$

Here, ρ is the density of the materials. V_p and V_s are the pressure wave velocity and the shear wave velocity, c_1 and c_2 are relaxation coefficients that have been introduced in order to improve the effect of the absorption. According to Psarrapaulos et al (2005), the efficiency of viscous dashpots considered in the theory of the absorbent boundaries is quite acceptable.

CHAPTER 5

A COMPARISON OF PREVIOUS TEST RESULTS WITH FINITE ELEMENT METHOD SOLUTIONS

5.1 General

Objective of this chapter is to verify the results of finite element code used in the analyses. For this purpose, previous experimental studies are modeled by finite element approach. Experimental and numerical results are compared. Besides this, a one-dimensional ground response analysis is performed to check the results of Plaxis dynamic module.

5.2 A verification example: Comparison of Shake91 and Plaxis results

One dimensional ground response analyses for an 8 meters high sand column which is assumed to have constant shear modulus through the depth of the profile are carried by using Shake91 code (Schnabel et al, 1972). Base of the theoretical soil column is excited with a sinusoidal acceleration time history with duration of 4 seconds. Maximum amplitude and frequency of the acceleration is taken to be 0.1g and 3 Hz, respectively. Soil parameters used in the Shake91 analyses are shown in Table 5-1.

Table 5-1 Parameters used in Shake91 analyses

Parameter	Value
Average unit weight	18 kN/m^3
Young's modulus	40000 kPa
Poisson's Ratio	0.33
Damping ratio	5%
Height of the soil column	8 m.

In Plaxis, 8 meters deep, 100 meters wide sand deposit resting on rigid bedrock is modeled to obtain the ground response.

Finite element mesh is shown in Figure 5.1. Absorbent boundary concept is utilized for simulating wave radiation in an infinite medium.

Time step for the dynamic finite element analyses is selected as 0.02 which assures that the calculations of each step can be obtained without letting the waves propagate through the length of the single element. Soil is modeled with Mohr-Coulomb criterion, by taking the parameters shown in Table 5-2. Damping is defined in terms of Rayleigh α and β parameters. In Figure 5.2 , surface responses obtained by one dimensional wave propagation study and finite element modeling study are compared for time duration of 5 seconds. Results are similar for the two different analysis methods. Rayleigh α and β parameters are selected as 0.001 and 0.03 respectively for a better fit of the results.

Table 5-2 Parameters used in Plaxis analyses

Parameter	Value
Average unit weight	18 kN/m^3
Young's modulus	40000 kPa
Poisson's Ratio	0.33
Internal Friction Angle	35^0
Cohesion	0.1 kPa
Rayleigh α	0.001
Rayleigh β	0.03

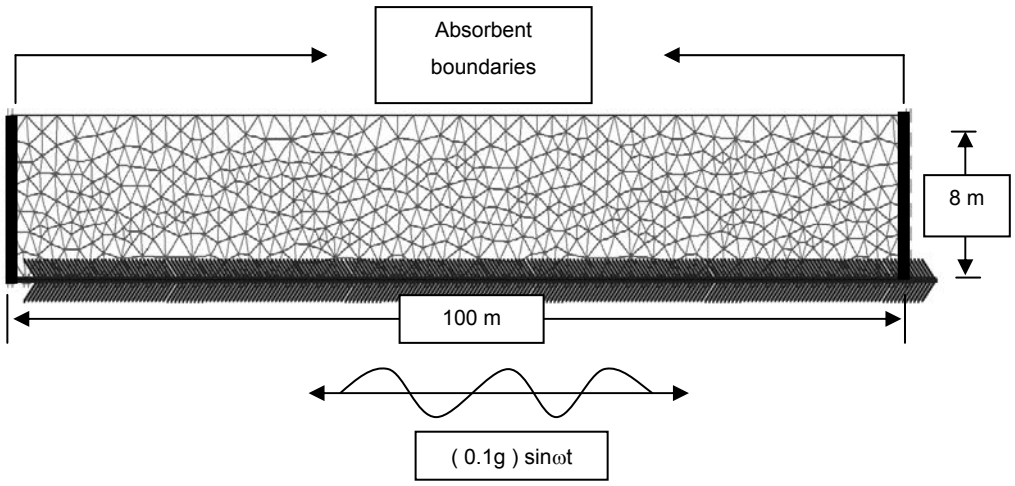

Figure 5.1 Finite element model used for ground response analysis

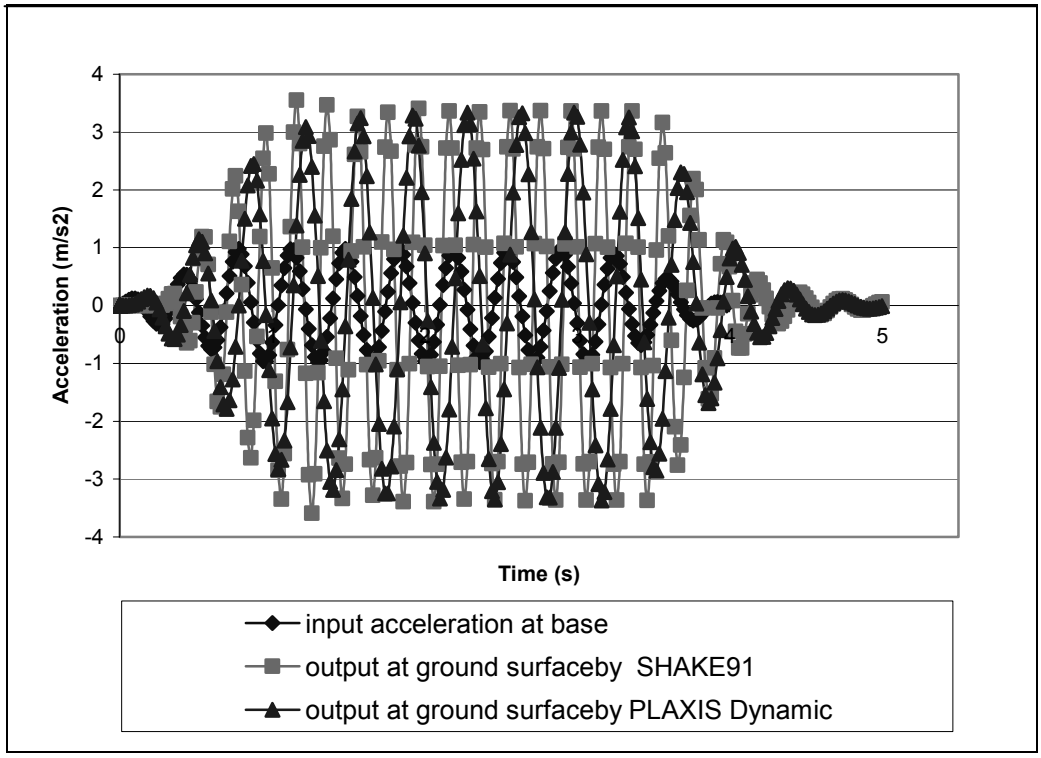

Figure 5.2 Comparison of Plaxis Amplification analyses by SHAKE91 results

5.3 Modeling of Previous Shake Table Studies by Dynamic Finite Element Method

Various experimental studies are performed to investigate the dynamic response of earth-retaining structures. These physical modeling studies can be divided into two groups: laboratory shake table tests and centrifuge tests. Shake table experiments are easier to conduct, but do not have the ability to account for the stress dependency of the soils in most cases. Still they are used for obtaining qualitative information on the behavior of retaining structures.

Laboratory shake table tests are used extensively to verify the Mononobe-Okabe theory. In these tests, small model walls are subjected to harmonic excitations of different frequencies. According to the results of the experiments, Mononobe-Okabe theory estimates total seismic thrust values reasonably well but it is not good at predicting dynamic pressure distributions. For this reason, application points of the seismic thrusts on the walls calculated by pseudo static approach may not be realistic.

Three recent 1-g shake table studies conducted at METU Civil Engineering Department for investigating the seismic behavior of retaining walls provide valuable data for further studies.Çalışan (1999) conducted an extensive experiment program for modeling various kinds of walls including gravity retaining walls and laterally braced (fixed walls). Following this study, Yunatçi (2003) examined the performance of laterally braced sheet pile walls. In this study, the effects of wall stiffnesses and base motion characteristics on the response of retaining structures are observed in a qualitative manner. In a more recent study, Çilingir (2005) performed a group of experiments to observe the surcharge effects.

A simulation of these tests by dynamic finite element method is performed in this part of the study. This is also considered to serve as a benchmark study for the following parametric analyses.

5.3.1 1-g Shake Table Model of a Gravity Retaining Wall

Çalışan (1999) carried out shake table tests for investigating the dynamic behavior of gravity type and horizontally braced rigid retaining walls. A soil box with dimensions of 200cm (length), 100 cm (height) ,100 cm (width) was used in the study.

The model wall was 70 cm high, 99 cm wide and 1 cm thick steel with a base width of 30 cm. The total weight of the wall was 89.15 kg. For increasing the total weight of the wall plates of extra weight had been located on top of the foundation part of the wall. For inducing friction between soil and wall base, emery paper was utilized. A schematic representation of the wall and the place of the transducers can be seen in Figure 5.3. During the tests sinusoidal harmonic motions were applied at the base of the soil box. Tests were repeated for various displacement amplitudes and frequencies of the base excitation motion and for different wall weights.

The soil used in the experiments was found to be sand with 3% fines and 4% gravel. The maximum and minimum dry densities of the soil sample were determined as 18.33 kN/m^3 and 14.99 kN/m^3 respectively. Average density of the backfill was about 16.9 kN/m^3 corresponding to a relative density of 61%.

During the tests, incremental seismic lateral earth pressures were measured by earth pressure cells attached to the model wall at three locations. The accelerations of the soil wedge behind the wall were registered by accelerometers placed at the earth pressure cell elevations within the soil wedge. The wall displacements were measured by the two displacement transducers located at the top and the bottom of the wall.

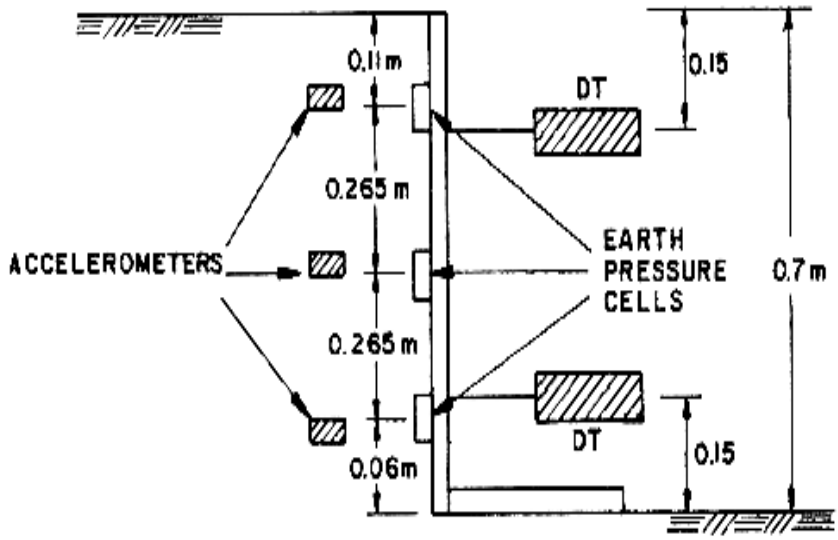

Figure 5.3 Schematic representation of the test setup (after Çalışan,1999)

5.3.2 Modeling the Test by Finite Element Method

By using Plaxis program, a two dimensional plane strain model of the test set-up is created with the same geometrical parameters.

Hardening soil model (Schanz, 1999) is used for representing soil behavior. Parameters used in hardening soil model are shown in following Table 5-3.

Secant stiffness modulus, E_{50} is calculated as 13340 kPa from triaxial test data obtained under cell pressure (σ_3) of 80 kPa. This value is converted to 14900 kPa (E_{50}^{ref}) for p_{ref}=100 kPa by using equation (3.13). To calculate this value, stress dependency coefficient, m, is taken as 0.5 which is suggested for most of the clean sands.

Table 5-3 Hardening Soil Parameters

Parameter	Value
E_{50}^{ref} (Secant Stiffness for p^{ref})	14900 kPa
p^{ref}	100 kPa
m (stress dependent stiffness parameter)	0,5 (for clean sands)
c	0,2 kPa
ϕ_{sand}	45^0
Ψ (calculated by using $\Psi=\phi_{sand}-30$)	15^0
E_{ur}^{ref} (unloading reloading stiffness) (Plaxis default: $E_{ur}^{ref}=3\ E_{50}^{ref}$)	44700 kPa
v_{ur} (Poisson's ratio for unloading/reloading)	0,2 kPa
R_f (failure ratio)	0,9

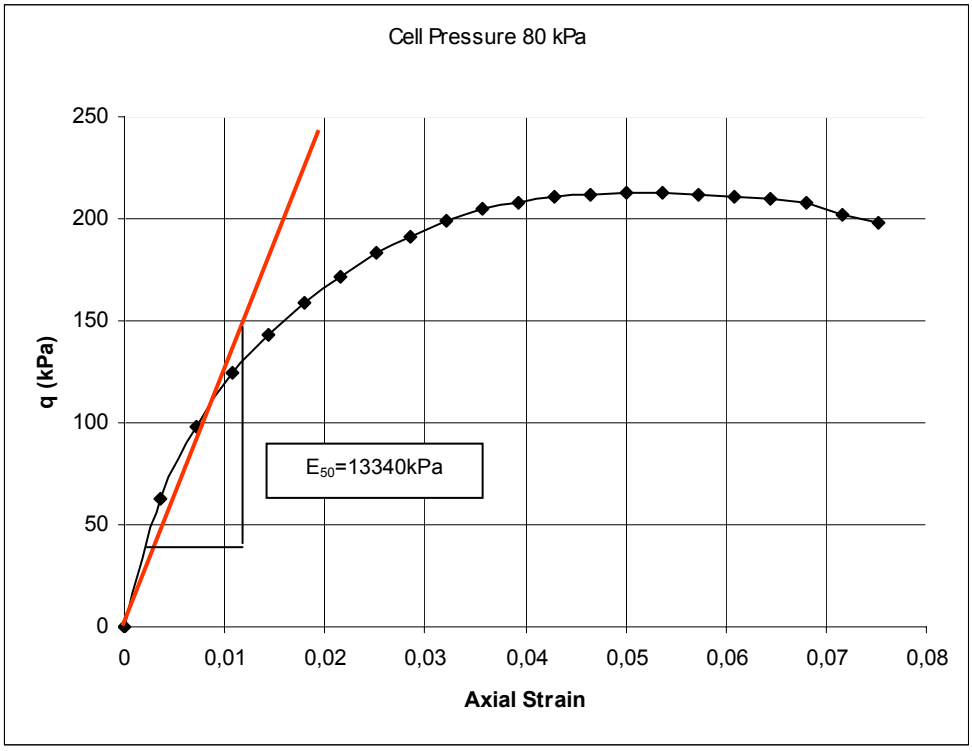

Figure 5.4 Calculation of E_{50} for triaxial test performed for σ_3=80 kPa

Internal friction angle of the cohesionless material is taken as 45 degrees. The order of dilatancy angle (ψ) for quartz sands is ϕ-30^0 (Plaxis v8.2 Reference Manual, page 3-45). By using this approximation, dilatancy angle is calculated as 15^0 . Average unit weight is taken as 16.9 kN/m^3. Finite element model used in the analyses is shown in Figure 5.5.

In the experiments, mass of wall model is 89.15 kg. Additional mass is provided by placing metal weights on the foundation of the wall. Total mass of the wall used in the experiments was reported to be 215.49kg. In FEM modeling, this extra weight is taken into account by increasing unit weight of the beam elements. The properties of the wall in finite element model are shown in Table 5-4.

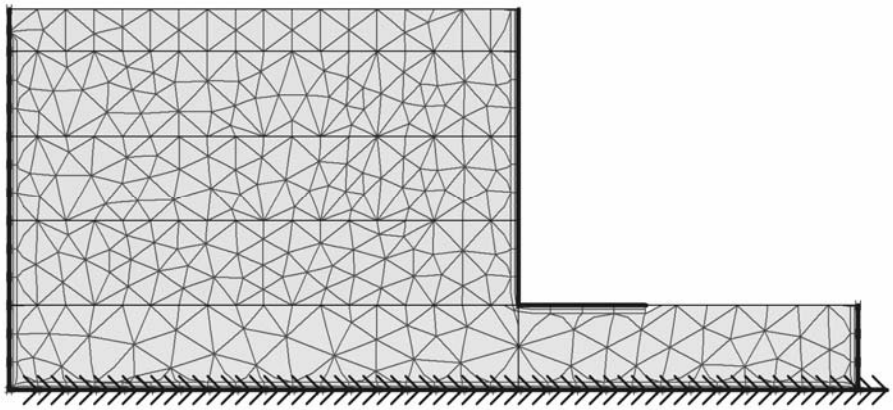

Figure 5.5 Finite element geometry used in the model

Absorbent boundary conditions are not used in finite element modeling of the experiment. Standard fixities are used together with prescribed dynamic displacements at lower boundary of the finite element model. Shaking bin is modeled by considering 2 cm thick steel plates. Interface elements are used between the soil elements and structural elements. Interface strength reduction factor, R_{inter} is taken as 0.75 . The details of these interface elements are given in chapter four.

Initial stresses are set up by applying the soil self weight in four plastic calculation steps. At first plastic calculation step, foundation soil, wall model and first 20 cm of the backfill is activated under gravitational loading. In second and third steps, 20 cm of backfill is activated and plastic loading analyses are performed. In last step, only 10 cm of the backfill is considered.

In each step , total multiplier associated with the staged construction process , ΣM_{stage} is taken as 1.0. In all the stages, prescribed conditions are successfully reached. Following these static analysis steps, the dynamic calculation phase is performed by applying harmonic base excitations. At the beginning of the dynamic calculation phase, displacements are reset to zero. Application of the harmonic loading is performed by defining dynamic prescribed displacements at the lower boundary of the model by using input module of Plaxis. In calculation module, dynamic loading is selected as calculation type and harmonic load multipliers are defined. Displacement amplitude is selected to be 2.2 mm. Frequencies are 3.03, 3.23, 3.75 and 4.6 Hz respectively. Total duration of the excitation is taken as 30 seconds. In the analyses, Plaxis changes its dynamic calculation sub-steps for satisfying the critical time step criterion which is mentioned in section 4.5.4. Stresses and displacements are calculated at those points corresponding to transducer locations.

Table 5-4 Parameters of beam elements

Parameter	Value
E (Young's Modulus)	190 GPa
Thickness of the beam element	0.01 m
EI	1583 KN.m^2/m
EA	1,900E+06 kN/m
γ (unit weight of the beam elements)	210,7 kN/m^3 (Modified for obtaining 215.5 kg total wall mass)

5.3.3 Comparison of FEM Results by Experimental Study of Çalışan (1999)

The experimental results recorded by Çalışan (1999) are compared with the numerical analyses results performed by Plaxis software. Lateral dynamic earth pressure profiles, peak thrust values, position of the application points of these forces, and the backfill accelerations are compared for the two groups of analyses. The set of input base excitation parameters used in a group of tests taken from Çalışan (1999) are reproduced in Table 5-5. Acceleration and pressure values registered by the transducers in the experiment are compared with the ones obtained at finite element nodes selected at transducer locations. In Table 5-6 and Table 5-7 , results obtained from experiments are shown. Following Table 5-8 and Table 5-9 gives numerical modeling results.

Table 5-5 Input motion parameters (after Çalışan, 1999)

Test Set	wall mass(kg)	properties of the input sinusoidal motion			
		displacement amplitude (mm)	frequency (Hz)	Maximum Velocity (m/s)	Maximum acceleration (*g)
3.1	215.49	2.2	3.03	0.04	0.08
3.2	215.49	2.2	3.23	0.05	0.09
3.3	215.49	2.2	3.75	0.05	0.13
3.4	215.49	2.2	4.6	0.06	0.19

Table 5-6 Dynamic pressures and incremental thrusts (after Çalışan, 1999)

Test Set	Measured Earth Pressures Corresponding to the Maximum Total Thrust (kPa)			Max. Horizontal seismic incremental thrust		
	top cell	middle cell	bottom cell	magnitude (kN)	seismic press. Coeff.	pt of app. (*H)
3.1	0.1	0.4	0.2	0.2	0.04	0.43
3.2	0.1	0.6	0.3	0.2	0.05	0.4
3.3	0.8	0.8	1.1	0.5	0.12	0.4
3.4	0.6	1.5	0.8	0.6	0.15	0.45

Table 5-7 Backfill accelerations and wall displacements (after Çalışan, 1999)

Test Set	Registered Maximum Accelerations (*g)			Maximum Displacements (mm)		Rotation (deg)
	top acc.	middle acc.	bottom acc.	TOP	BOTTOM	
3.1	0.18	0.11	0.11	0.6	0.1	0.08
3.2	0.23	0.17	0.16	0.5	0.1	0.05
3.3	0.43	0.27	0.25	5.9	0.5	0.77
3.4	0.87	0.68	0.49	10.2	1.0	1.33

Table 5-8 Dynamic pressures and incremental thrusts obtained by Plaxis

Finite element model of Test	Earth Pressures Corresponding to the Maximum Total Thrust (kPa)			Maximum Horizontal Seismic Incremental Thrust		
	top cell	middle cell	bottom cell	Magnitude (kN)	Seismic press. Coeff.	pt of app. (*H)
3.1	0.24	0,27	0.85	0.24	0.07	0.45
3.2	0.49	0,98	1,14	0.31	0.08	0.44
3.3	0,94	1,26	1,31	0.78	0.21	0.43
3.4	1,13	1,34	1,46	0.96	0.26	0.41

Table 5-9 Backfill accelerations and wall displacements obtained by Plaxis

Finite element model of Test	Maximum Accelerations (*g)			Maximum Displacements (mm)		Rotation (deg)
	top acc.	middle acc.	bottom acc.	TOP	BOTTOM	
3.1	0.092	0.088	0.087	0.109	0.047	0.05
3.2	0.101	0.100	0.098	1.76	0.14	0.09
3.3	0.147	0.143	0.140	7,95	1,63	0.21
3.4	0.238	0.231	0.225	14,71	4,69	0.56

In Figure 5.6 horizontal wall displacements recorded at the tests are compared with results of FEM analyses for various base excitation frequencies. Maximum horizontal displacements registered at the top LVDT are predicted quite similarly by finite element methodology. At lower LVDT elevation, higher displacements are obtained.

In Figure 5.7, maximum rotation angles of the wall base are compared with values obtained from numerical modeling study. In considered base acceleration amplitude range, FEM analyses predict smaller rotation angles when compared with the experimental results. Sliding of the wall base is more significant according to numerical analyses.

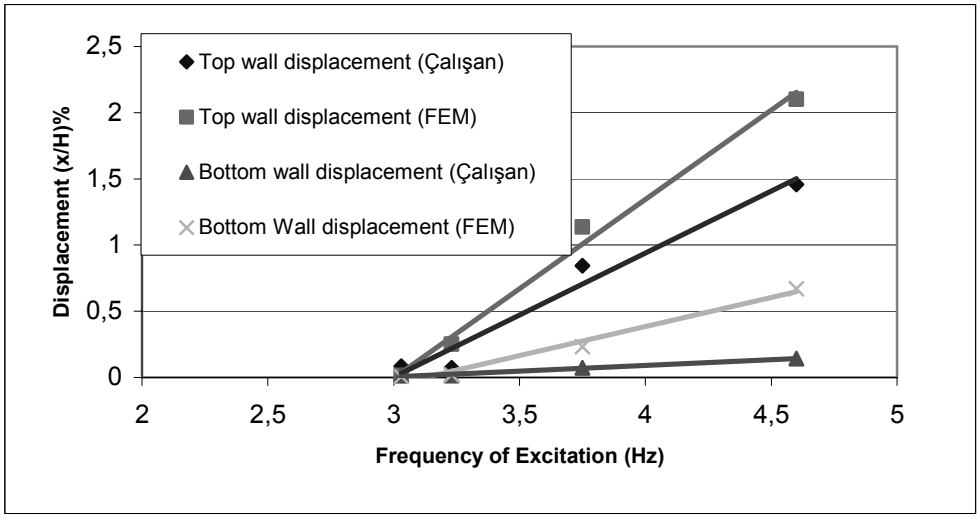

Figure 5.6 Comparison of experimental and numerical modeling results for wall displacement

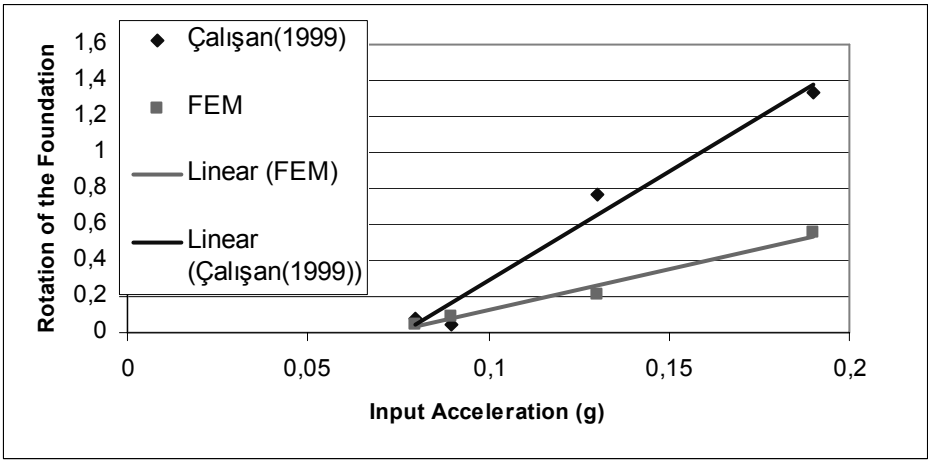

Figure 5.7 Comparison of angle of rotations of wall base for experimental and numerical modeling cases

In Figure 5.8, values of incremental seismic thrust obtained in Çalışan's study are plotted together with Plaxis results. In both studies, values of dynamic thrust increase with increasing excitation frequency values. A comparison is also made for the locations of the thrust application points in Figure 5.9.The ratios indicate heights of the thrust application points from the base of the wall to the total wall height.

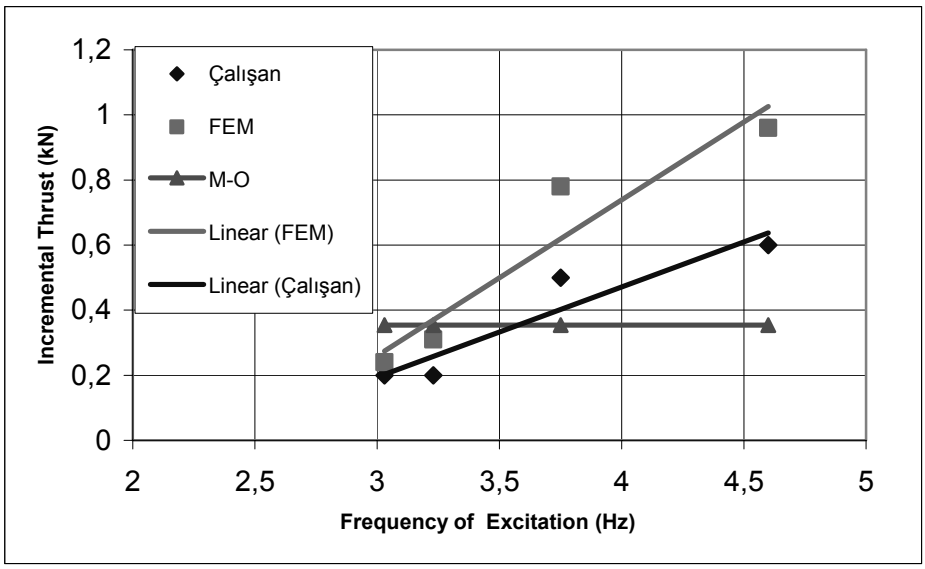

Figure 5.8 Comparison of experimental and numerical value of incremental dynamic thrust

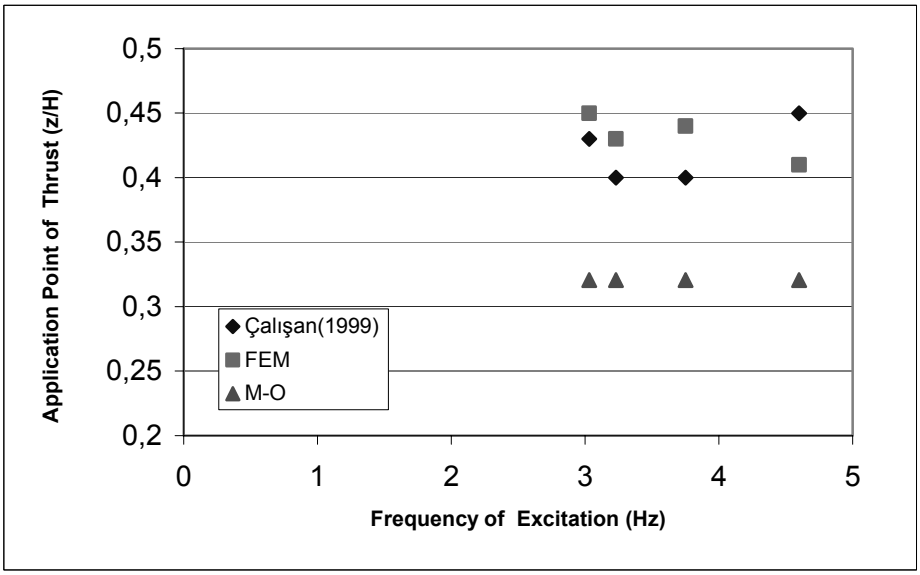

Figure 5.9 Point of application of dynamic thrust versus base excitation frequency
(z is the vertical distance from the base of the wall to the point of application)

Values of horizontal incremental seismic pressure coefficient, ΔK_{ae}*cosδ, are calculated by dividing the maximum seismic incremental thrust by 0.5*γ*$H^2$to compare with experimental values in Figure 5.10. Symbol, δ is the soil-wall friction angle in degrees.

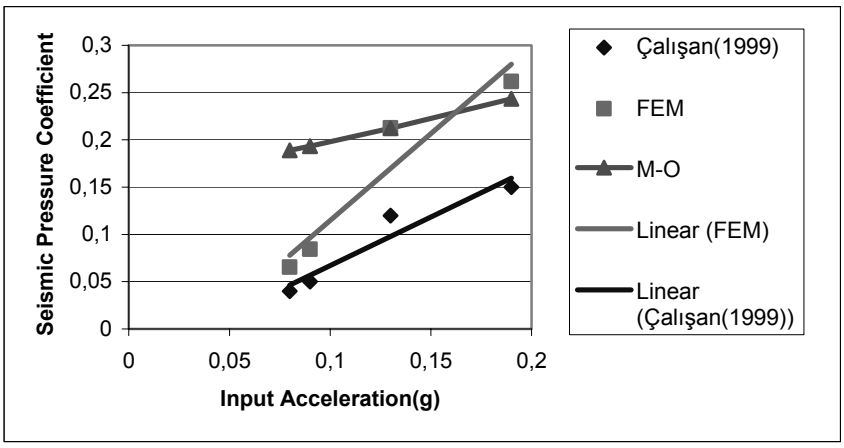

Figure 5.10 Comparison of seismic pressure coefficients for experimental and numerical modeling cases

5.3.4 Shake Table Test of a Laterally Braced Wall Model

A series of shaking table tests were conducted by Yunatçı (2003) for observing dynamic response of laterally braced sheet pile walls. Shaking box used in previous study was utilized in this experiment group. The model wall used was a 3 mm thick, single piece steel sheet with dimensions of 65 cm height and 99 cm width. The plate had a surface of smooth in texture and straight in geometry. A schematic representation of the model wall and instrumentation is given in Figure 5.11. Excitations defined in Table 5-10 were applied to the base of the model. Soil used throughout the study was air-dried sand (SP) with specific gravity,2.675. Initial average density of the sand was evaluated as 16.93 kN/m3. Angle of internal friction was determined as 45^0 by triaxial tests.

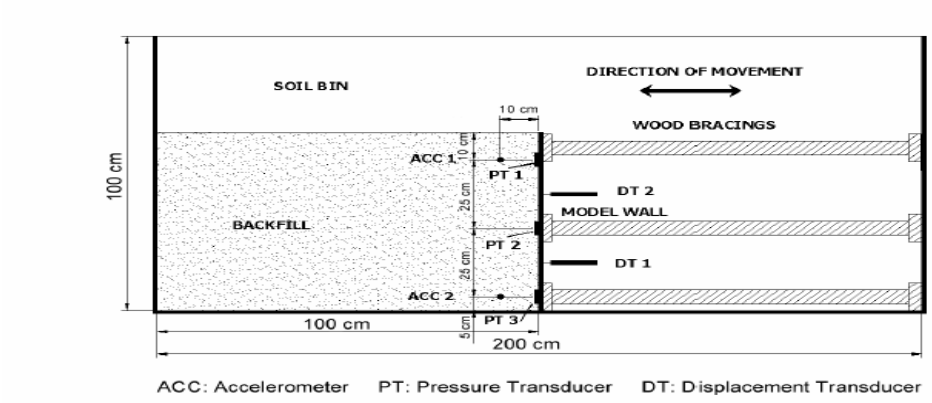

Figure 5.11 Schematic representation of test setup (after Yunatçı, 2003)

Three dynamic earth pressure cells were located on the wall at 10 cm below the surface of the backfill, at mid-depth and 5 cm above the base of the shaking box. Two accelerometers were placed in the backfill, one at the bottom and the other at the top. They were arranged to be at the same elevations with the pressure transducers. Two displacement transducers were placed on the wall for registering wall movements.

Table 5-10 Properties of a set of input motions in Yunatçı's study

Test Set	Test No.	Properties of the Input Motion		
		Initial Disp. (mm)	Frequency (Hz)	Acc. of the Box (*g)
3	Test 3-1	4.63	2.94	0.161
	Test 3-2		3.23	0.194
	Test 3-3		3.7	0.255
	Test 3-4		4.55	0.386

5.3.5 Finite Element Modeling of Experiment

Experiment setup shown in Figure 5.11 is modeled by a two dimensional plane strain model by using Plaxis code. Sand used in the experiments is modeled as a strain hardening material. Constitutive modeling parameters of sand are same with the ones used previously (See section 5.3.2).

Structural parameters of the model wall which is produced from 3mm thick steel sheet are calculated by taking Young's Modulus of steel as 190 GPa and unit weight as 87.5 KN/m^3. The wooden struts used for supporting the wall are idealized by utilizing the node to node anchor model of Plaxis which very well suits the modeled case. Anchors are modeled to be located at the positions of the struts. The geometry used in Plaxis modeling can be seen in Figure 5.12.

At the boundaries of the finite element model, standard fixities are used together with dynamic displacements prescribed for the dynamic excitation case. During input stage of the finite element modeling, dynamic prescribed boundary displacements are defined and activated at the beginning of the dynamic calculation step. Same displacement amplitudes and frequencies used in the experiments are utilized during dynamic analyses. Yunatçı (2003) performed the experiments for three different excitation amplitudes and four different frequencies. In this study, for comparison, only one set of these experiments (4.63 mm excitation amplitude with four different frequencies i.e. 2.94Hz, 3.23Hz, 3.70Hz, 4.55Hz) is modeled.

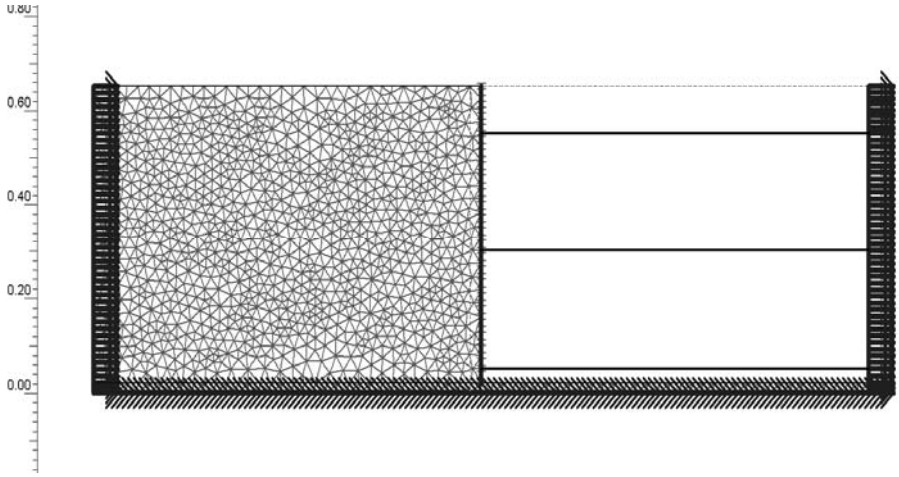

Figure 5.12 Geometry of the finite element model used in the analyses

5.3.6 Comparison of Physical Modeling and Finite Element Method Results

In Figure 5.13 , incremental thrusts at different excitation amplitudes are compared. Numerical study results are seen to be higher than experimental results for low acceleration amplitudes. For higher acceleration amplitudes, better accordance is observed with experimental results. Figure 5.14 indicates the point of application of the dynamic active thrust. According to Mononobe-Okabe predictions and experimental results, maximum dynamic thrust acts at a distance of approximately H/3 from the base. For acceleration amplitudes of 0.16g and 0.19g, results of finite element analyses indicate that dynamic thrust acts at approximately 0.5H from the base.

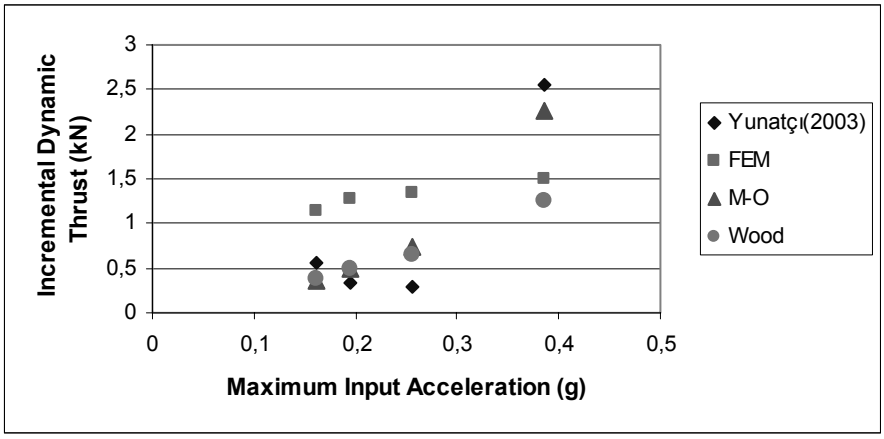

Figure 5.13 Comparison of incremental seismic thrust obtained by various methods

Laterally braced wall model used in the experiments make deflections in unbraced portions due to the high flexibility of the relatively thin metal sheets forming the wall. In Figure 5.15 and Figure 5.16 , residual horizontal displacements recorded by displacement transducers used in the experiments are compared with the values obtained from numerical solutions. In experimental cases, residual values are increasing for larger acceleration amplitudes. Same trend is obtained in numerical studies but magnitudes of displacements are underpredicted in FEM approach. Numerical modeling study predicts approximately 0.1 mm displacement at the location of upper transducer which records 0.3 mm maximum displacement during the experiment.

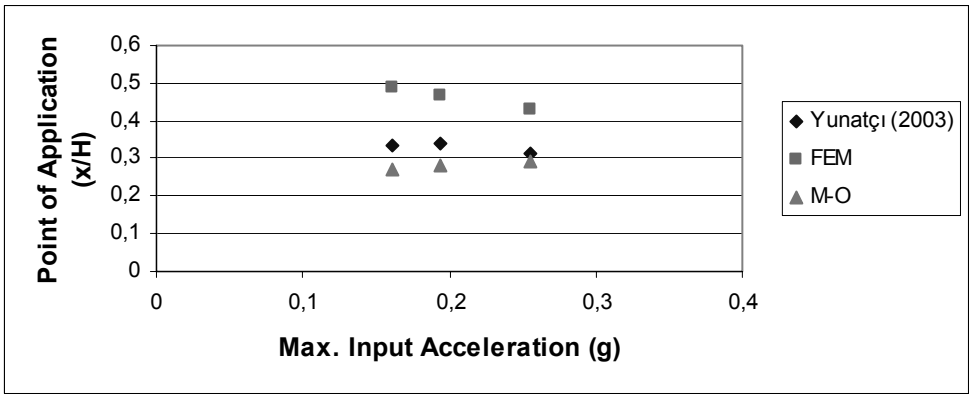

Figure 5.14 Points of application of dynamic thrust versus input acceleration amplitude

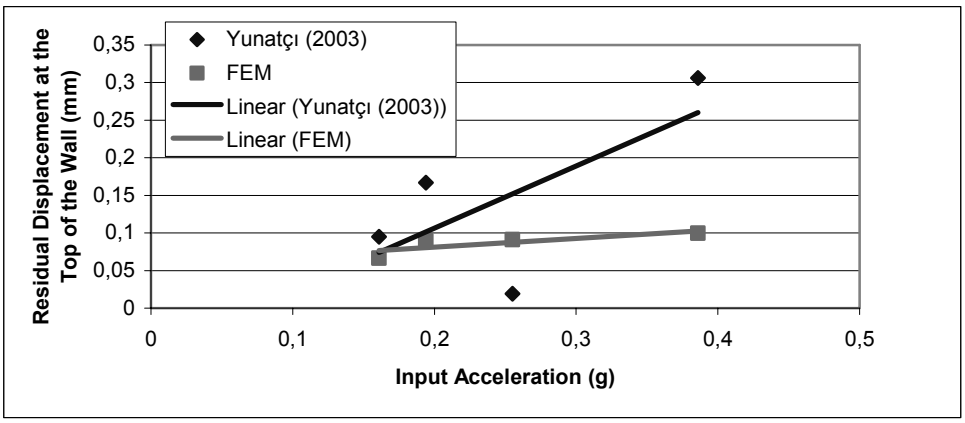

Figure 5.15 Residual wall displacements at the top of the wall versus input acceleration amplitude

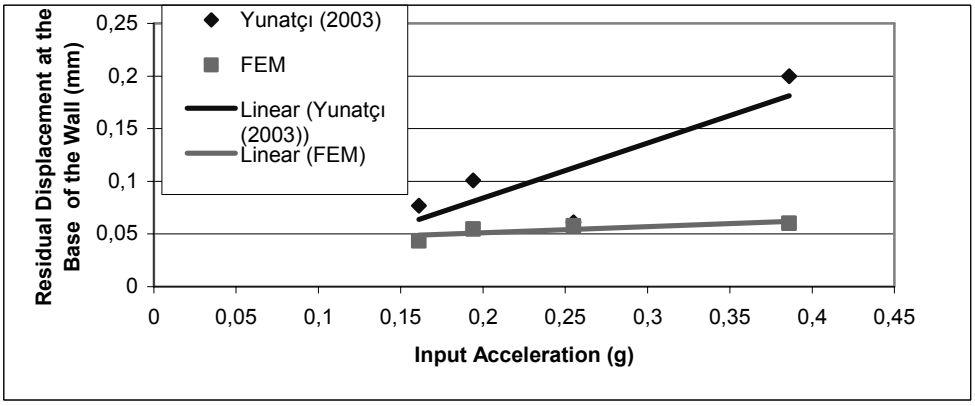

Figure 5.16 Comparison of residual wall displacements for the base of the wall

CHAPTER 6

PARAMETRIC STUDY

6.1 Introduction

In this chapter, the results of a parametric study performed by Plaxis dynamic finite element modeling software are presented. It is aimed to investigate the effects of base excitation characteristics (i.e acceleration amplitude and frequency), soil strength and wall flexibility on the dynamic response of concrete cantilever retaining walls. Important points related to the analyses are summarized in the following lines:

(a) Soil is modeled as a strain hardening material. Non-linear stress-strain behavior of the soils is represented by hardening soil model which is based on plasticity theory .

(b) Finite element code used in the analyses solves incremental dynamic equations of each time step by an implicit solver based on Newmark's Time Integration Scheme. In all of the analyses, time steps are selected in accordance with the critical time step criterion which is mentioned in section 4.5.4.

(c) Use of ordinary zero displacement boundaries utilized in the static geotechnical analyses is not adequate for dynamic problems. These kind of boundaries do not let waves propagate. Scattering waves reflect at these boundaries. For this reason, a modification must be made for preventing the reflection of the waves from boundaries. Otherwise, additional stresses are caused in soil medium and affect numerical solution. At boundaries of the considered finite element geometry, dashpot systems which have components in horizontal and vertical directions are used to absorb the radiated energy.

(d) In finite element modeling of contact problems, special element types are required for taking into account of the slipping and gapping between the different finite element media. In Plaxis, soil-wall interface is modeled by conditional interface elements which let slippage and gapping during interaction of the soil and the structural components. Detailed explanation of the interface elements used in Plaxis is given in section 4.4.

(e) Before the dynamic analysis phase, staged construction of the wall is modeled. Initial stresses are applied by gravity loading phase.

(f) Considered finite element systems are dynamically excited by base motions in terms of harmonic sinusoidal acceleration time histories.

Before the presentation of the results, several background issues including the geometry of the analyzed model, characteristics of the input motions, and natural frequency of the system are discussed to set the context for the interpretation of the results.

Results obtained from finite element analyses are compared with analytical solutions widely used in the design of the retaining structures. The comparisons are first made for some selected cases and then an assessment of the parametric effects is made.

6.2 Preliminaries

6.2.1 Finite Element Modeling of the Investigated Systems

Two dimensional finite element model is used throughout the study. According to the analytical studies performed by Veletsos and Younan (2000), dynamic wall pressures on the retaining systems are proportional with the height of the wall. In this study , a model wall of 8 m. height is analyzed. Thickness of the concrete wall stem is taken as 0.50 meters. However, walls stems with different thicknesses are also analyzed for studying the effect of wall flexibility on the dynamic response of retaining walls.

Analyses are performed for the backfill retained by a vertical, flexible wall. Figure 6.1 depicts the cross section of the problem. In the analyses, backfill length is taken as ten times the height of the wall. It is intended to use the rotational springs at wall base for simulating rocking motion of the foundation slab which is assumed to rest on a soil layer. According to this finite element model, foundation of the cantilever wall will not slide but rotate by the effect of inertial forces caused by the excitation of the wall and the backfill.

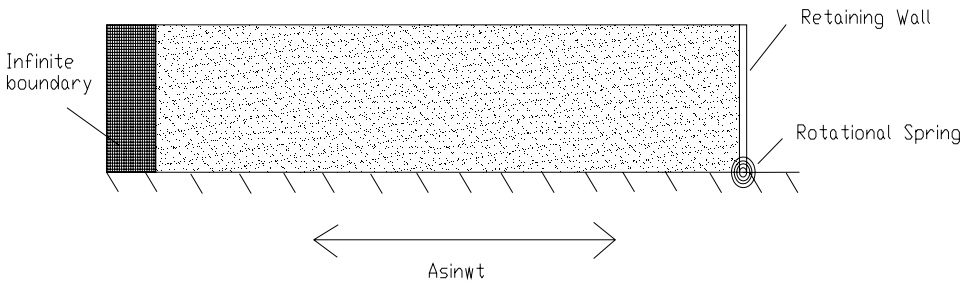

Figure 6.1 Geometry of the system

For determining the spring coefficients which will be used in the analyses, a relation proposed by Dobry and Gazetas (1986) for strip footings are used .The proposed formulation is:

$$R_{\theta} = \frac{\pi G_f B^2}{8(1-\upsilon_f)}\left(1+\frac{1}{10}\frac{B}{H_f}\right) \qquad (6.1)$$

In this formulation G_f is the shear modulus, H_f is the thickness, and v_f , Poisson's ratio for the underlying soil layer. B is the width of the foundation of the wall.

Rotational spring constant is calculated by assuming the width (B) of the foundation and underlain soil layer thickness (H_f) as 4 m. and 8 m. respectively for all the analyses. For a foundation slab width of 4 meters, resting on an 8 meters thick sand layer with $v_{f,}$,0.33 and G_f, 40000kPa, rotational spring coefficient is found to be 393800 kN.m/rad .

Discretisation of the soil medium is made by 15 noded triangular, plane strain elements. Absorbent boundaries are utilized to simulate the radiation of S and P waves outside the finite element mesh. The formulation of this boundary type is given in equations 4.34.The distance to the absorbent boundaries can be taken as ten times the height of the wall which was also suggested by Psarrapoulos et. al (2005).Discretisation of the wall is made by beam elements. Theory of the plate elements used in the study is summarized in section 4.3. A representative discretisation of the considered model is shown in Figure 6.2.

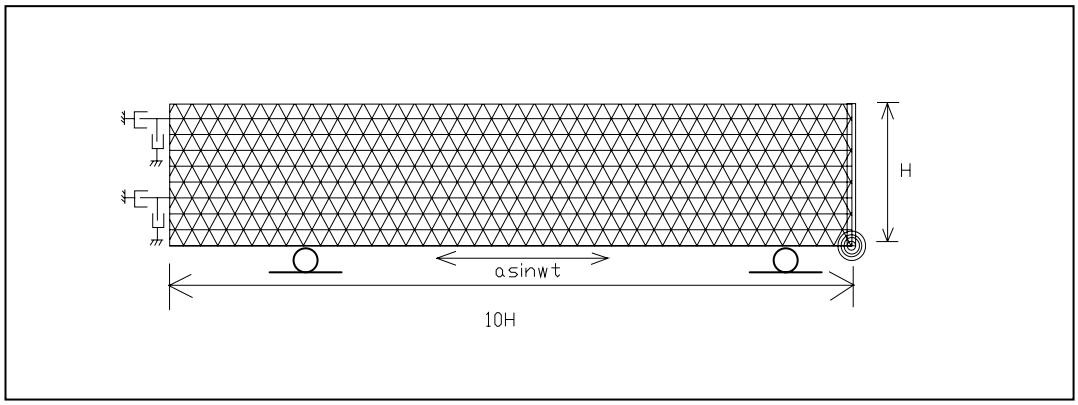

Figure 6.2 Finite element discretisation of the system

For modeling the interface between the wall and the soil, Plaxis has an elasto-plastic model which has the ability to distinguish between elastic behavior where small displacements can occur within the interface and plastic interface behavior when permanent slips may occur. When the interface used remains in the elastic range, then both slipping (relative movement parallel to the interface) and gapping or overlapping (relative displacements perpendicular to the interface) could be expected to occur. More detailed information on the interface elements used in Plaxis are given in section 4.4.

6.2.2 Constitutive Model Properties of the Considered Systems

Beam elements which are utilized to model the concrete structural components are set to behave linearly elastic. Wall parameters used in the studies are shown in Table 6-1.

Table 6-1 Material properties for the plate elements

Parameter	Value
Material	Concrete
Unit weight	22 kN/m^3
Young's Modulus (E)	230 Gpa
Poisson's Ratio (v)	0.2

Backfill is considered to behave as a non-linear material which obey the hardening soil model proposed by Schanz et al (1999). Soil model is explained in full detail in chapter three. Constitutive properties selected for the backfill are shown in Table 6-2.

Table 6-2 Constitutive material properties for the backfill

Parameter	Value
Unit weight of the backfill material	18 kN/ m^3
Poisson's Ratio (v) for backfill material	0.33
Young's Modulus (E_{50}) for backfill material	35000 kPa
Cohesion of the backfill material	0.1 kPa
Internal Friction Angle for the backfill material	30^0 in all groups (except the analyses where effect of friction angle of the backfill is under concern)
Dilatancy angle for the backfill	5^0
R_f (failure ratio)	0.9
m	0.5
Soil Wall friction angle	0.75φ

Interface elements which were used to model the contact interactions between the soil and structural elements obey the Mohr-Coulomb failure criterion as explained in section 5.4. Each interface data set has an strength reduction factor *(R_{inter})* , associated to the strength properties of the soil which it interacts . In this study an interface strength reduction of 0.70 is used.

6.2.3 Characteristics of the Base Excitations Applied to the Models

The excitation is applied as a prescribed harmonic acceleration time history at the base of the whole model. Acceleration amplitudes are calculated according to the following formula.

$$A(t)=\alpha\sin(\omega t) \qquad (6.2)$$

where α represent peak amplitude in g and ω represent circular frequency of the excitation(rad/s) . A sample acceleration time history is shown in Figure 6.3.

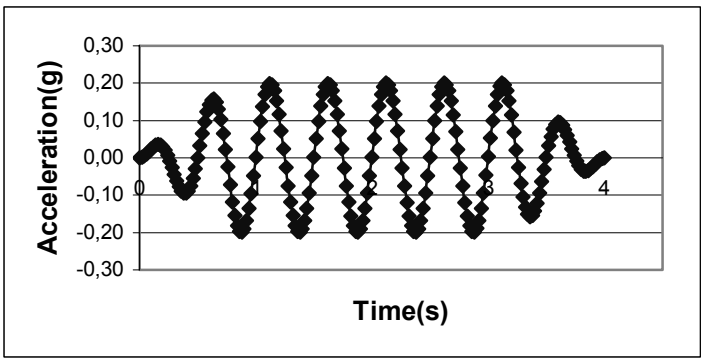

Figure 6.3 A sample prescribed acceleration-time history of 0.2g amplitude and 2Hz frequency

The natural frequency is calculated as 2.83 Hz for the considered system by using the formula $4H/V_s$ where H represents the thickness of the soil layer and V_s is the shear wave velocity of the backfill. H is taken as 8 meters and V_s is taken as 90 m/s. In the studies, special care is given to the case where excitation frequency coincides with natural frequency of the system.

6.2.4 Variable Parameters of the Study

As explained in the aim of the study, the effect of a group of parameters on the dynamic response of cantilever retaining walls are being investigated. These parameters are summarized in Table 6-3.

Table 6-3 Variable parameters of the study

Parameters Investigated	Range
Input base excitation amplitude	0.05g – 0.30g
Input base excitation frequency	2.0 Hz – 10 Hz
Wall flexibility	0.0006 m^2/kN - 0.033 m^2/kN
Internal friction angle	25^0-40^0

Flexibility parameter is defined as H^4/EI where E is the Young's Modulus of the wall material, H , wall stem height (m) and I , wall's moment of inertia .In the analyses, different flexibilities are examined by changing the thickness of concrete wall from 0.4 m to 1 m.

Following response parameters are studied:

(a)Total and incremental dynamic thrusts

(b) Point of application of the dynamic thrust

(c) Bending moment profiles on the wall stem

6.3 Presentation of the Results

6.3.1 Effects of Input Excitation Amplitude

The effect of input acceleration on the response parameters listed above is studied. Structural parameters used for modeling the wall are summarized in Table 6-1. Analyses are carried out for 5 different amplitudes of 0.05g, 0.1g, 0.12g, 0.15g and 0.20 g. The frequency of the acceleration time history is taken as 2 Hz.

Table 6-4 Model wall parameters

Wall height	8 m.
Wall thickness	0.50 m.
Wall flexibility	0,0170 m2/kN per meter
$K_{rot\ .spring}$	394000 kN.m /rad per meter
EI	808600 kN/m2 per meter
EA	17250000 kN/m per meter

Geometry and important parameters of the model are presented in Figure 6.4. Values of total dynamic active thrust for different acceleration amplitudes are presented in Figure 6.5 together with values calculated by Mononobe-Okabe and Steedman-Zeng methods. It is obvious from the figure that increasing amplitudes increase the differences between the

numerical and analytical solutions. This difference reaches three times the value of thrust calculated by M-O solution for the acceleration amplitude of α=0.2g.

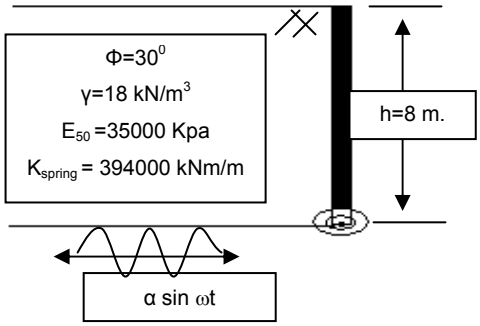

Figure 6.4 Geometry of the model and important parameters

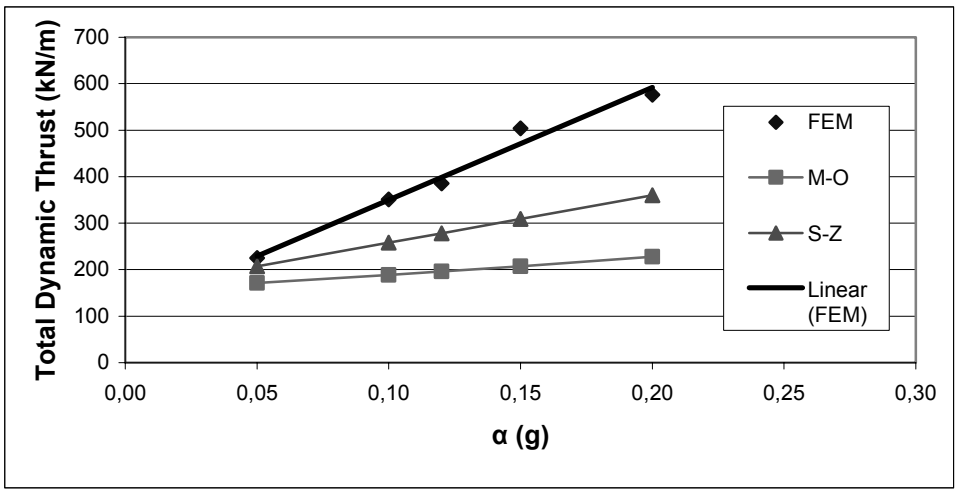

Figure 6.5 Total dynamic thrust on the wall versus peak base acceleration

Location of application points of total dynamic thrust (static + incremental dynamic thrust) for different acceleration amplitudes are shown in Figure 6.6. Figure 6.7 (a,b,c,d) present bending moment profiles on wall stem for different base excitation levels.

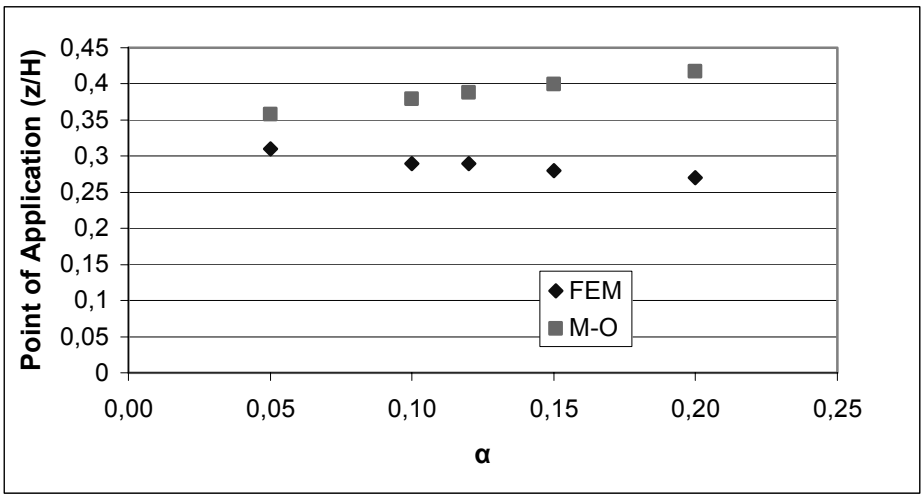

Figure 6.6 Location of application point of total dynamic thrust versus base acceleration amplitude (z is the vertical distance from wall base to application point of thrust)

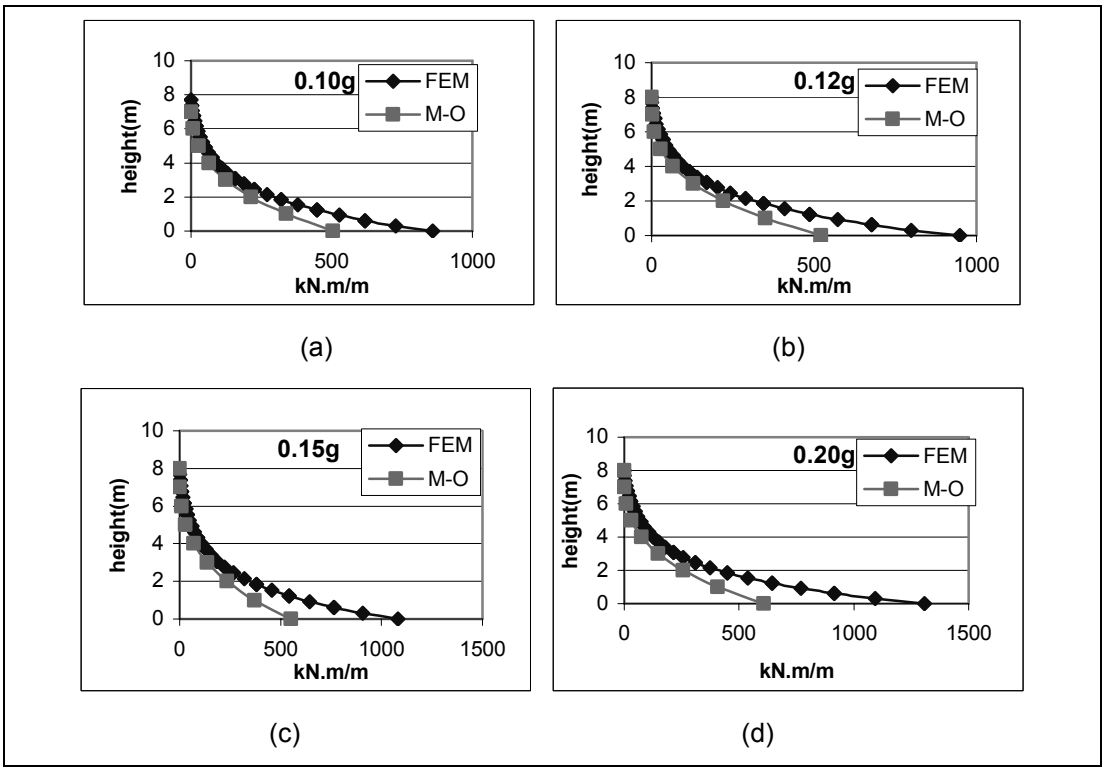

Figure 6.7 (a,b,c,d) Bending moment profiles for different acceleration amplitudes

In Figure 6.8 , dimensionless bending moments are shown along the wall height. Dimensionless parameters are defined as:

A = z/h where z is the distance from wall base in meters and h is the wall height

B = $M/\gamma h^3$ where M is the moment value at location z.

α = maximum base acceleration in g.

Similarly in Figure 6.9, incremental dimensionless bending moments are plotted against dimensionless wall height. Incremental moments are obtained by subtracting the moments caused by static lateral pressures acting on the wall from maximum total moments reached during excitation. In both figures, it is observed that an increase in acceleration amplitude results in an increase of the moments.

Soil wedge occurring when maximum thrust acts against the wall , is shown as total displacement contours in Figure 6.10. Time variation of horizontal wall displacements and dynamic lateral pressures against the wall for 0.10g, 0.20g and 0.30g acceleration amplitudes are shown in Figure 6.11 and figure 6.12 at the base, midheight and top of the wall stem.

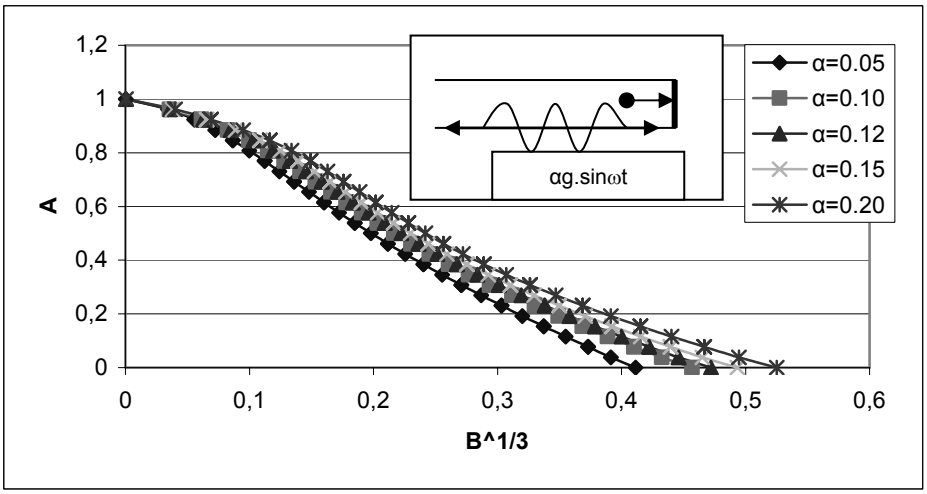

Figure 6.8 Dimensionless total dynamic moments obtained from FEM analyses ($\omega=2\pi f_{excitation}$)

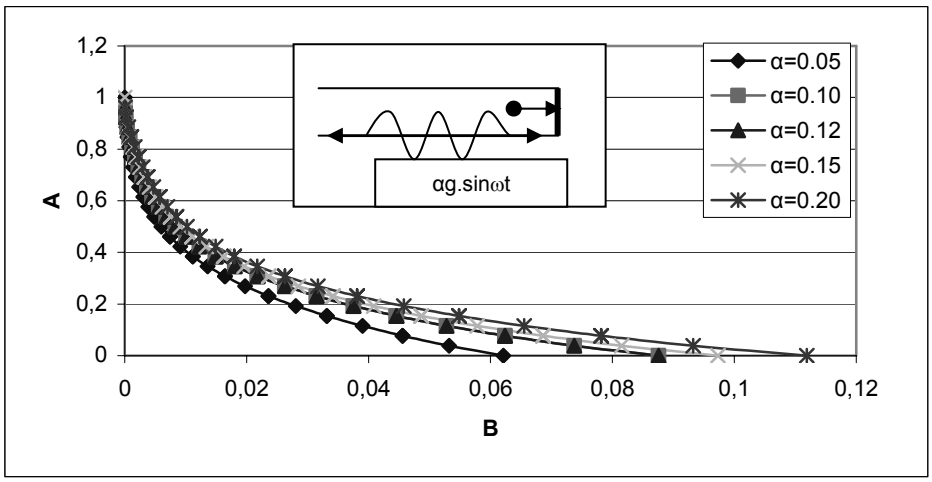

Figure 6.9 Dimensionless incremental dynamic moments obtained from FEM analyses ($\omega=2\pi f_{excitation}$)

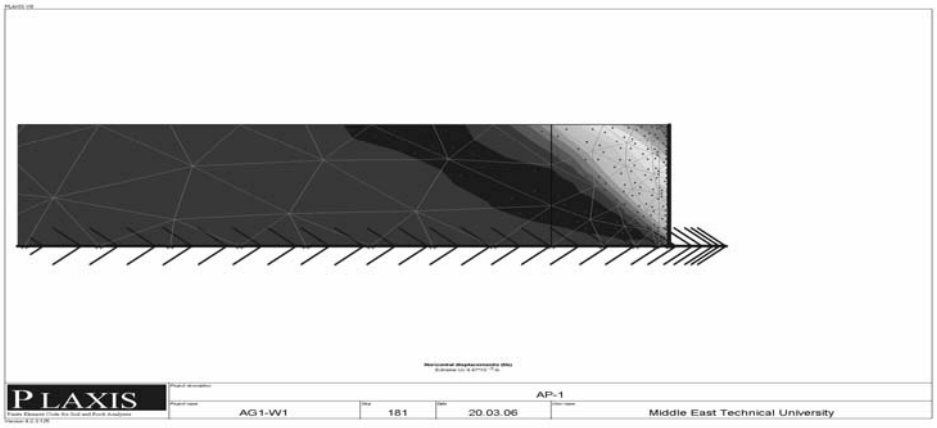

Figure 6.10 Failure wedge at the instant of maximum thrust

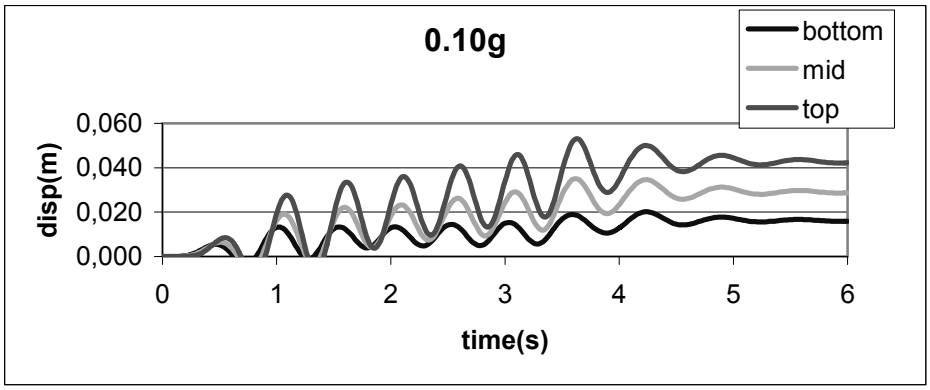

(a)

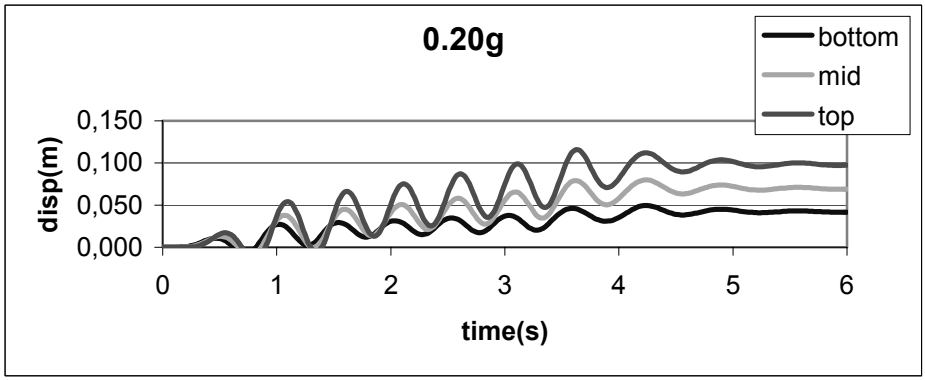

(b)

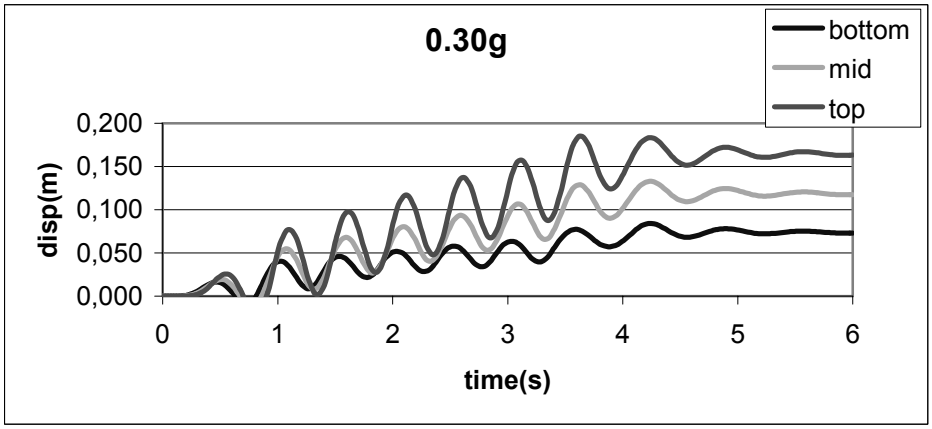

(c)

Figure 6.11 Time histories for horizontal wall displacements for (a)0.10g,(b)0.20g,(c)0.30g

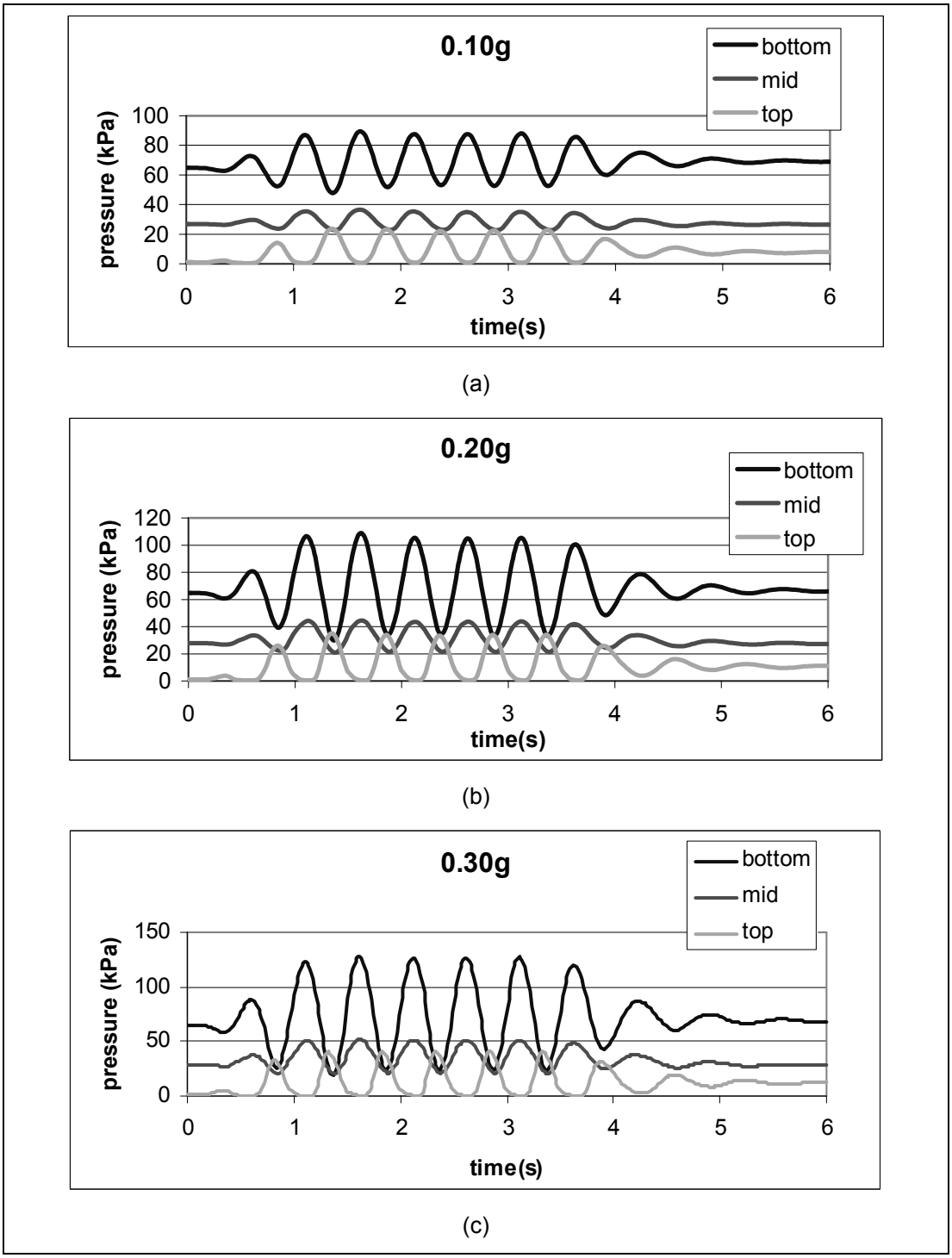

Figure 6.12 Time histories for lateral earth pressures for (a)0.10g,(b)0.20g,(c)0.30g

6.3.2 Effects of the Input Excitation Frequency

For constant base acceleration amplitude of 0.1g, a group of finite element analyses are performed for excitation frequencies indicated in Table 6-5. Wall geometry and all the other parameters are same with the ones indicated in Table 6-2 and Table 6-4.

Table 6-5 Parameters used in frequency analyses

excitation amp.(g)	excitation Freq.(Hz)	soil parameters	wall parameters
0.1g	2	same with the values indicated in Table 6.2	same with the values indicated in Table 6.4
0.1g	2.83(Resonance)		
0.1g	5		
0.1g	8.5		
0.1g	10		

Soil natural period is calculated as 0.35 seconds. Corresponding natural frequency is 2.83 Hz

The ratio of the frequency of base excitation to the natural frequency of the system is defined as frequency ratio and shown by symbol ξ .Maximum thrust values are plotted against frequency ratios in Figure 6.13. According to numerical study, maximum thrust occurs when the excitation frequency coincides with the natural frequency of the wall. There is agreement with Mononobe-Okabe and Steedman-Zeng methods for the base excitation frequencies outside the vicinity of the natural frequency of the system. Location of application points for the maximum total thrust are given against frequency ratios in Figure 6.14 .

Figure 6.15 and Figure 6.16 indicate dimensionless total and incremental moment profiles. As can be observed from these figures, maximum moments occur at the resonance. Dimensionless overturning moments at the wall base are plotted against frequency ratio (ξ) in Figure 6.17.

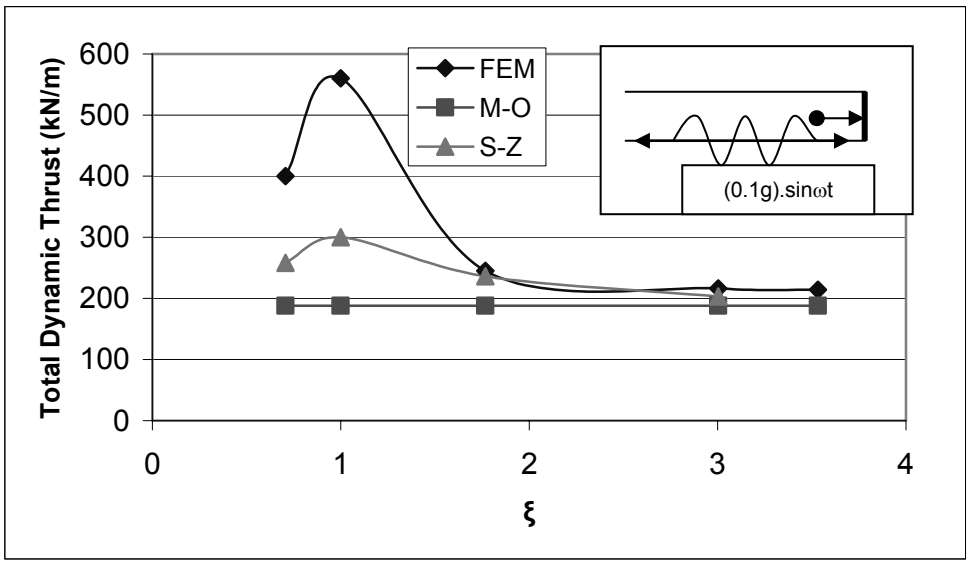

Figure 6.13 Total dynamic thrust versus frequency ratio (ξ)

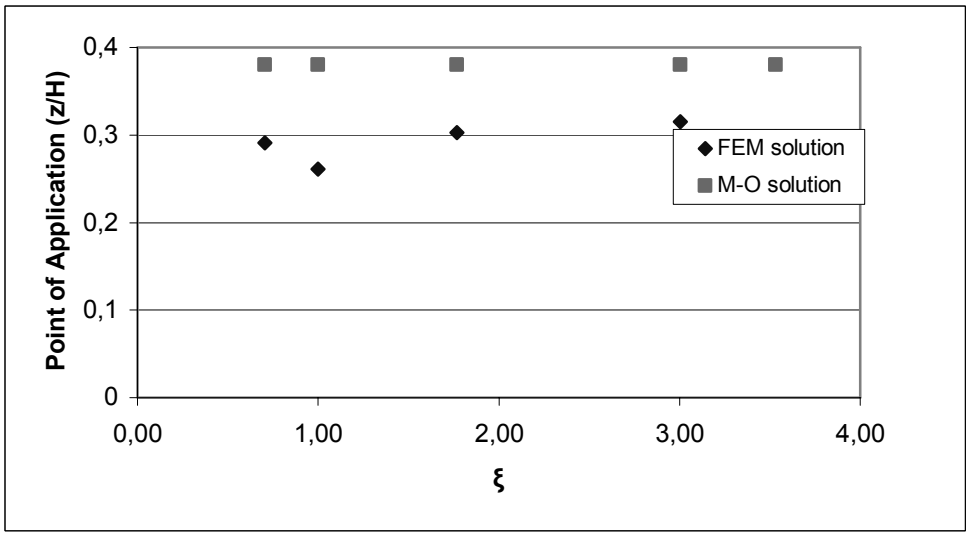

Figure 6.14 Points of application of the total dynamic thrust versus frequency ratio (z is the vertical distance from wall base to application point of thrust)

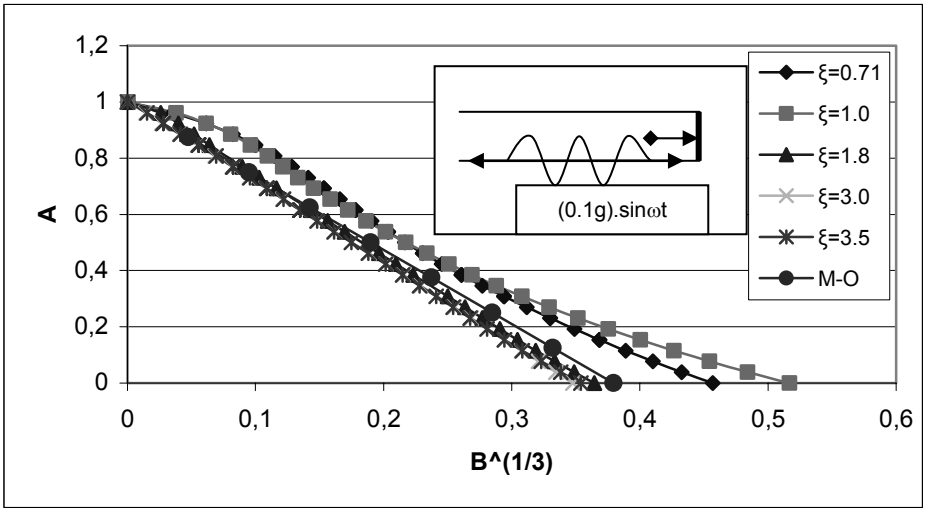

Figure 6.15 Total dynamic bending moments along the wall height for different base excitation frequencies (In dimensionless terms)

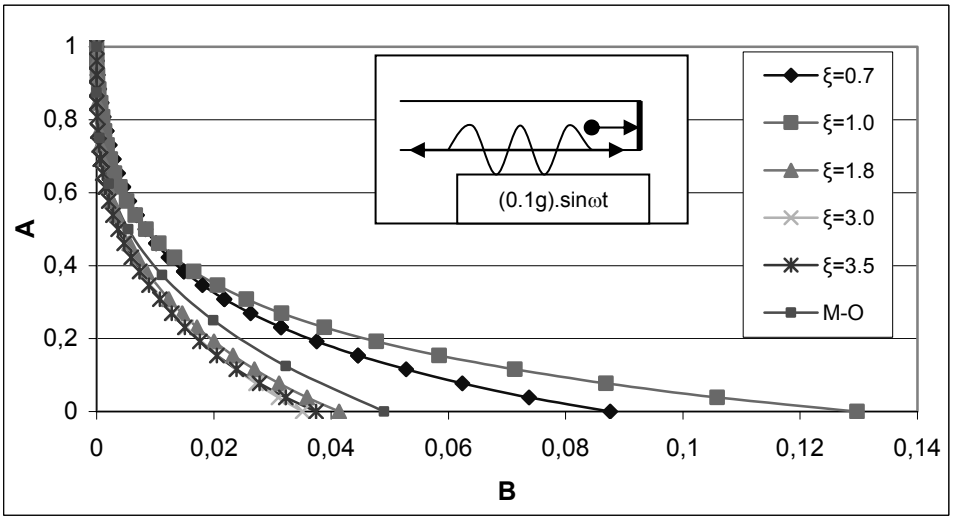

Figure 6.16 Incremental dynamic bending moment profiles along the wall height for different base excitation frequencies (In dimensionless terms)

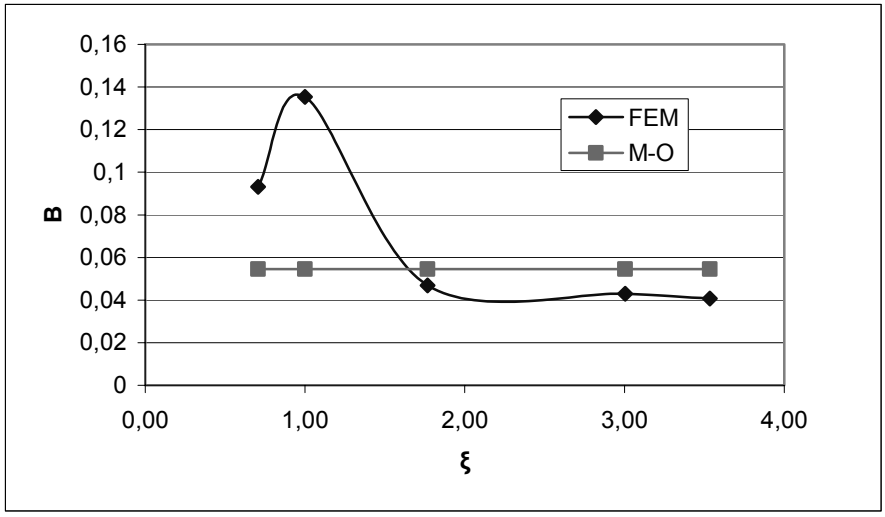

Figure 6.17 Maximum dimensionless wall moment versus frequency ratio

6.3.3 Effects of the Soil Strength

This parametric study is carried out to investigate the effects of the soil strength of the backfill on the dynamic response of the soil-retaining wall systems. For this purpose, internal friction angle of the backfill is taken as the variable parameter. Analyses are carried out for the range of $\varphi=25^0$ to $\varphi=40^0$ while keeping the other soil parameters constant. Wall properties and geometry are kept same as in the previous analyses . Input base motion acceleration time history having an amplitude of 0.1g, frequency of 5Hz and a duration of 5 seconds is applied to the base of the system

Figure 6.18 and Figure 6.19 present total and the incremental dynamic active thrust values for different internal friction angles. Maximum thrust values obtained from FEM analyses closely fits to the results of pseudo static analyses. In Figure 6.20, positions of application points obtained from FEM study are compared with M-O results. Points of application for maximum total active thrust are predicted to be located at approximately 0.30 H above the base by FEM analysis. According to this result, application points are located closer to the base of the wall as compared to 0.37 H corresponding to M-O approach. Figure 6.21 and Figure 6.22 summarize the moment profiles at the time of maximum thrust. In figure 6.23, moments obtained by FEM solution are compared with M-O results.

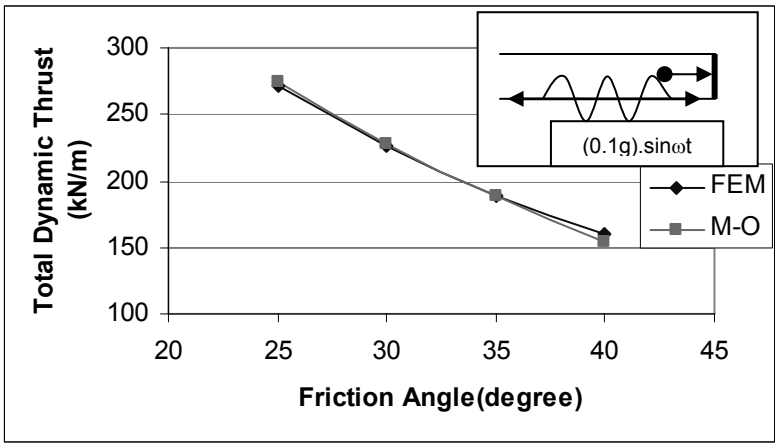

Figure 6.18 Total dynamic thrust versus internal friction angle

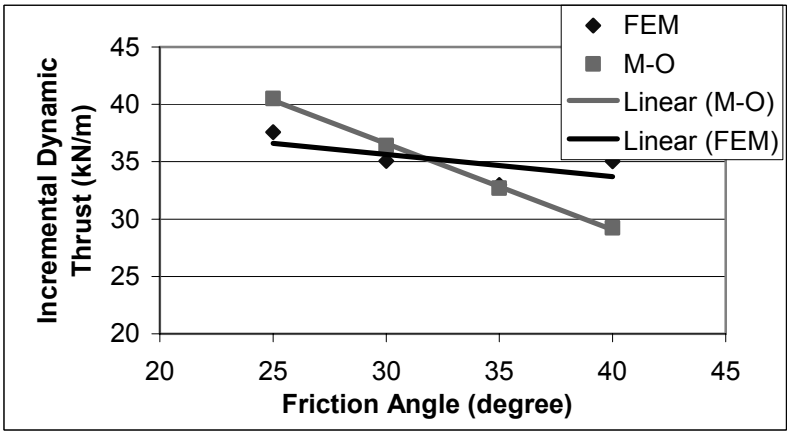

Figure 6.19 Incremental dynamic thrust versus internal friction angle

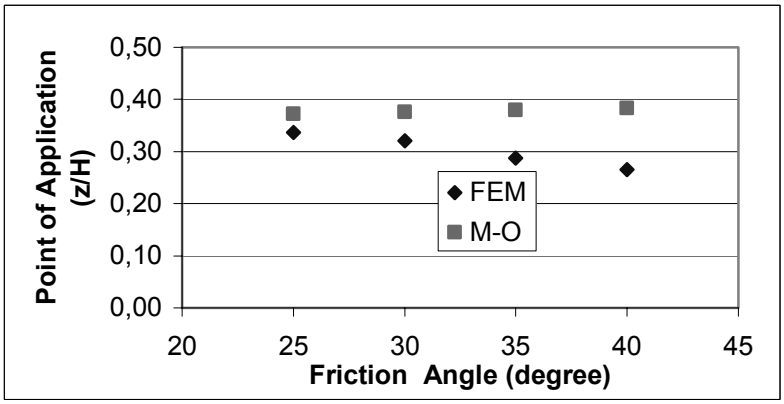

Figure 6.20 Point of application value for total dynamic thrust versus friction angle (z is taken to be from the base of the wall)

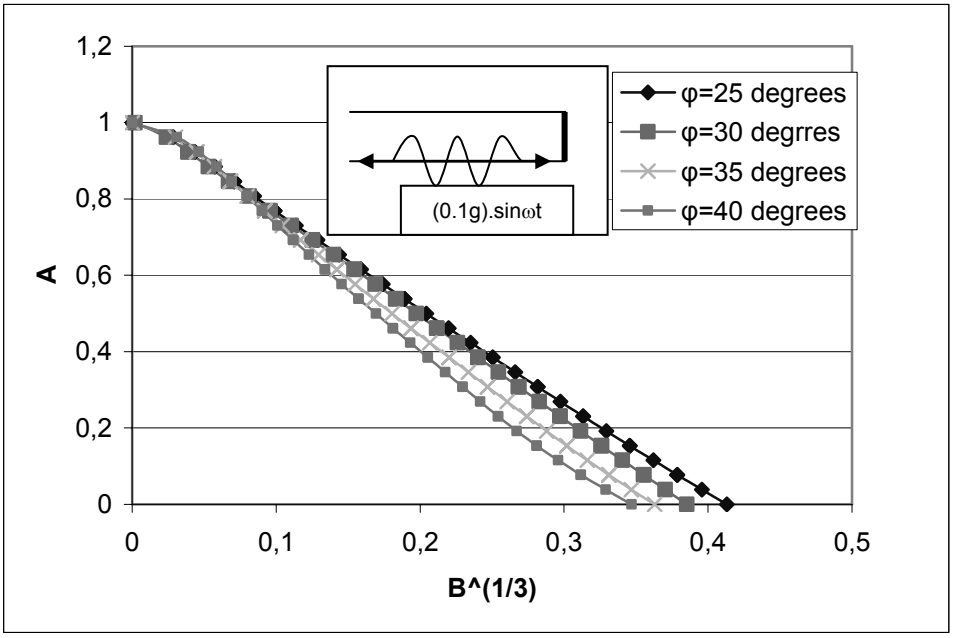

Figure 6.21 Dimensionless total dynamic moment profiles

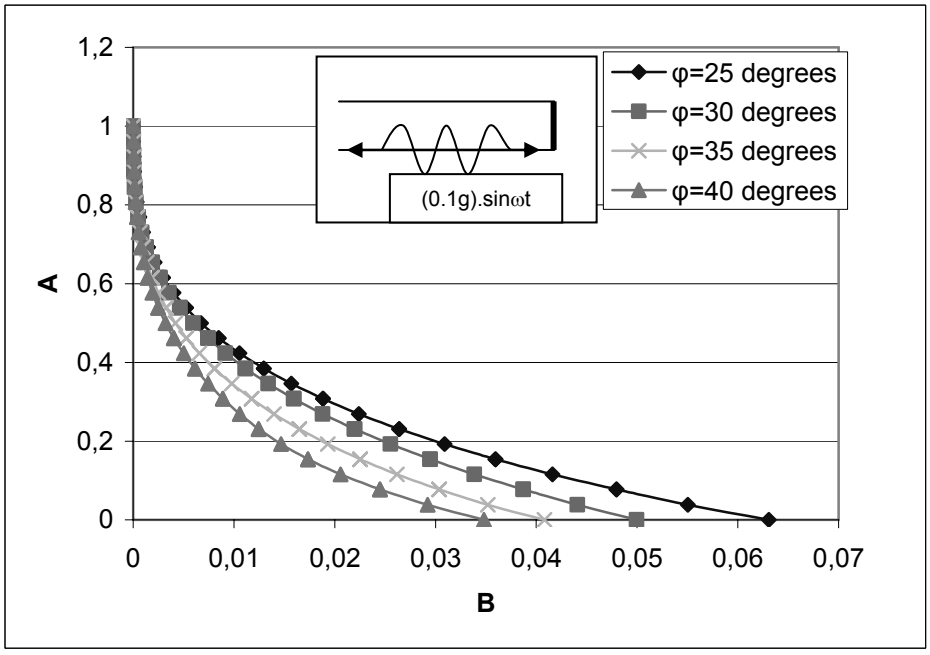

Figure 6.22 Dimensionless incremental dynamic moment profiles

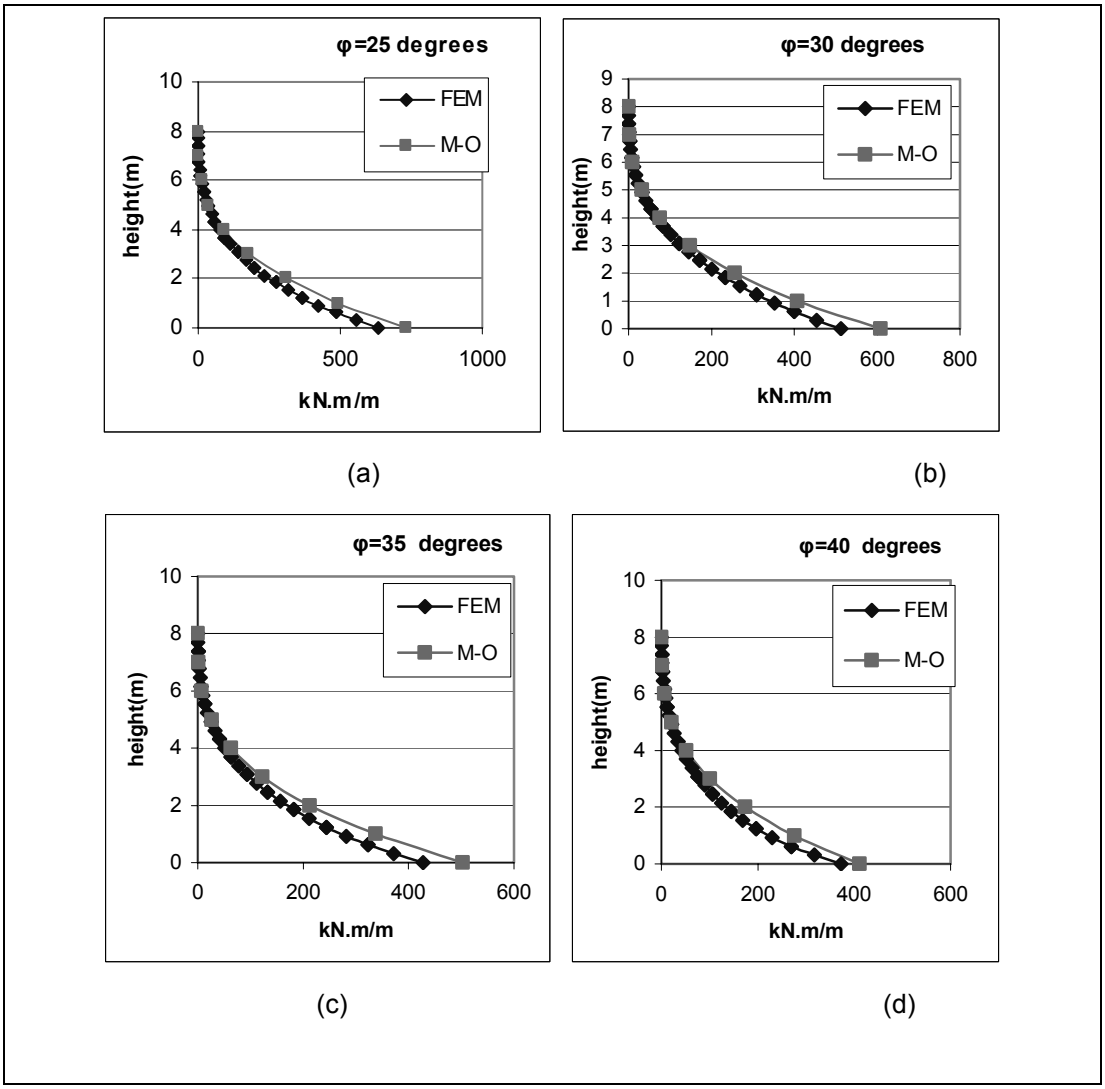

Figure 6.23 Bending moment profiles for different internal friction angles of the backfill

6.3.4 Effects of the Wall Flexibility

In this part of the study, the effect of wall flexibility on the dynamic response of the retaining walls is examined. Soil parameters are taken as described in Table 6-2.

Wall flexibility parameter (f) is defined as H^4/EI where E is the Young's Modulus of the wall material, H , wall stem height (m) and I , moment of inertia of the wall section. Using this definition, the flexibilities for five different wall configurations shown in Table 6-6 are studied By Plaxis dynamic module. In the analyses, wall flexibilities are changed by changing wall thicknesses.

Table 6-6 Parameters used in flexibility analyses

wall width (m)	f (m^2/kN /m)	wall height (m)	input base excitation	soil parameters
0.4	0.0334	8	0.1g 5Hz	Described in Table 6.2
0.5	0.0170	8	0.1g 5Hz	
0.75	0.0051	8	0.1g 5Hz	
1.0	0,0021	8	0.1g 5Hz	

In Figure 6.24 and Figure 6.25, maximum total active thrust values are plotted against wall thickness and wall flexibility, respectively. According to FEM study, increasing flexibility of the wall decreases dynamic thrust on the wall. For flexibility values greater than 0.01, magnitudes of dynamic thrust calculated by numerical method are quite consistent with the ones calculated by Steedman-Zeng method.

Figure 6.26 shows the location of application points of total active force on the wall for different flexibility values. According to FEM study, total dynamic thrust act at 0.3H above the base of the wall. Significant change is not observed for different wall flexibilities.

The normalized bending moment profiles are shown in Figure 6.27 and Figure 6.28. Bending moment profile is also calculated by using standard Mononobe-Okabe method. Flexibility is not a variable in the M-0 method. However, the moments obtained from FEM analyses are functions of flexibility. From the results it can be observed that Mononobe-Okabe gives nearly identical results with finite element analysis for the rigid wall which has flexibility value of 0.02 but overestimates the moments for flexible walls. Dimensionless overturning moments at the wall base versus flexibility of the wall is shown in Figure 6.29. For rigid walls, there is a significant increase in overturning moments.

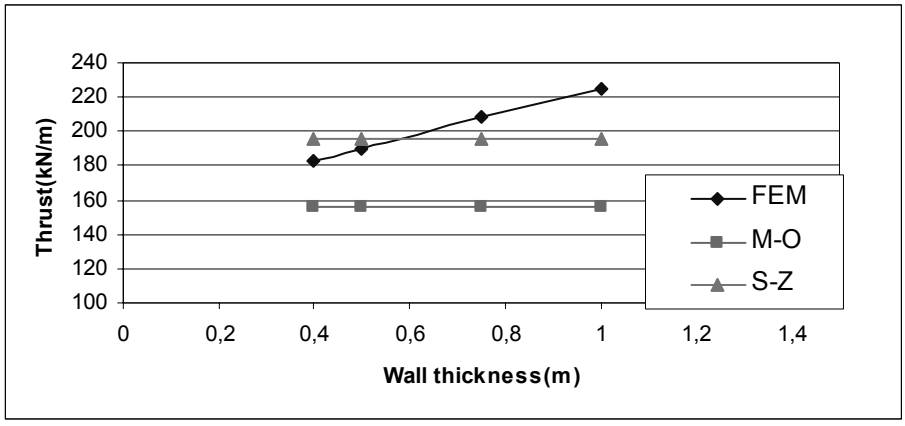

Figure 6.24 Maximum total dynamic thrust versus wall thickness

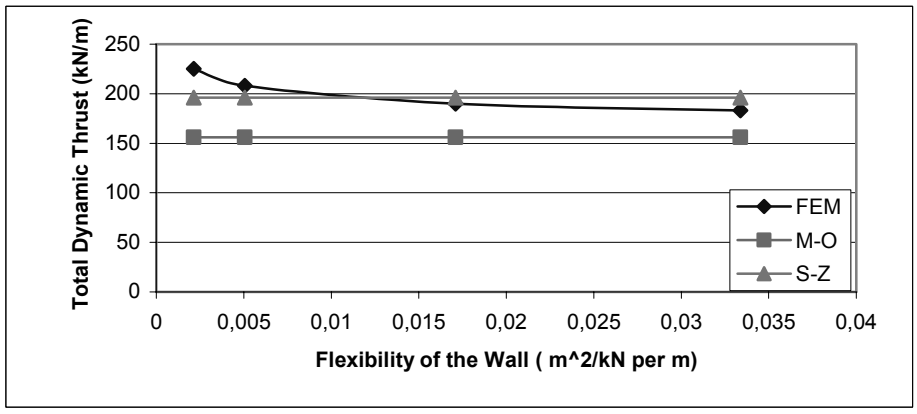

Figure 6.25 Maximum total dynamic thrust versus wall flexibility

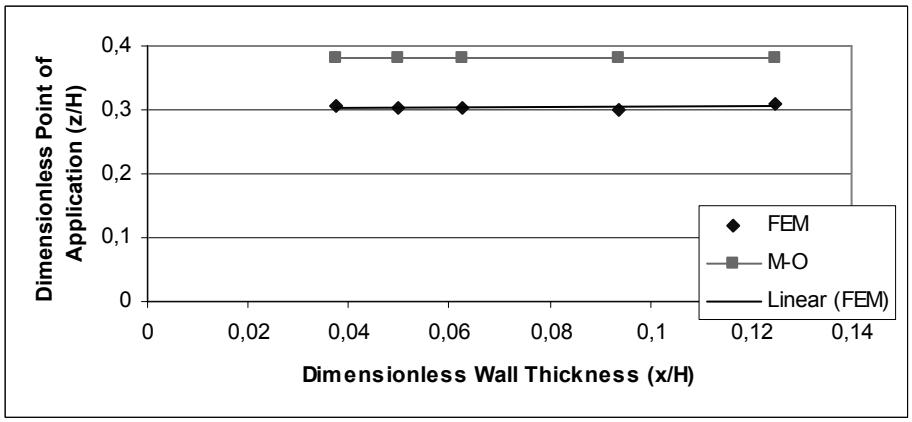

Figure 6.26 Point of application of total dynamic thrust versus wall thickness

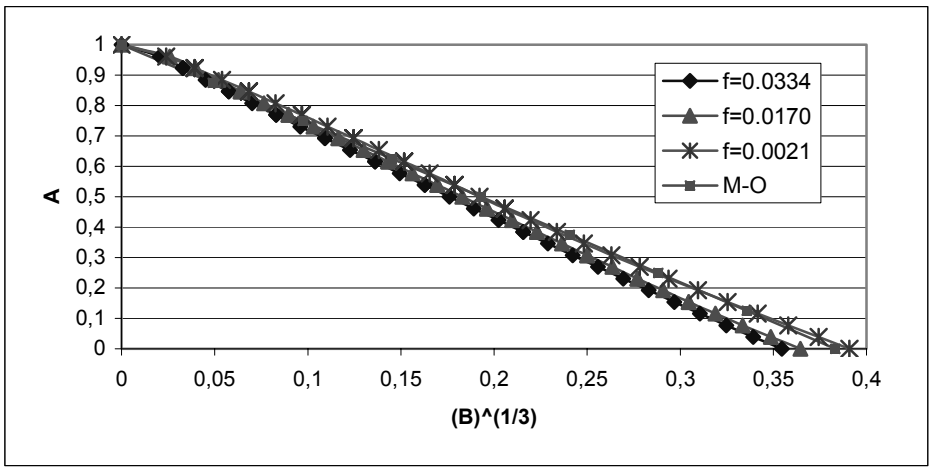

Figure 6.27 Dimensionless total bending moment profiles

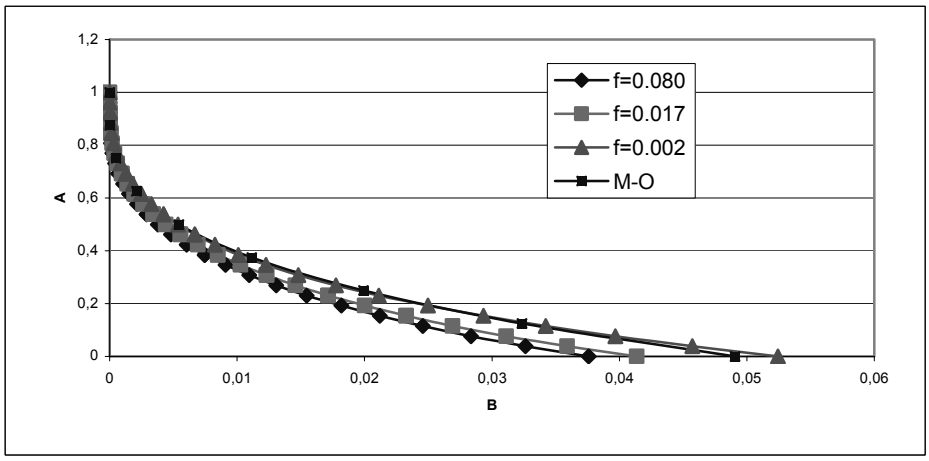

Figure 6.28 Incremental dimensionless dynamic bending moment profiles

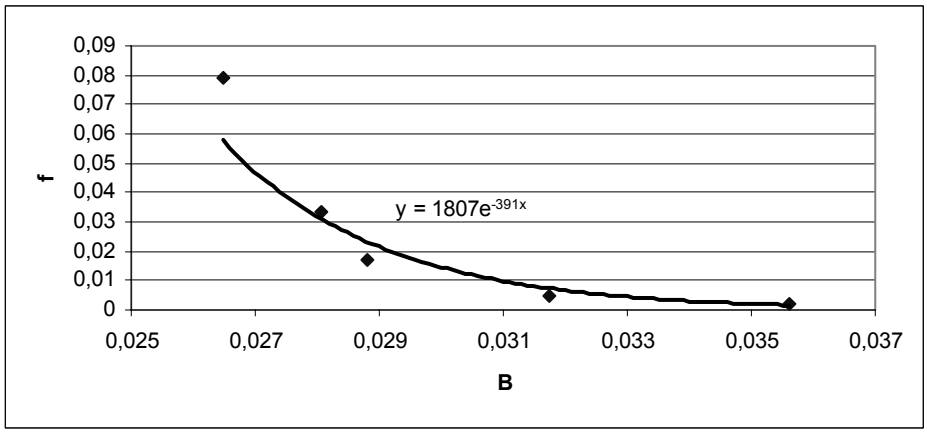

Figure 6.29 Dimensionless base moment versus wall flexibility

CHAPTER 7

SUMMARY AND CONCLUSIONS

A numerical study is performed in order to investigate the effects of input base excitation characteristics (peak acceleration amplitude and frequency of the excitation), soil strength and wall flexibility on the dynamic response of cantilever earth-retaining walls.

In this study, Plaxis v8.2 dynamic finite element code is used for the analyses. Previous experimental studies are modeled and solved by finite element approach. Results of two different shake table model tests conducted in METU Civil Engineering Department Geotechnics laboratory are compared with values obtained from finite element approach. Besides this, a one-dimensional ground response analysis is performed to check the results of Plaxis dynamic module.

Comparison of experimental and numerical results for dynamic thrusts, maximum horizontal displacements at the top of the wall, foundation rotations and application points of the thrusts indicated that the dynamic finite element code has the ability to model the experimental setups. Once calibrated, the code was capable of predicting the deflection and bending moment profiles of the wall stems. In the light of these validation and calibration studies, a parametric study is carried o for real wall geometries.

In the parametric study, an 8 meters high vertical concrete retaining wall supporting the same height of dry cohesionless backfill is modeled. Base of the system is excited by simple harmonic acceleration time histories. Foundation of the retaining wall is not modeled; instead, a rotational spring is used at the wall base to represent the rotational rigidity of the foundation in the presence of foundation subsoil.

Total and incremental dynamic thrusts, points of application and dimensionless bending moment profiles on the walls are presented together with commonly used pseudo static Mononobe-Okabe method and Steedman-Zeng approach.

Analyses performed for cantilever retaining walls indicate that acceleration amplitude of base motion is the major effective parameter on magnitudes of dynamic thrust acting on the walls. Significant increase is observed in values of thrust between the base excitation amplitudes of 0.05g to 0.20g.

Increase of thrust is predicted higher as compared to M-O and S-Z results. In FEM study, points of application for the thrust are found to be located at approximately 0.30 H from the base of the wall and decrease slightly when excitation amplitude increases. According to Mononobe-Okabe solution, location of application points increase with increasing acceleration amplitude.

Base motion frequency becomes an important factor on magnitudes of dynamic thrust when it approaches to natural frequency of the system. At resonance case, value of total thrust obtained by numerical study is approximately three times larger than the value obtained by Mononobe-Okabe method due to the fact that this method do not take into account the effect of excitation frequency. When base motion frequency is outside the vicinity of natural frequency of the system, magnitude of dynamic thrust is predicted close to analytical approaches. Points of application are found to be located at approximately 0.3 H above the base except the resonance case. By performing Mononobe-Okabe analysis, this value is found as 0.37H for the whole range of base motion frequency.

Effect of soil strength on the dynamic response is investigated in terms of internal friction angle of the backfill. As expected, smaller thrust and overturning moments are observed for increasing internal friction angle of the backfill. Values of thrust obtained from finite element study closely fits the results of M-O method which takes into account the soil strength. According to finite element modeling study, dynamic active thrust acts at 0.34 H above base for an internal friction angle of 25^0 whereas, it acts at 0.26H for an internal friction angle of 40^0. Numerical analyses are predicting the point of application of the thrust 5% to 25 % lower when compared with the values obtained by Mononobe-Okabe method.

Two wall parameters, height and stiffness are presented by a single parameter called flexibility. Thickness of the wall is changed to have different flexibility values while height of the wall is kept constant. It is observed that dynamic thrust acting on the wall stem due to base motion is indeed a function of flexibility. As the flexibility increased, the magnitude of active dynamic thrust and bending moment decreased. It is observed that Mononobe-Okabe method underestimate dynamic thrust for the considered flexibility values. Discrepancy between the predictions increase for rigid walls ($f \leq 0.02$ m^2/kN per meter). FEM predictions are in better accordance with solutions of Steedman-Zeng method which takes into account the amplification of motion through the height of the backfill.

Results of numerical analyses for the idealized wall-backfill system appear to be reasonable and in agreement with predictions of the pseudo-static methods in most cases. However, further analyses of actual case histories must be performed to confirm the computed prediction with the actual earthquake damage observations.

In considered wall-backfill model, wall is fixed to the base. There exists only a rotational constraint to simulate the foundation rotations during dynamic motion. However, sliding displacement of the wall base will also affect the behavior of the retaining wall. Analyses for the backfill-wall system resting on foundation soils must also be carried out for investigating this case.

REFERENCES

1. Aggour, M.S. and C.B. Brown, "Retaining Walls in Seismic Areas", Proceedings, 5th World Conference on Earthquake Engineering, Rome, Italy, pp. 2624-2627, June, 1973.

2. Alampalli, S., "Earthquake Response of Retaining Walls; Full Scale Testing and Computational Modeling", Ph. D. Thesis, Rensselaer Polytechnic Institute, Troy, New York, USA, 1990.

3. Bangash, A.A. ”Nonlinear Dynamic Finite Element Analysis of Tiedback Retaining Walls

4. Biggs, J.M., Introduction to Structural Dynamics. New York.McGrawHill;1964

5. Byrne, P.M. and F. Salgado, "Seismic response of retaining structures", Proceedings, International Conference on Recent Advances in Geotechnical Earthquake Engineering and Soil Dynamics, April 26 - May 3, St. Louis, MO, 1981.

6. Chen,W.and Mizuno, E.(1990), Nonlinear Analysis in Soil Mechanics

7. Çalışan, O., “A Model Study On The Seismic Behavior Of Gravity Retaining Walls”, Ph.D Dissertation, Middle East Technical University, Ankara, Turkey, January 1999

8. Clough, G.W. and Duncan, J. M, “Finite Element Analysis of Retaining Wall behavior”, Journal of Soil Mechanics and Foundations division,ASCE,Vol.97, No.SM12,pp.1657-1674

9. Çilingir,U, “A Model Study on the Effects of Wall Stiffness and Surcharge on Dynamic Lateral Earth Pressures”, M.S Thesis , Middle East Technical University, Ankara, Turkey, July 2005

10. Das, B. M., Fundamentals of Soil Dynamics , Elsevier Science Publishing co. Inc, New York,1983

11. Franklin, A.G. and F.K. Chang, "Earthquake Resistance of Earth and Rock-Fill Dams", Report 5, Permanent Displacement of Earth Embankments by Newmark Sliding Block Analysis, Misc. Paper S-71-17, Soils and Pavements Laboratory, U.S. Army Waterways Experiment Station, Vicksburg, MS, Nov., 1977.

12. Gazetas G, Psarropoulos PN, Anastasopoulos I, Gerolymos N.Seismic behaviour of flexible retaining systems subjected to short duration moderately-strong excitation. Soil Dynamics and Earthquake Eng 2004;24:537–50.

13. Green et al. (2003), Proceedings of The Sixth US Conference and Workshop on Lifeline Earthquake Engineering (TCLEE2003), ASCE, August 10-13, 2003, Long Beach, CA

14. Hardy, S. “The implementation and application of dynamic finite element analysis to geotechnical problems” Ph.D thesis, Department of Civil and Environmental Enginnering, Imperial College of Science, Technology and Medicine, March 2003, London

15. Jacobson, P.N., "Translational behavior of gravity retaining walls during earthquakes", Research Report 80-9, Dept. of Civil Eng., Univ. of Canterbury, New Zealand, 1980.

16. Koseki J. Seismic performance of retaining walls—case histories and model tests. Proceedings of the Fourth Forum on Implications of Recent Earthquakes on Seismic Risk, Japan: Tokyo Institute of Technology; 2002. p. 95–107.

17. Kramer, S. Geotechnical earthquake engineering, NJ,USA, Prentice Hall ;1996

18. Lambe,W.T.,Whitman, R.V. ,Soil Mechanics , SI version , John Wiley and Sons,1969

19. Lysmer J., Kuhlmeyer R.L. (1969) “Finite Dynamic Model for Infinite Media” ASCE J. of the Eng. Mech. Div., p.859-877

20. Mononobe, N. and H. Matsuo; "On the Determination of Earth Pressures During Earthquakes"; Proceedings, World Engineering Conference, Vol. 9, p. 176,1929.

21. Nadim, F. and R.V. Whitman, "A numerical model for evaluation of seismic behavior of gravity retaining walls", Research Report R82-33, Dept. of Civil Engineering, M.I.T., 1982.

22. Nazarian, H.N. and A.H. Hadjian, "Earthquake-Induced Lateral Soil Pressures on Structures", ASCE Journal of Geotechnical Engineering, Vol. 105, No. GT9, pp. 1049-1066, September, 1979.

23. Newmark, N.M.; "Effects of Earthquakes on Dams and Embankments"; Fifth Rankine Lecture, Geotechniques, Vol.15, No.2,pp 139-160, 1965.

24. Okabe, S.; "General theory of earth pressure and seismic stability of retaining wall and dam", Journal. Japanese Soc. of Civil Eng., Vol. X, No. 6, Dec., 1924.

25. Okabe, S.; "General Theory of Earth Pressure"; Journal, Japanese Society of Civil Engineers, Vol. 12, No. 1, 1926.

26. Plaxis Scientific Manual, edited by Brinkgrieve R.B.J. , Delft University of Technology, 2002 , The Netherlands

27. Prakash, S. and B.M. Basavanna; "Earth Pressure Distribution Behind Retaining Wall During Eathquake"; Proceedings, Earthquake Engineering, Fourth World Conference, Vol. HI, Chile, 1969.

28. Psarrapaulos ,P.N.," Seismic Earth Pressures on rigid and flexible retaining walls", Soil Dynamics and Earthquake Engineering, Elsevier, 25(2005),795-809

29. Richards Jr., R. and D. Elms; "Seismic behavior of gravity retaining walls", Research Report No. 77-10; University of Canterbury, Christchurch, New Zealand, 1977.

30. Richards Jr., R. and D.G. Elms; "Seismic Behavior of Gravity Retaining Walls"; ASCE Journal of Geotechnical Engineering, Vol. 105, No. GT4, pp. 449-464, April, 1979.

31. Schanz,T., Vermeer,P.A.,Bonnier P.G.,(1999).Formulation and verification of the Hardening –soil model. In .R.B.J. Brinkgrieve, Beyond 2000 in Computational Geotechnics , Balkema Rotterdam:281-290

32. Seed, KB. and R.V. Whitman; "Design of Earth Retaining Structures for Dynamic Loads"; Lateral Stresses in the Ground and Design of Earth-Retaining Structures, ASCE Specialty Conference, Cornell Univ., Ithaca, N. York, June 22-24,1970.

33. Siddharthan, R_ and E. Maragakis, "Seismic Performance of Flexible Retaining Walls Supporting Dry Cohesionless Soils", Developments in Geotechnical Engineering #45, Structures and Stochastic Methods, A.S. Cakmak (ed.), 1987.

34. Siddharthan, R_ and E.M. Maragakis; "Performance of Flexible Retaining Walls Supporting Dry Cohesionless Soils Under Cyclic Loads"; International Journal for Numerical and Analytical Methods in Geomechanics, Vol. 13, pp. 309-326,1989

35. Sluys, L.,J. (1992),Wave Propogation, Localisation and Dispersion in softening solids, Dissertation, Delft University of Technology

36. Stadler, A.,T., ”Static and Dynamic Behavior of Cantilever Retaining Walls”, Ph.D Thesis, University of Colorado, USA , 1996

37. Steedman, R.S. and X. Zeng; "Centrifuge modeling of the effects of earthquakes on free cantilever walls"; Centrifuge '91, Ko (ed.), Balkema, Rotterdam, 1991.

38. Steedman, R.S., "Modeling the Behavior of Retaining Walls in Earthquakes", Ph.D. Thesis, Cambridge University, , England, 1984.

39. Veletsos, A. S., and Younan, A, H. (1994a). "Dynamic soil pressures on rigid retaining walls." *Earthquake Engrg. and Struct. Dyn.,* 23(3), 275-301.

40. Veletsos, A. S., and Younan, A, H. (2003). "Dynamic response of flexible retaining walls “ *Earthquake Engrg. and Struct. Dyn.,* 29,1815-1944.

41. Veletsos, A. S., and Younan, A. H. (1994b), "Dynamic modeling and response of soil-wall systems." *J. Geotech. Eng.,* ASCE, 120(12), 2155-2179.

42. Wood,J.H. (1973),”Earthquake Induced Soil Pressures on Structures”. Report EERL 73-05, California Institute of Technology

43. Yıldız ,E. , “Lateral pressures on rigid retaining walls: A neural network approach” M.S Thesis , Middle East Technical University, Ankara, Turkey, August 2003

44. Yunatçı,A.A, “A Model Study on the Seismic behavior of the laterally braced sheet pile walls”, M.S Thesis , Middle East Technical University, Ankara, Turkey, January 2003 .

45. Zarrabi, K., "Sliding of Gravity Retaining Wall During Earthquakes Considering Vertical Acceleration and Changing Inclination of Failure Surface", Master's Thesis, Department of Civil Engineering, M.I.T., Cambridge, Mass., 1979.